Juel-4393

Jülich Center for Hadron Physics (JCHP)
Institut für Kernphysik (IKP)
COSY

Precision Proton-Proton Elastic Scattering Data

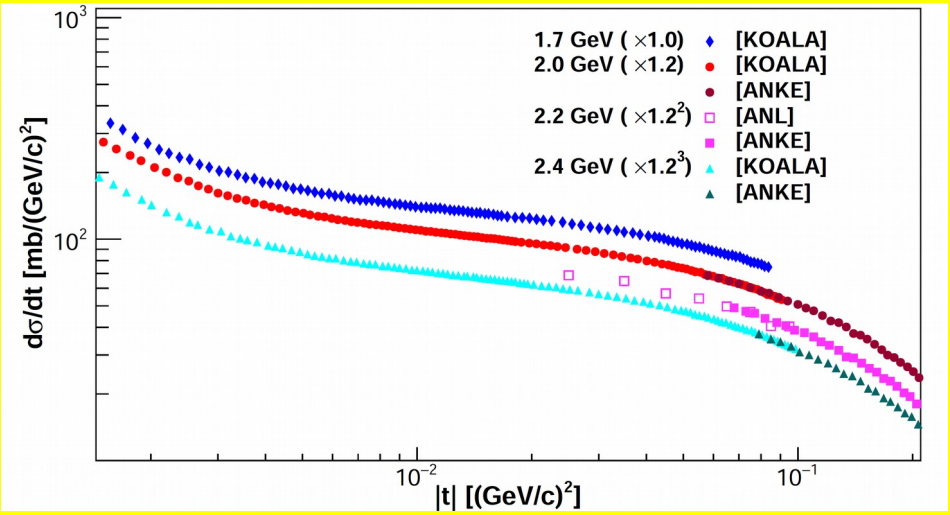

Record Spin Coherence Time for EDM Searches

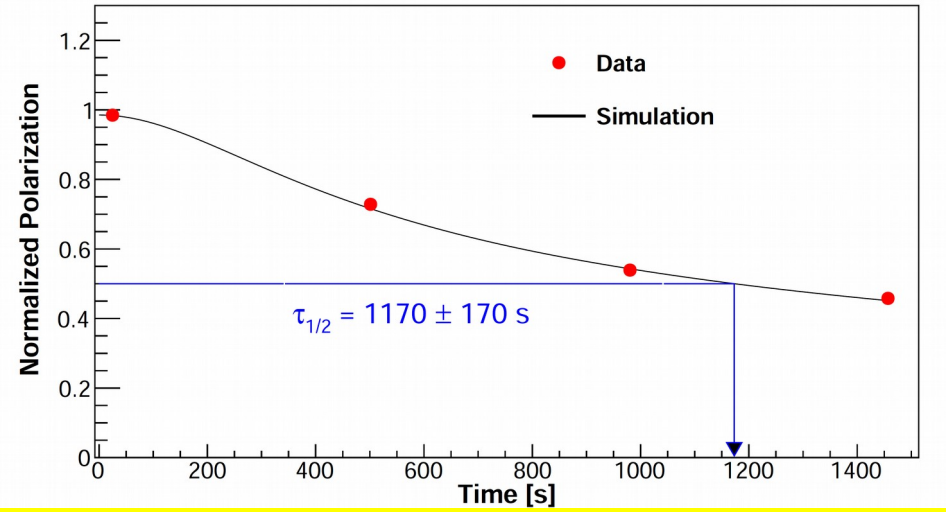

Annual Report 2015

JÜLICH
FORSCHUNGSZENTRUM

Annual Report 2015

Jülich Center for Hadron Physics / Institut für Kernphysik / COSY

Cover picture:
The (upper) cover picture shows the normalized differential cross section of proton-proton elastic scattering at small angles for 4 different beam energies as a function of the squared 4-momentum transfer |t|. The experiments were conducted at COSY using the ANKE spectrometer and the KOALA detection system designed for the measurement of antiproton-proton elastic scattering at HESR. The COSY measurement achieved, not only unprecedented small |t| data in the CNI region, but also precise differential cross sections (for details see sections 1.1 and 1.2).
The (lower) plot follows, as a function of time, the spin polarization in the ring plane of a deuteron beam circulating in the COSY storage ring at 0.97 GeV/c. Such a beam could be used to look for the small rotation that can arise if the radial electric field interacts with some electric dipole moment (EDM) that might be aligned with the particle spin axis which relies on the beam staying polarized. This beam polarization has been preserved for a half-life of 1173 ± 172 s, creating a new record lifetime that is about a thousand times greater than the previous limit for electron beams (for details see page 13).

Contents

Preface

With the start of the third programme-oriented funding period (PoF-3) in 2015 the IKP has completed the process of focusing its scientific portfolio to the two topics PANDA and HESR at FAIR and storage ring EDM search (srEDM).
After a long period of uncertainty about the realizing of the FAIR project, especially concerning the antiproton pillar, the FAIR council made a clear positive statement. All four pillars of FAIR including the PANDA experiment should be completed simultaneously. That's a clear signal to go on with the PANDA detector development and the HESR preparations.
The ongoing project srEDM promoted by the international JEDI collaboration gained a high scientific reputation as a potential flagship project in basic research. Measurements or at least the extension of the limits of charged particle EDMs will try the limits of the Standard Model and constrain models of supersymmetry.
A complementary project in the leptonic sector started recently with the new IKP group of Prof. Ludhova, resulting from the HGF recruiting initiative, for the study of neutrino physics.
The experimental activities at COSY have changed from hadron physics to high precision spin physics and FAIR related component tests. About half of the user beam time in 2015 was used for srEDM related studies and the other half was devoted to tests of HESR and FAIR detector components.

Apart from results originating from our hadron physics activities at COSY the following highlights have been achieved in 2015:

- **FAIR:** The preparation of HESR is on schedule, first dipoles and quadrupoles were delivered and the test procedures have started. Test measurements for the Straw Tube Tracker, the MVD and the DAY-1 KOALA experiment have been successfully performed.

- **srEDM:** A record long spin coherence time has been achieved and various developments are on the way towards the precursor experiment, like e.g. BPM, RF-Wien-filter, and polarimeter. The precision in the spin manipulation techniques has reached such a high level that it provides a diagnostics tool for probing spin motion effects in storage ring not accessible before.

- **Theory:** The theory group worked on various fields with exciting results. Examples are first ab initio calculations of alpha-alpha scattering, a fundamental ingredient of the nucleosynthesis, the precise determination of the pion-nucleon σ-term or the investigation of pentaquark-like structures and XYZ states.

In spite of the recognized high scientific value of our research the board of directors suggested a transition of the IKP after the contractual deliverables of the main activities FAIR and srEDM within POF-3 are fulfilled. We are convinced that curiosity-driven basic research, the main topic at IKP is indispensable for a research center with the demand for a high scientific reputation. We believe that an excellent approach for IKP or its future new structure will be to keep the tripod of basic research with experiment, theory and accelerator science. Presently the discussions about the future of IKP are ongoing and there will be for sure changes.

Finally I would like to thank all IKP members, the colleagues of the infrastructure departments and our national and international collaboration partners for their activities and support.

Jülich, March 2016 James Ritman

1 COSY - highlights from hadron physics

1.1 The absolute differential cross section of pp-elastic scattering at small angles

For beam energies above about 1 GeV there are relatively few measurements of proton-proton elastic scattering available at centre-of-mass (c.m.) angles θ from 10° to 30°, i.e., between the region of major Coulomb effects and the larger angles where the EDDA collaboration has contributed so extensively. The lack of information on the differential cross section and analysing power inevitably leads to ambiguities in any pp partial wave analysis (PWA) at high energies. The ANKE collaboration has published [PLB **739** (2014) 152] proton analysing powers in this angular domain at 796 MeV and five other beam energies between 1.6 and 2.4 GeV using a polarised proton beam and these led to a revision of the SAID PWA in order to accommodate the data. The major uncertainty in such a measurement is the precision to which the beam polarisation can be determined, beam-target luminosity and equipment acceptance playing only secondary roles. This is far from being the case for the differential cross section where, in order to provide accurate absolute values, both the luminosity and acceptance must be mastered with high precision.

The present studies of the differential cross section were carried out at the ANKE spectrometer using an unpolarised proton beam at eight different beam energies, $T_p = 1.0, 1.6, 1.8, 2.0, 2.2, 2.4, 2.6$, and 2.8 GeV, interacting with a hydrogen cluster-jet target. Only the forward detector, which measured fast protons from elastic pp scattering over a range of up to $12^\circ - 30^\circ$ in c.m. polar angles was used in the analysis. The biggest challenge that has to be faced when measuring the absolute value of a cross section in a storage ring experiment is to establish the beam-target luminosity at the few percent level. It has been shown that this can be achieved by studying the energy loss through electromagnetic processes as the coasting uncooled beam passes repeatedly through the target chamber. There is a resulting change in the frequency of the machine that can be determined with high accuracy by studying the Schottky power spectrum of the beam. The amount of electromagnetic interaction is proportional to that of the strong proton-proton scattering, whose measurement was the goal of the experiment.

Detailed analysis has identified several contributions to the overall systematic uncertainty of the pp elastic scattering data at the eight energies studied. No single contribution is dominant, which means that it would be hard to reduce the systematic error to much below the 2.5–3.5% total uncertainty. Any angular dependence in the total systematic uncertainty is smaller than the statistical errors.

The variation of the ANKE data over the ranges in angle and energy studied can be seen most clearly in the differential cross section with respect to the four-momentum transfer t and these results are shown in Fig. 1. Also shown are exponential fits to the measured data made on the basis of

$$\frac{d\sigma}{dt} = A \exp\left(-B|t| + C|t|^2\right), \qquad (1)$$

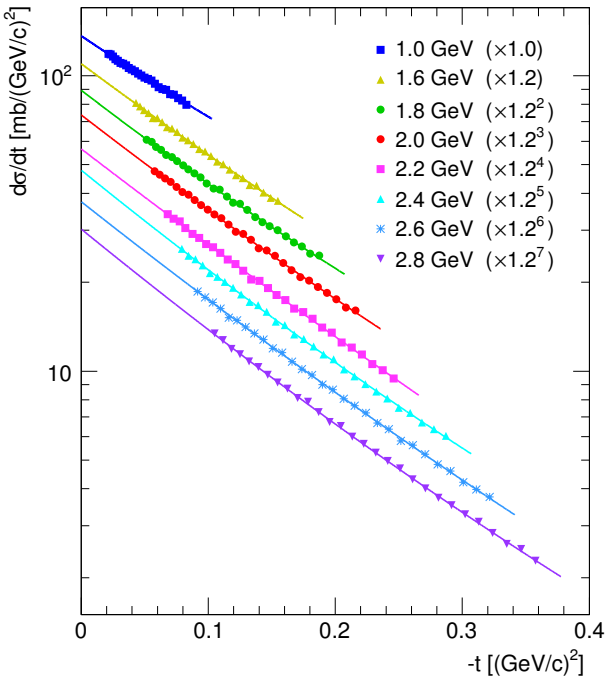

Fig. 1: Combined ANKE data set of differential cross sections with respect to the four-momentum transfer t compared to fits made on the basis of Eq. (1). Systematic errors are not shown and the statistical errors are smaller than the sizes of the symbols. The correct values are shown at 1.0 GeV but, for clarity of presentation, the other data are scaled down sequentially in energy by factors of 1.2. Thus the data have to be multiplied by the factors of 1.2^n given in the brackets in order to obtain the true results.

Table 1: Parameters of the fits of Eq. (1) to the differential cross sections measured in this experiment. In addition to the statistical errors shown, the second uncertainty in the value of A in the second column represents the combined systematic effects. The corrected values of the forward cross section, A(Corr.), were obtained using the SAID fit discussed in the text.

T_p GeV	A $\frac{\text{mb}}{(\text{GeV}/c)^2}$	B $(\text{GeV}/c)^{-2}$	C $(\text{GeV}/c)^{-4}$	A(Corr.) $\frac{\text{mb}}{(\text{GeV}/c)^2}$
1.0	$136.4 \pm 1.3 \pm 3.8$	6.7 ± 0.4	4.0 ± 3.8	136.7 ± 3.8
1.6	$131.7 \pm 1.9 \pm 4.5$	7.4 ± 0.3	2.7 ± 1.7	131.1 ± 4.5
1.8	$128.6 \pm 1.7 \pm 4.4$	7.6 ± 0.2	3.4 ± 1.0	127.6 ± 4.3
2.0	$127.3 \pm 1.7 \pm 4.5$	7.7 ± 0.2	2.5 ± 0.8	124.0 ± 4.3
2.2	$117.2 \pm 1.8 \pm 3.0$	7.6 ± 0.2	1.4 ± 0.7	113.1 ± 2.9
2.4	$119.2 \pm 1.8 \pm 3.7$	8.0 ± 0.2	2.7 ± 0.5	112.8 ± 3.5
2.6	$111.9 \pm 1.7 \pm 3.4$	7.8 ± 0.2	2.0 ± 0.4	108.8 ± 3.3
2.8	$108.5 \pm 1.8 \pm 2.8$	8.1 ± 0.2	2.4 ± 0.4	105.0 ± 2.7

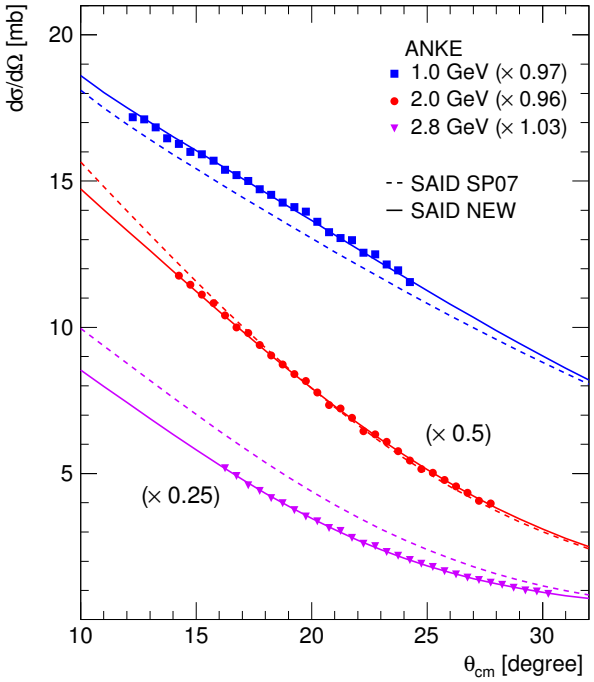

Fig. 2: Scaled ANKE proton-proton elastic differential cross sections at 1.0, 2.0, and 2.8 GeV, where the statistical errors are smaller than the sizes of the symbols. The results are compared to the SAID SP07 solution (dashed line) and a modified ("new") partial wave solution (solid line) where the ANKE data have been taken into account. For presentational reasons the 2.0 and 2.8 GeV data and curves have been reduced by factors of 0.5 and 0.25, respectively. The best agreement with the new partial wave data was achieved by scaling the ANKE data with factors 0.97, 0.96, and 1.03 at the three energies.

where the values of the resulting parameters are given in Table 1. The results clearly have an impact on the current partial wave solutions. This is demonstrated in Fig. 2, where the ANKE cross sections at 1.0, 2.0, and 2.8 GeV are compared to both the SAID SP07 solution and a modified one that takes the present data at all eight energies into account. Scaling factors in the partial wave analysis, consistent with the overall uncertainties have been included in the figure. It should be noted that the modified SAID solution does not weaken the description of the ANKE proton analysing powers.

The precise EDDA measurements were undertaken for c.m. angles of 35° and above whereas the ANKE data finish well below this and the gap looks even bigger in terms of the momentum-transfer variable t. Nevertheless, the modified SAID solution shown in Fig. 2 fits the ANKE 1.0 GeV cross section when reduced by 3%. This solution also describes the EDDA data at 1014.4 MeV.

In the forward direction the number of proton-proton elastic scattering amplitudes reduces from five to three and the imaginary parts of these amplitudes are de-

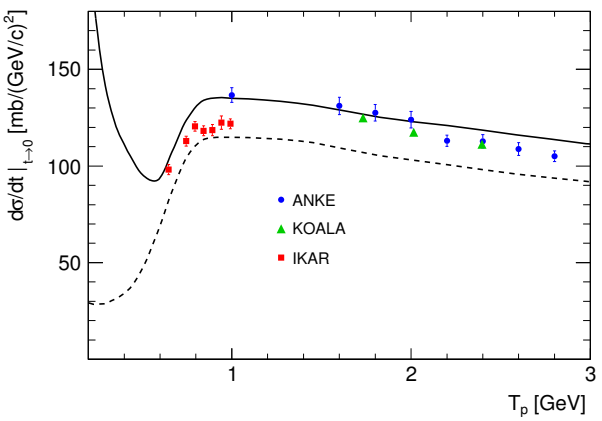

Fig. 3: The predictions of Grein and Kroll for the values of the forward pp elastic differential cross section A(GK) (solid line), the corresponding lower limit provided by the spin-independent optical theorem being indicated by the broken line. The extrapolated ANKE data, corresponding to the A(Corr.) parameter of Table 1, are shown with their quoted errors by the (blue) circles, whereas the (red) squares are the published IKAR values [Nucl. Phys. B **214** (1983) 1]. Also shown are three points obtained by the KOALA experiment and discussed elsewhere in this report. Although these results are still preliminary, the agreement with the ANKE values and the Grein and Kroll curves is very satisfactory.

termined completely by the spin-averaged and spin-dependent total cross sections with the help of the generalised optical theorem. The corresponding real parts have been estimated from forward dispersion relations, where these total cross sections provide the necessary input. All the terms contribute positively to the value of A and, using the optical theorem, the lower bound, $A \geq (\sigma_{\rm tot})^2/16\pi\hbar^2$, is obtained by taking the pp spin-averaged total cross section $\sigma_{\rm tot}$. This lower bound and the full Grein and Kroll estimates A(GK) [Nucl. Phys. A **377** (1982) 505] are both shown in Fig. 3 where, for consistency, the same values of $\sigma_{\rm tot}$ were used in the two calculations.

The agreement of the ANKE data with the theoretical curve in Fig. 3 is encouraging and would be even slightly better if the normalisation factors found in the fits to the cross sections in Fig. 2 were implemented.

The new ANKE data have a significant influence on a partial wave analysis of this reaction, as illustrated at three energies in Fig. 2. In the revised solution, the $^1S_0$ and $^1D_2$ waves in particular change at high energies and this will be made clearer in an update to the SAID SP07 solution. On a more practical level, the measurements will also be a valuable tool in the normalisation of other experiments.

For further details see Phys. Lett. B **755** (2016) p.92-96.

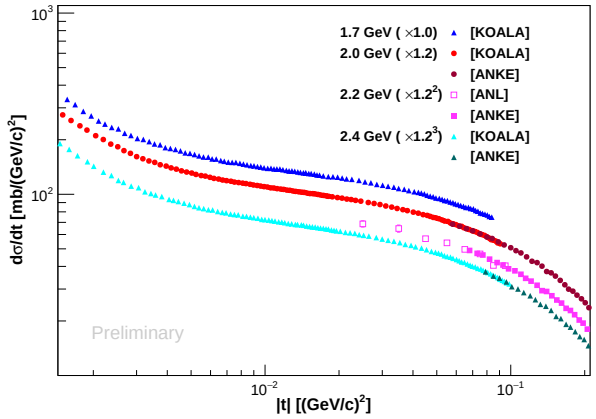

Fig. 4: The normalised KOALA differential cross section of proton-proton elastic scattering at different beam energies as a function of the squared 4-momentum transfer $|t|$. The errors are generally smaller than the size of the symbols. The correct values are shown at 1.7 GeV but the other data should be multiplied by the factor shown in the appropriate bracket.

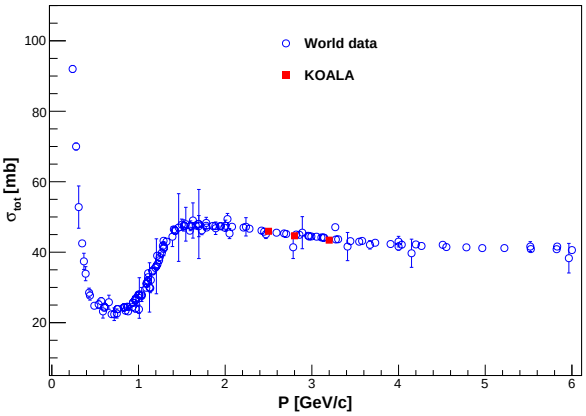

Fig. 5: The total cross section of proton-proton interactions determined through the optical theorem at three beam momenta. The KOALA data, plotted as red solid squares, show consistency with the global data set of proton-proton total cross sections measured in transmission experiments.

1.2 The differential cross section of *pp*-elastic scattering in the CNI region

The precise measurement of proton-proton elastic scattering in the Coulomb-Nuclear-Interference (CNI) region provides, not only the data needed as an input to a phase-shift analysis, but also the possibility to determine the total cross section of proton-proton interactions through the optical theorem. The KOALA experiment has been proposed to measure the differential cross section of antiproton-proton elastic scattering over a large range of the squared 4-momentum transfer t at HESR, including the CNI region. The idea is to measure the scattered beam particles at forward angles by tracking detectors and the recoil target protons near 90° by energy detectors. The recoil detector will measure both the kinetic energy and the polar angle of the recoil protons, noting that t is directly proportional to the proton's kinetic energy T_{p}, i.e., $|t| = 2m_{\mathrm{p}}T_{\mathrm{p}}$. The recoil detector will measure the energy of the recoil protons within an angular range (recoil angle defined as $\alpha \equiv 90^\circ - \theta_{\mathrm{lab}}$) $0^\circ < \alpha < 19^\circ$.

The recoil detector was commissioned at COSY by measuring proton-proton elastic scattering since the recoil particles are exactly the same for both antiproton-proton elastic scattering at HESR and proton-proton elastic scattering at COSY. The commissioning experiment with one recoil detector was performed at the ANKE hydrogen cluster target station at COSY.
Data of proton-proton elastic scattering at the beam energies of 1.7, 2.0, and 2.4 GeV were taken in the commissioning beam time. After energy calibration, acceptance correction and background subtraction the t-distribution has been reconstructed from the measured energy of the recoil protons. The distributions have been fitted with the standard (spin-independent) parameterisation in which the differential cross sections of the Coulomb scattering, the nuclear scattering, and their interference are involved. Since the measured t-distributions extend into the region where the Coulomb peak, with its easily calculable cross section, is dominant, the luminosity was determined from these distributions with the expected small uncertainty. In this way the normalised differential cross sections of proton-proton elastic scattering has been obtained at three beam energies and the results are shown in Fig. 50.

Several existing experimental data set of proton-proton elastic scattering measurements at 2.0, 2.2 and 2.4 GeV, which do not extend to such small values of $|t|$, have also been plotted [Phys. Lett. B (2016) 755: 92, Phys. Rev. D (1974) 9: 1179]. It shows consistency between the KOALA data and the existing results. The total cross sections of proton-proton interaction at the three beam energies have been derived through the optical theorem. As shown in Fig. 5, the values of the total cross sections determined with KOALA are in good accord with the global data set.

The agreement of the KOALA data with published data is encouraging and the differential cross sections should have a major impact on the proton-proton phase shift analysis. The precise data of the differential cross section at CNI region will also be a valuable tool in the luminosity normalisation of other experiments. With such promising precision data on proton-proton elastic scattering, one can also look forward to seeing excellent results for antiproton-proton elastic scattering.

For further details of the KOALA experiment and detectors, see Eur. Phys. J. A (2014) 50: 156.

1.3 Measurement of the spin correlation parameters in the $pd \to {}^3\mathrm{He} + \pi^0$ reaction

Two-body pion production in the interaction of protons with few-nucleon systems is of interest, both from the point of view of studying the reaction mechanism, and from that of determining the structure of light nuclei. The success of microscopic models with explicit Δ-excitation for two-nucleon systems suggests that these models should be tested in the three-nucleon case, where production of Δ is intimately linked to 3N forces. The phenomenological approach, using impulse approximation with $pp \to d\pi^+$ cross section, as input was successful near the reaction threshold but only partial progress has been achieved at higher energies [W.R. Falk *et al.*, Phys. Rev. C 50 (1994) 1574].

In general six invariant amplitudes are required to describe the $pd \to {}^3\mathrm{He} + \pi^0$ reaction and these amplitudes will be functions of the angle between the incident proton and outgoing pion in the c.m. frame. The number of independent functions reduce to two at threshold or in the forward/backward directions. These may be written as [J.-F. Germond and C. Wilkin, J. Phys. G 16 (1990) 381]

$$F(dp \to {}^3\mathrm{He}\pi^0) = \sqrt{\frac{1}{2}}\bar{u}_\tau \vec{p}\cdot(A\vec{\varepsilon} + iB\vec{\varepsilon}\times\vec{\sigma})u_p. \quad (2)$$

Here $\vec{\varepsilon}$ is the deuteron polarisation vector, $\vec{p}$ and $\vec{k}$ the proton and pion centre-of-mass momenta and u_p and u_τ the initial and final fermion spinors. The amplitude should be multiplied by a $\sqrt{2}$ factor if the $pd \to {}^3\mathrm{H} + \pi^+$ reaction is being considered.

If only the two amplitudes A and B are retained, the unpolarised c.m. differential cross section, deuteron tensor analysing power, and vector transverse spin correlation become

$$\frac{d\sigma}{d\Omega} = \frac{kp}{3}(|A|^2 + 2|B|^2), \quad (3)$$

$$T_{20} = \sqrt{2}\frac{|B|^2 - |A|^2}{|A|^2 + 2|B|^2}, \quad (4)$$

$$C_{y,y} = -\frac{2Re(A^*B)}{|A|^2 + 2|B|^2}, \quad (5)$$

whereas iT_{11} and T_{22} , as well as the proton analysing power A_y, must all vanish.

The $pd \to {}^3\mathrm{He} + \pi^0$ and $pd \to {}^3\mathrm{H} + \pi^+$ reactions have been studied experimentally over many decades and a wealth of data on the differential cross sections and analysing powers has been collected for these processes. However, the double polarisation observables have been explored far less and information on the spin correlations is still very scarce. The ANKE spectrometer equipped with an internal polarised target together with the polarised deuteron beam of COSY offer a unique opportunity to conduct measurements of the transverse spin correlation coefficients in these reactions.

Two double-polarisation experiments have been performed at ANKE with a polarised deuteron beam and a polarised hydrogen target, at the beam energies of 363 and 600 & 1115 MeV per nucleon (COSY proposals #172 and #205). The data at the two lower energies were analysed to obtain the spin correlations in the $pd \to {}^3\mathrm{He} + \pi^0$ reaction. These results can be used together with the existing data on the differential cross section and the tensor analysing power T_{20} [C. Kerboul *et al.*, Phys. Lett. B 181 (1986) 28] to extract information on the forward amplitudes A and B from eq. 3-5.

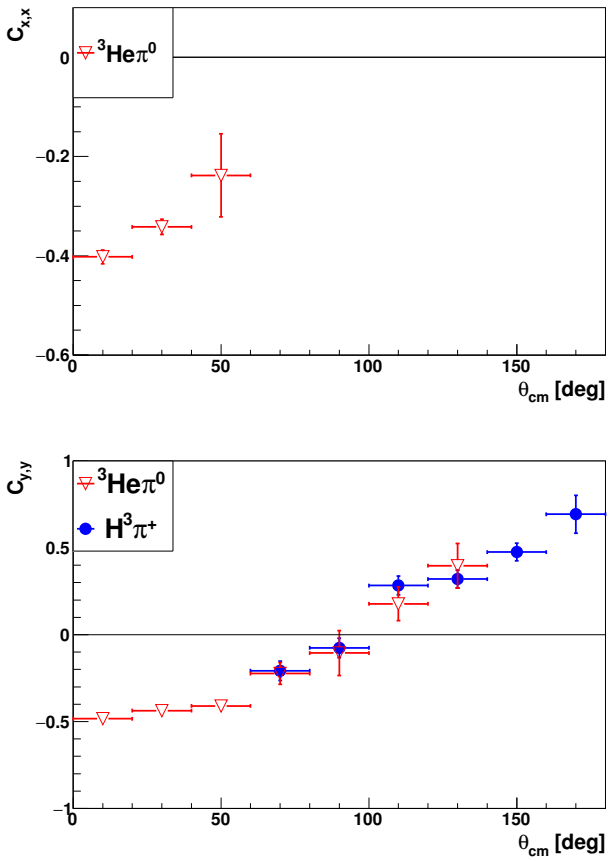

Fig. 6: Transverse spin correlation coefficients $C_{x,x}$ and $C_{y,y}$ in the $\vec{d}\vec{p} \to {}^3\mathrm{He} + \pi^0$ and $\vec{d}\vec{p} \to {}^3\mathrm{H} + \pi^+$ reactions at 363 MeV per nucleon.

Preliminary results at 363 MeV/n are presented in Fig. 6. Both ^{3}He and ^{3}H production processes could be investigated at this energy and the results in the angular range of $60-140^o$ covered by the both reactions are completely compatible. The ANKE detector acceptance is limited by the size of the gap in the analysing magnet D2 and is concentrated around $\phi = 0^\circ$ and 180° regions. This leads to a better definition of the $C_{y,y}$ coefficient as compared to $C_{x,x}$.

Since a clean selection of tritium by the energy loss in the scintillation hodoscope is no longer feasible at 600 MeV/n per nucleon, only data on the $pd \to {}^3\mathrm{He} + \pi^0$ reaction are shown at this higher energy. The $C_{x,x}$ and $C_{y,y}$ coefficients measured at small

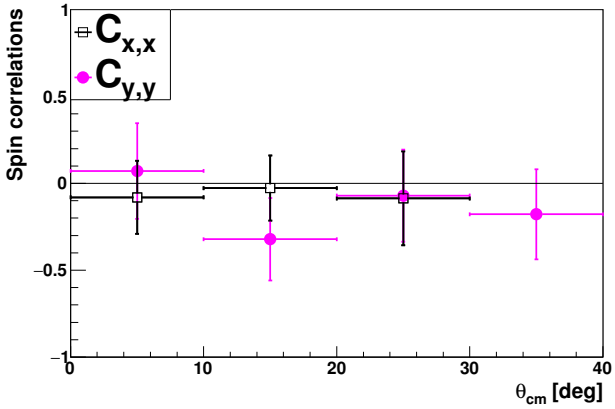

Fig. 7: Transverse spin correlation coefficients $C_{x,x}$ and $C_{y,y}$ in the $\vec{d}\vec{p} \to {}^3\mathrm{He} + \pi^0$ reaction at 600 MeV per nucleon.

angles are presented in Fig. 7. In addition to these spin correlation parameters, the proton and deuteron vector analysing powers can also be extracted from these data. At 363 MeV/n, A_y^p can be compared to the data of [J.M. Cameron *et al.*, Nucl. Phys. A 472 (1987) 718] and to the high statistics ANKE measurement with a polarised proton beam and a deuterium cluster-jet target [V. Shmakova *et al*, IKP Annual report 2010]. The new results from the double-polarisation experiment are completely compatible with the existing data.

1.4 Parametrization of the NΣ Cusp in the COSY-TOF pK$^+$Λ Data

In 2010 and 2012 $pp \to pK^+\Lambda$ data were measured with a beam momentum of 2.95 GeV/c. These data show in the pΛ invariant mass distribution a clear enhancement at the threshold of NΣ. In Fig. 8 (middle) the deviation of the measured invariant mass distribution from the phase space is plotted. The distribution is corrected for the detector acceptance and the reconstruction efficiency, which is given in the bottom figure.

The deviation from the phase space can be described by the final state interaction of the proton and Λ (in the lower part of the invariant mass), the NΣ cusp (around the threshold of 2.13 GeV/c^2), and reflection of nucleon resonances affecting the whole range of this invariant mass. The cusp is parameterized with the Flatté formalism [S. M. Flatte, Phys. Lett. B63(1976), 224]. In this paper Flatté described the ηπ (ππ) interaction at the two kaon threshold. He assumed that the $a_0(980)$ ($f_0(980)$) resonance changes its width due to the opening channel of KK, which induces a cusp structure. This formalism is adapted to the pKΛ channel by assuming a virtual bound state of pΛ, which decays into pΛ and NΣ. The cross section of the cusp is given by

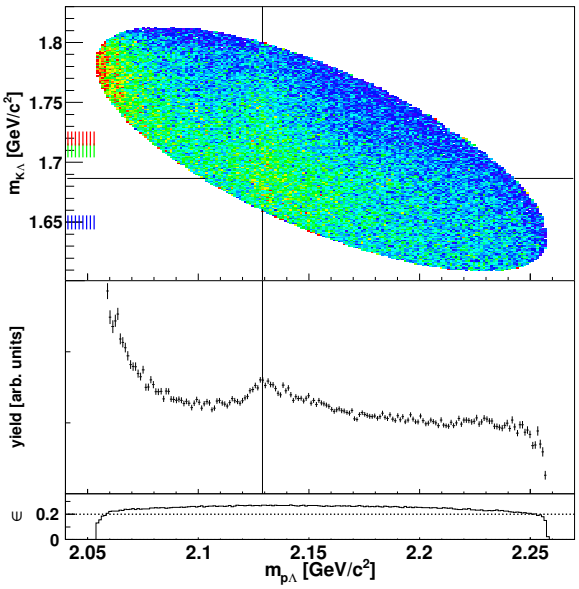

Fig. 8: Top: The linear Dalitz plot with acceptance and reconstruction efficiency corrections. In order to enhance the visibility of the structures the color code is truncated. The black lines indicate the KΣ and the NΣ threshold. The red area at the ordinate indicates the mass of the N*(1720) resonance, the green area indicates the N*(1710) resonance, and the blue area the N*(1650) resonance. Middle: The projection on the invariant mass pΛ shows the deviation from the phase space. It is corrected by the combined detector and reconstruction efficiency ε, which is shown in the bottom frame.

$$\frac{\mathrm{d}\sigma}{\mathrm{d}m_{\mathrm{p}\Lambda}} \equiv |A_{cusp}|^2 = \left| \frac{m_\mathrm{r}\sqrt{C\Gamma_0 \cdot \Gamma_{\Lambda\mathrm{p}}}}{m_\mathrm{r}^2 - m_{\Lambda\mathrm{p}}^2 - i m_\mathrm{r}(\Gamma_{\Lambda\mathrm{p}} + \Gamma_{\Sigma\mathrm{N}})} \right|^2 \quad (6)$$

m_r and Γ_0 are the mass and the total width of the virtual pΛ state. C is a normalization parameter. $\Gamma_{\Lambda\mathrm{p}}$ and $\Gamma_{\Sigma\mathrm{N}}$ are the partial decay widths of the virtual state, which are given by:

$$\Gamma_{\Lambda\mathrm{p}} = g_{\Lambda\mathrm{p}} \cdot q_{\Lambda\mathrm{p}} \quad \text{and} \quad \Gamma_{\Sigma\mathrm{N}} = g_{\Sigma\mathrm{N}} \cdot q_{\Sigma\mathrm{N}}$$

$g_{\Lambda\mathrm{p}}$ and $g_{\Sigma\mathrm{N}}$ are the coupling constants of the two decay channels to the virtual pΛ state and $q_{\Lambda\mathrm{p}}$ and $q_{\Sigma\mathrm{N}}$ are the cm momenta in the corresponding two-body subsystems. The characteristics of the Flatté formula is that the partial decay width $\Gamma_{\Sigma\mathrm{N}}$ is imaginary below the NΣ threshold and real above the threshold. At the threshold this width is zero. The coupling constants and the mass of the virtual state are determined by a fit procedure, which includes a parametrization of the final state interaction and

of the reflection due to the nucleon resonances. Possible interference terms between the cusp and these effects are neglected. As the coupling constants and the virtual resonance mass are correlated [V. Baru et al., Eur. Phys. J. A 23(2005)523], the fit results can only be interpreted to give the ratios of the virtual resonance parameters and its couplings to the decay channels. The normalization parameter C cannot be separated from the unknown total width Γ_0. Therefore, the product $C\cdot\Gamma_0$ is treated as one parameter. The fit result is shown in Fig. 9, which is a zoom of the middle of Fig. 8. The virtual resonance mass results to be 2.13 GeV/c^2 and the coupling to the NΣ channel is 1.25. The coupling to the pΛ channel is set to 1 as input for the fit. $C\Gamma_0$ is 0.311 . Details of the fit are given in the corresponding publication [S. Jowzaee et al., Eur. Phys. J. A. 52(2016) 7].

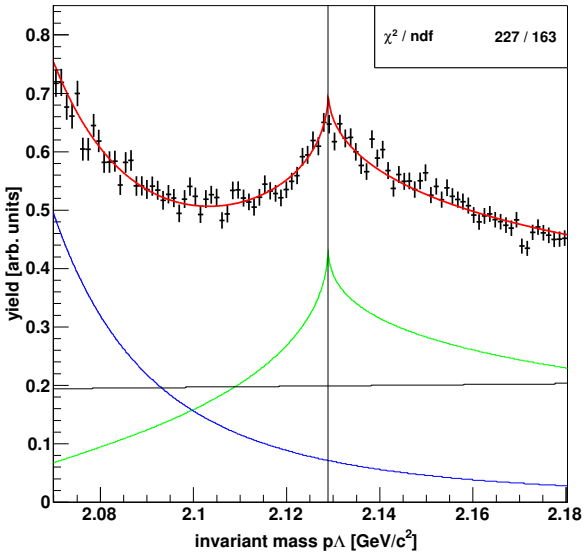

Fig. 9: Description of the NΣ Cusp region by the Flatté formalism. The fit result is given by the red line. It is composed of the FSI part (blue line), the part of the reflections (black line), and the Flatté-distribution (green line). The NΣ threshold is marked with the vertical black line.

The characteristic behavior of the Flatté-distribution at the threshold can be revealed by separating the real part and the imaginary part of the amplitude A_{cusp} as shown in Fig. 10 left part. The spike of the cusp arises from the real part of the amplitude. (If the mass of the virtual resonance is below the threshold, the imaginary part of the amplitude will have the spike form). By replacing in the nominator of the cusp amplitude formula the term $C\Gamma_0$ with $\Gamma_{p\Lambda}$ this formula describes below the $N\Sigma$ threshold the elastic channel of the virtual resonance m_r. In the Argand plot it can be seen, that the trajectory follows counter clock wise the unitary circle up to the threshold and due to the opening of the NΣ channel it turns to the

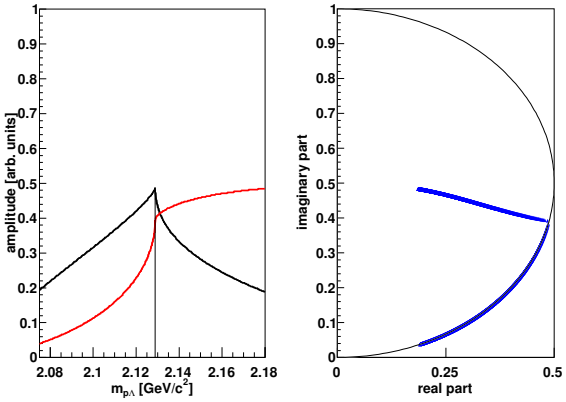

Fig. 10: Cusp amplitude and Argand plot. Left: The real part of the cusp amplitude is shown with the black line, the imaginary part with the red line. Right: The Argand plot is shown with the unitary circle (black) and the complex amplitude of the modified Flatté formula (blue line).

left by 90° (see Fig.10 right part).

1.5 The $d^*(2380)$ dibaryon resonance – status and perspectives

In one of the first measurements conducted with the hermetic WASA detector at COSY a narrow resonance-like structure was observed in the $np \to d\pi^0\pi^0$ reaction, which displayed a near to perfect Lorentzian structure sitting upon only little background in the energy dependence of the total cross section.
Fitted with a Breit-Wigner resonance ansatz this structure corresponds to a mass of 2.37 GeV and a decay width of only 70 MeV. The analysis of the angular distributions yields an angular momentum of three, so that in total the quantum numbers associated with this structure are $I(J^P) = 0(3^+)$. From the Dalitz plot we infer that this structure is associated with a deeply bound ΔΔ system, *i.e.* a system bound by about 90 MeV relative to the nominal ΔΔ threshold.
In subsequent experiments this resonance structure was traced in all two-pion production channels, which were at least partially of isoscalar character. Besides the purely isoscalar channel $d\pi^0\pi^0$ these are the channels $d\pi^+\pi^-$, $pn\pi^+\pi^-$, $pn\pi^0\pi^0$ and $pp\pi^0\pi^-$, which have both isoscalar and isovector components. In all cases the resonance structure has been observed. The $pn\pi^+\pi^-$ reaction has been investigated by HADES at GSI.
From the strength of the observed resonance effects in the various channels we may extract the branching of the anticipated resonance into these channels. We find that the branching into the various $NN\pi\pi$ channels is in full agreement with the isospin rules for a decay of an isoscalar ΔΔ system into the $NN\pi\pi$ channels.
In order to prove that the observed structure corresponds

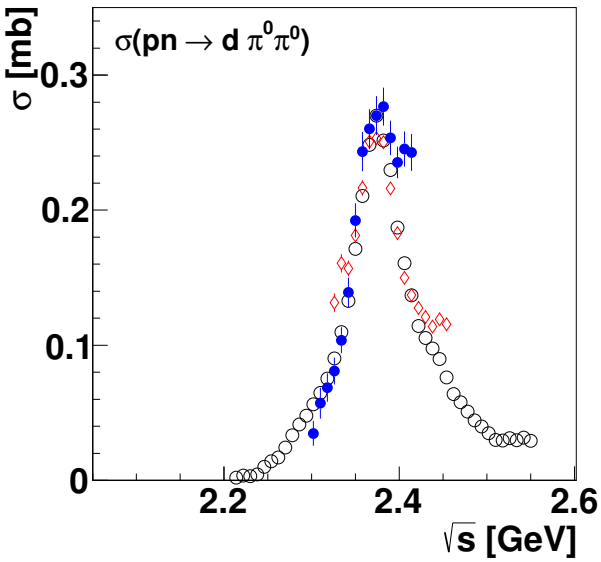

Fig. 11: $d^*(2380)$ in the "golden" reaction channel $np \to d\pi^0\pi^0$. The symbols representing the data refer to three independent measurements under different kinematic and experimental conditions.

to a genuine resonance, *i.e.* is a *s*-channel phenomenon and not just made by *t*-channel meson exchange in the course of the nucleon-nucleon collision, a corresponding resonance pole has to be found in the ${}^3D_3 - {}^3G_3$ coupled partial waves of *np* scattering. From the measured decay branchings into the various two-pion channels we can estimate the resonance contribution in the *np* channel to be in the order of 0.17 mb, which is tiny compared to the total *np* cross section of nearly 40 mb. Hence the only observable, which could possibly sense such a tiny contribution, is the analyzing power, since it is composed of only interference terms in the partial waves.

Therefore, in a final experiment on this issue, polarized *np* scattering was measured at WASA in inverse kinematics by having a polarized deuteron beam hitting the hydrogen pellet target. By detecting the fast spectator proton in the forward detector and the scattered proton and neutron in forward as well as central detectors of WASA we achieved again kinematically complete measurements covering practically the full angular range over the energy region of interest. The analyzing power data exhibit again the resonance structure as expected from the resonance hypothesis. With the new data implemented into the SAID data base the partial-wave analysis, indeed, produces a pole in the ${}^3D_3 - {}^3G_3$ coupled partial wave at $(2380 \pm 10) - i(40 \pm 5)$ MeV – in perfect agreement with the resonance hypothesis results from two-pion production. Following the nomenclature used for hadron excitations the notation $d^*(2380)$ has been adopted by now for this dibaryon resonance.

Parallel to polarized *np* scattering also the analyzing power of the $np \to d\pi^0\pi^0$ reaction could be measured in the energy region of $d^*(2380)$.

The WASA measurements of the double-pionic fusion to ^{3}He and ^{4}He reveal that $d^*(2380)$ is also produced in these reactions. Though the resonance appears there strongly broadened by Fermi motion and collision damping, it is obviously strong enough to survive even in nuclear surroundings.

In retrospect COSY with its high-resolution beam of protons and deuterons was ideally suited for the search of narrow resonances in the nucleon-nucleon collision process. Hence it is of no surprise that the first, non-trivial dibaryon resonance was established at this machine by combining it with the WASA detector, which was able to measure the four-momenta of both neutral and charged ejectiles in hitherto unprecedented quality.

From the experimental point of view the only remaining decay channels to be still measured are $d^* \to NN\pi$ and $d^* \to d\gamma$. An analysis of suited WASA data on the isoscalar single-pion production in the d^* energy region is in progress. The electromagnetic excitation of the deuteron to the d^* resonance by real or virtual photons is being investigated at MAMI and JLAB. Evidence for dilepton production via $d^*(2380)$ has been found in *pn* collision experiments from DLS and HADES.

Meanwhile a number of theoretical calculations based on QCD or hadronic interaction find this dibaryon state at the proper mass. However, so far only a single one can accommodate the measured narrow width by relating it to the hidden color aspect. According to this particular calculation $d^*(2380)$ is a compact hexaquark system with a radius of only 0.8 fm.

Having found now one genuine dibaryon state the question immediately arises, are there possibly more? To this end the existing WASA data base on two- and four-pion production is being searched for other dibaryon resonances – predicted now by those model calculations, which were successful in properly describing $d^*(2380)$.

1.6 The η-mesic helium - status and perspectives

A *mesic nucleus* is one of the theoretically predicted and still not experimentally confirmed exotic objects. In contrast to the already discovered mesonic atom, where a negatively charged pion is trapped in the Coulomb potential of the atomic nucleus, this kind of mesonic matter consists of a nucleus bound exclusively via strong interaction with a neutral meson such as η, η', K, or ω. One of the most promising candidates is the η-mesic nucleus, postulated by Haider and Liu over thirty years ago. The coupled-channel studies of the $\pi N \to \pi N$, $\pi N \to \pi\pi N$ and $\pi N \to \eta N$ reactions indicated that in the close-to-threshold region the η-nucleon interaction is attractive and strong enough to form an η-nucleus bound system.

Initially, it was indicated that due to a relatively small value of the ηN scattering length, η-mesic nuclei could only be formed with nuclei having masses greater than 12. However, current research shows that the η-nucleon

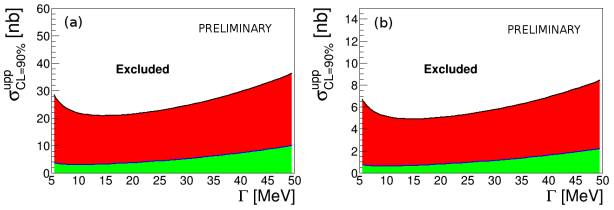

Fig. 12: Preliminary upper limit of the total cross-sections for (a) $dd \to ({}^4\mathrm{He}-\eta)_{\mathrm{bound}} \to {}^3\mathrm{He}n\pi^0$ and (b) $dd \to ({}^4\mathrm{He}-\eta)_{\mathrm{bound}} \to {}^3\mathrm{He}p\pi^-$ as a function of the width of the bound state. The binding energy was fixed to 30 MeV. The green areas denote the systematic uncertainties.

interaction is considerably stronger than it was expected earlier. A wide range of possible values of the ηN scattering length $a_{\eta N}$ allows the creation of η-nucleus bound states for a light nuclei such as ^{4}He, ^{3}He, T or even for a deuteron.

In 2008 and 2010 the WASA-at-COSY collaboration performed first dedicated measurements to search for ^{4}He-η bound states in the deuteron-deuteron fusion reaction. The η-mesic nuclei were searched via studying the excitation functions for $dd \to {}^3\mathrm{He}p\pi^-$ (2008 and 2010) and $dd \to {}^3\mathrm{He}n\pi^0$ (2010) in the vicinity of the ^{4}Heη threshold. A maximum below the threshold would indicate the production of a $^4\mathrm{He}-\eta$ bound state produced via the reaction $dd \to ({}^4\mathrm{He}\text{-}\eta)_{\mathrm{bound}} \to {}^3\mathrm{He}N\pi$. During the experiment in each acceleration cycle the beam momentum was increasing slowly and continuously crossing the threshold for the $dd \to {}^4\mathrm{He}\eta$ reaction. In the first experiment, the beam momentum was changed in an interval corresponding to a range in excess energy Q from about -51 MeV to 22 MeV, while in the second one the excess energy range $Q \in$(-70,30) MeV was used.

Although already the first results were by almost two orders of magnitude more sensitive with compared to previous measurements, they did not reveal any statistically significant signal for an η-mesic ^{4}He nucleus. The upper limit for the cross-section for the bound state formation and decay via $dd \to ({}^4\mathrm{He}\text{-}\eta)_{\mathrm{bound}} \to {}^3\mathrm{He}p\pi^-$ process was determined at a 90% confidence level. This upper limit depends mainly on the width of the bound state, but only weakly on the binding energy. It varies from 20 nb to 27 nb as the width of the bound state varies from 5 MeV to 35 MeV.

In 2015 the analysis of the 2010 data — with 20 times larger statistics compared to the 2008 data — has been completed. Excitation functions have been determined for the $dd \to {}^3\mathrm{He}p\pi^-$ and $dd \to {}^3\mathrm{He}n\pi^0$ processes, which — still — do not show any narrow structure that could be interpreted as a signature of a bound state with a width less than 50 MeV. The improved upper limits for the formation and decay of a η-mesic ^{4}He nucleus are presented in Fig. 12. We achieved a sensitivity of the cross-section of the order of a few nb for $dd \to ({}^4\mathrm{He}-\eta)_{\mathrm{bound}} \to {}^3\mathrm{He}p\pi^-$, which is about four times better in comparison with those obtained from the 2008 data. In addition, the excitation function for $dd \to ({}^4\mathrm{He}-\eta)_{\mathrm{bound}} \to {}^3\mathrm{He}n\pi^0$ was investigated for the first time.

In order to conclude the experiments on η-mesic helium with WASA-at-COSY, in May 2014 a final measurement on η-mesic ^{3}He has been performed. The data are currently being analysed.

1.7 Branching ratios for η decays into charged particles

During previous years the WASA-at-COSY collaboration has collected in total $3 \cdot 10^7$ events with η-mesons produced in the reaction $pd \to {}^3\mathrm{He}\eta$ at a beam energy of T = 1.0 GeV. Using a minimum bias data sample of η mesons (tagged by a missing mass analysis based on the reconstructed ^{3}He in the WASA Forward Detector) and the reconstruction capabilities of the WASA Central Detector (most notably the charged particle tracking and particle identification) pure samples of several decay modes have been isolated. While the cross section of the $pd \to {}^3\mathrm{He}\eta$ reaction is too small to collect statistics for rare and very rare decays, these samples are used to benchmark the detector performance and the analysis algorithms for the high statistics data sets taken for $pp \to pp\eta$ aiming at very rare decay modes. It is also important to note that these are the only current results on η decays where the η-mesons are produced in hadronic interactions, therefore they feature complementary experimental conditions compared to the results of other experiments which use photoproduction or e^+e^- collisions for meson production.

The analysis on the whole data set has been finalized in 2015 and branching ratios of the decays $\eta \to \pi^+\pi^-\gamma$, $\eta \to e^+e^-\gamma$, $\eta \to \pi^+\pi^-e^+e^-$ and $\eta \to e^+e^-e^+e^-$ have been extracted. All branching ratios are normalized to the $\eta \to \pi^+\pi^-\pi^0$ decay. Table 2 shows a summary of the results for the relative and absolute branching ratios together with the most recent values from PDG. For the higher abundant η-decays the systematic uncertainty of the result dominates the statistical one. It is smaller for the relative branching ratios as the systematic uncertainty of the normalization channel $\eta \to \pi^+\pi^-\pi^0$ does not contribute. The main sources for the systematic uncertainties are rate effects, luminosity determination and detector calibration.

The deduced value for $\Gamma(\eta \to \pi^+\pi^-\gamma)/\Gamma(\eta \to \pi^+\pi^-\pi^0)$ is $0.206 \pm 0.003_{stat/fit} \pm 0.008_{sys}$. It is in good agreement with the older experiments, but is 2.6 and 2.5 standard deviations above the recent values from CLEO and KLOE, respectively. The branching ratio for $\eta \to e^+e^-\gamma$ is consistent with the most recent Particle Data Group fit $(6.9 \pm 0.4) \cdot 10^{-3}$ but it is more precise by 20% (using a combined statistical and systematic error). The absolute branching ratios for $\eta \to \pi^+\pi^-e^+e^-$ and $\eta \to e^+e^-e^+e^-$ decays are in good agreement with the values reported by KLOE. The measured CP-violating, dihedral angle asym-

$\Gamma(\eta \to X)/\Gamma(\eta \to \pi^+\pi^-\pi^0)$	
WASA-at-COSY	PDG
$\eta \to \pi^+\pi^-\gamma$	
$0.206 \pm 0.003_{stat} \pm 0.008_{sys}$	0.1847 ± 0.0030
$\eta \to e^+e^-\gamma$	
$(2.97 \pm 0.03_{stat} \pm 0.13_{sys}) \cdot 10^{-2}$	$(3.00 \pm 0.19) \cdot 10^{-2}$
$\eta \to \pi^+\pi^-e^+e^-$	
$(1.2 \pm 0.1_{stat} \pm 0.1_{sys}) \cdot 10^{-3}$	-
$\eta \to e^+e^-e^+e^-$	
$(1.4 \pm 0.4_{stat} \pm 0.2_{sys}) \cdot 10^{-4}$	-

$\Gamma(\eta \to X)/\Gamma_{\text{tot}}$	
WASA-at-COSY	PDG
$\eta \to \pi^+\pi^-\gamma$	
$(4.67 \pm 0.07_{stat} \pm 0.19_{sys}) \cdot 10^{-2}$	$(4.22 \pm 0.08) \cdot 10^{-2}$
$\eta \to e^+e^-\gamma$	
$(6.72 \pm 0.07_{stat} \pm 0.31_{sys}) \cdot 10^{-3}$	$(6.9 \pm 0.4) \cdot 10^{-3}$
$\eta \to \pi^+\pi^-e^+e^-$	
$(2.7 \pm 0.2_{stat} \pm 0.2_{sys}) \cdot 10^{-4}$	$(2.68 \pm 0.11) \cdot 10^{-4}$
$\eta \to e^+e^-e^+e^-$	
$(3.2 \pm 0.9_{stat} \pm 0.5_{sys}) \cdot 10^{-5}$	$(2.40 \pm 0.22) \cdot 10^{-5}$

Table 2: Summary of the measured η-decays. Top: branching ratios relative to the decay $\eta \to \pi^+\pi^-\pi^0$). Bottom: absolute branching ratios. The numbers are compared to averaged world data sets by PDG.

metry, A_ϕ for $\eta \to \pi^+\pi^-e^+e^-$ has been determined to be consistent with zero: $A_\phi = (-1.1 \pm 6.6_{stat} \pm 0.2_{sys}) \cdot 10^{-2}$. A corresponding publication has been submitted.

2 COSY – accelerator developments

2.1 Introduction

To serve the needs of future users, COSY is in an upgrade and transformation process. Strongest motor for this transformation is the JEDI precursor experiment. This high precision experiment not only requires excellent understanding of and expertise in beam cooling methods, spin manipulation, and ion source design or operation but also e.g. a modern orbit control system and further enhancements. Systematic effects need to be controlled that otherwise could mask the data of interest during polarization measurements.

The investigated options for an orbit control upgrade cover the whole chain from sensor, to read-out electronics, and to the interface to the control system. Concerning the sensors, electrostatic beam position monitors (BPMs) in different geometries as well as Rogowski type position monitors which measure the magnetic field induced by the particle flux are studied as described below.

The implementation of an automated orbit response matrix measurement (ORM, see below) on one hand allows for a reliable and fast orbit correction and on the other hand will be used to calibrate and correct linear optics. For this purpose a LOCO (Linear Optics from Closed Orbit) algorithm based on the analysis of measured ORMs is under development with the aim to improve the current COSY model.

In addition to the COSY related activities the accelerator group is responsible for the High Energy Storage Ring HESR at FAIR in Darmstadt (from design to commissioning). This activity is described in the chapter "Progress of the HESR".

Further effort goes into the collaboration with CERN for an ion source for the ELENA ring [https://espace.cern.ch/elena-project/SitePages/Home.aspx]. It decelerates antiprotons from 5.3 MeV to 100 keV. The preparation of the ring for users can be optimized with an ion source that is available independently from the antiproton beam. IKP developed a complete module adapted to the specific needs as e.g. very small phase space acceptance and severe restrictions on space. Jülich developed the turn key system for commissioning, delivered it in time to CERN and set it up in the destination area. Scope of the work covers the compact source, the vacuum system, controls including graphical user interface, safety system, short beam line and diagnostic devices for verification of beam properties. Presently, the source is being integrated into the ELENA facility. IKP staff will support the CERN colleagues during ELENA commissioning in 2016 and 2017.

2.2 Orbit measurement upgrade

By new requirements of the experiments performed at COSY, especially the JEDI precursor experiment, the necessity of more precise beam position measurements are seen. In order to achieve this goal several upgrade scenarios have been developed. The system still in operation at COSY is based on an analog processing of the beam position with a later digitization with 8 bit ADCs. Although the analog processing was state of the art at the time of construction and is still today a good solution, the drifts of the system would make a test signal calibration necessary, which is not found within the system today. This would include a complete exchange of the digital part, as the 30 year old system is not capable of handling a calibration procedure. But already now regular failures of the analog parts, with increasing problems of getting replacement parts, are making operation difficult. Therefore a complete upgrade of the read-out electronics was decided.

Several options were presented to a committee with experts from CERN, DESY and GSI in November 2015. The recommendation with respect to the read out electronics was to focus on a first test of the commercially available LIBERA system. This recommendation was a.o. based on the reason that the LIBERA system is the preferred system of the FAIR project, and in this way developments could be used commonly. A test system has been ordered and is expected to be delivered in early 2016.

2.3 Rogowski type beam position monitor

The primary concept composed of a torus wound with a wire to measure the current, is modified towards a device which measures the center of gravity of the current. The spatial sensitivity is reached by winding the torus in parts and measuring the induced voltages in these parts (see Fig. 13). One advantage of the new device is the length of 1 cm compared to the length of the existing BPMs of 13 cm. Due to that small dimension, the BPM can be installed at additional places in COSY.

The presented concept is based on the idea of determining

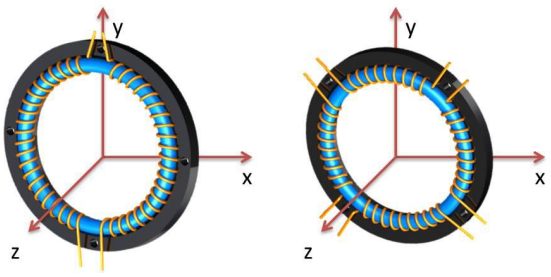

Fig. 13: Half and quarter wound Rogowski coils in the defined coordinate system. The shown configuration on the left enables a position measurement in x-direction. The configuration shown on the right corresponds to a measurement in both directions: x and y.

the position of the beam by measuring the magnetic field induced by the particle flux. The developed Rogowski coil BPM persists of a torus with the following geometric parameters: radius of the torus R = 50 mm; radius of the tube a = 5 mm. The tube of the torus is winded with one layer of copper wire. Dividing the wiring in four segments allows one to determine the beam position in both directions of the transverse plane.

To test the measurement principle in a real accelerator environment, a half wound Rogowski coil was installed at COSY. The measurements were performed with a bunched deuteron beam with a momentum of 970 MeV/c and a revolution frequency of 750 kHz. One series of measurements was dedicated to the response to a horizontal orbit shift of the beam at the position of the Rogowski coil BPM. This response was induced by applying a local orbit bump. The deflection of the bump was controlled by the change of two corrector magnets. A deuteron beam of about 10^9 particles was injected, accumulated and accelerated to its final momentum. Corrector magnets were powered to generate a horizontal local orbit bump at final momentum. The beam position was measured before and after the orbit bump. The pre-amplified signals of the Rogowski coils were fed into a two channel lock-in amplifier, the reference frequency being the beam revolution frequency as defined by the bunching cavity.

Since the existing BPM system at COSY does not provide a measurement of the beam position at the shown accuracy, a calibration against the existing system was not possible. An absolute calibration will be carried out with the new test system, described before. In addition to the precisely linear sensitivity of the BPM, its response to exciting a vertical orbit bump was studied. With a perfectly aligned BPM and no vertical-horizontal coupling, the measured displacement should be independent of the change of the beam position in y-direction. The result of the measurements is shown in Fig. 14. The horizontal sensitivity is $m = 0.5117(4) mm/\%$.

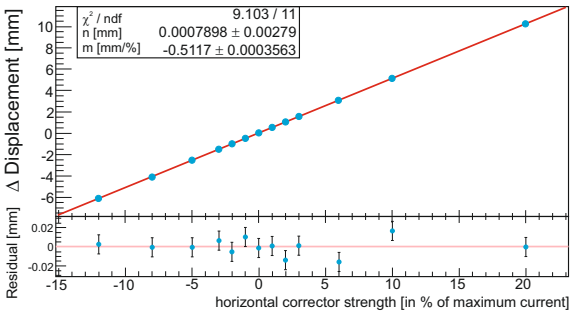

Fig. 14: Response of the Rogoswki coil BPM to horizontal orbit bumps. The fit quality ("Residual") is shown in the lower graph.

A similar measurement for vertical orbit bumps showed a slight linear dependece of $m = (1.3 \pm 0.4) \mu m/\%$ in the vertical response which may be due to tilts in the magnets or the BPM. In comparison to the horizontal case, the vertical sensitivity is about 400 times smaller.

To reduce the noise of the measured voltages and the resulting position uncertainty, the coils can be cooled. By changing the geometric form of the windings, the pick-ups may be used for measurements of higher moments of the beam distribution. To increase the sensitivity superconducting wires with a SQUID readout are considered as a next step in this development.

2.4 Automated orbit response matrix measurement

A model independent orbit correction is done by using an Orbit Response Matrix (ORM). Such an ORM is the response of the closed orbit at each Beam Position Monitor (BPM) to a change of each corrector magnet. A measurement of the ORM was done by manually changing a corrector magnet strength to three different magnetic fields values. For each of these fields the closed orbit was measured and saved to a data file. This procedure was repeated for all existing corrector magnets and the matrix was calculated. The complete measurement took roughly eight hours.

To have a faster and reliable method to measure the ORM an application was developed, which measures the ORM automatically. The application is connected via network to all BPMs, the timing system of COSY and all corrector magnets. In addition the application is connected to a database, where calibration factors for the corrector magnets are saved. Since the ORM is not a square matrix, the inversion is done by using the singular value decomposition algorithm. By choosing the number of used singular values, the correction strength and the resulting RMS value of the corrected orbit can be calculated. Fig. 15 depicts the calculated and measured RMS values in both planes depending on the number of used singular values. The comparison of the measurement with the theoretical prediction shows good agreement for low numbers of singular values. For higher number of singular values, which corresponds to higher correction strength, the measured value is higher than the calculated one. This effect is until now not understood and under investigation by using simulations. All in all the new developed tools, ORM measurement and orbit correction, work and improve the daily work at the accelerator.

2.5 High energy electron cooling

Dedicated beam studies were followed by HV conditioning procedures for the 2 MeV electron cooler up to 1.6 MV. Improved beam diagnostics and the recently commissioned correction schemes for the Larmor rotation of the electron beam allowed for electron current up to 1 A and faster electron cooling of the proton beam circulating

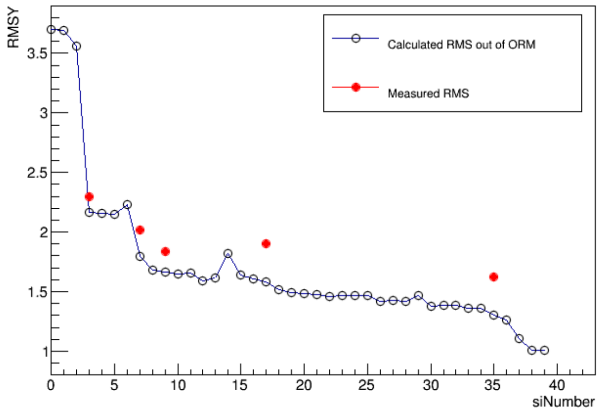

Fig. 15: Calculated (black) and measured (red) vertical RMS values for different numbers of singular values (black).

in the COSY ring. Longitudinal beam cooling resulting in a momentum spread of smaller than $5 \cdot 10^{-5}$ FWHM in less than 100 s was demonstrated for a DC proton beam at 1.66 GeV. Transverse cooling was significantly improved as well. A reduction of the horizontal beam emittance by one order of magnitude was achieved within 200 s (see Fig. 16). These experiments were performed with $3.6 \cdot 10^8$ protons circulating in the ring to make sure no collective effects are observed. The electron cooler performed well when used simultaneously with the stochastic cooling system. Cooling into a barrier bucket (Fig. 17) as well as cooling of bunched beams worked well.

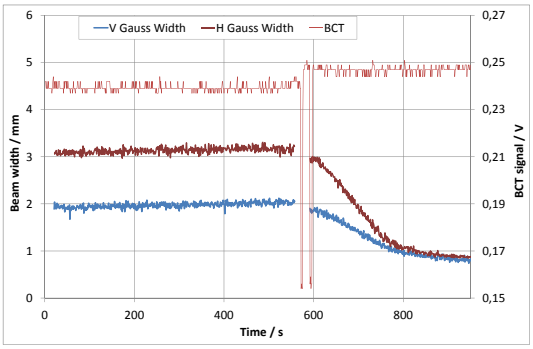

Fig. 16: Evolution of horizontal (black) and vertical (red) size of the beam core at 1.66 GeV during e-cooling with an electron current of 0.8 A.

The development of the physical model of the electron cooler and the automatic procedures for correction of so called larmor and galloping motion of the electron beam continues. The model based setup of the electron beam [A. Halama, IKP Annual Report 2015] is expected to be operational for the upcoming beam time in May-June 2016. This will allow for higher electron beam quality thus a better cooling performance. Furthermore, the time

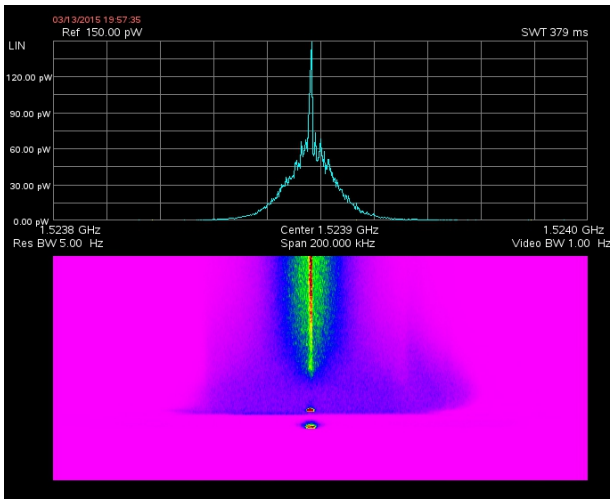

Fig. 17: Longitudinal electron cooling at 1.66 GeV with an electron current of 0.55 A with barrier bucket system on. The colored area shows the evolution over 550 seconds. Injection corresponds to the blue horizontal line.

for setting up the required cooler parameters can be shortened significantly.

3 Storage ring based EDM search – achievements and goals

3.1 Introduction

Electric dipole moments (EDM) are one of the keys to understand the origin of our Universe. Permanent EDMs of subatomic particles violate parity P and time reversal T symmetry. Assuming the CPT theorem, this leads to CP violation. The Standard Model predicts non-vanishing EDMs, their magnitudes, however, are expected to be unobservably small with current experimental techniques. The discovery of a non-zero EDM would be a signal for new physics and could explain the matter-antimatter asymmetry observed in our Universe.

The measurement of an EDM is based on the observation of a spin precession in the presence of a strong electric field. So far, only EDMs of electrically neutral systems have been examined except the EDM of the μ lepton. It has been proposed to perform charged-particle EDMs searches in storage rings [Phys. Rev. Lett. 93, 052001 (2004)], since the electric field is also the field that bends and closes the particle orbit. These experiments require a new class of high-precision storage ring built to provide improvements by orders of magnitude in the technology for polarized beam storage and measurement, as well as the knowledge of and control over the beam itself.

The COSY storage ring at the Forschungszentrum Jülich has proven to be an excellent platform for developing and demonstrating the necessary capabilities for a future dedicated EDM storage ring. That new storage ring to measure the EDM of deuterons must combine electric and magnetic bending fields chosen so that the polarization, placed initially parallel to the beam velocity, can remain for a time long enough to accumulate a measurable signal.

The JEDI Collaboration (Jülich Electric Dipole moments Investigations) has been formed to exploit and demonstrate the feasibility of such measurements and to perform the necessary R&D work towards the design of a dedicated EDM storage ring. As a first step R&D work at the Cooler Synchrotron COSY is pursued. Subsequently, an EDM measurement (precursor experiment) of deuterons will be performed at COSY with limited sensitivity within the present funding period. On a longer time scale, the design and construction of a dedicated EDM storage ring will be carried out.

3.2 Experimental achievements at COSY

For the measurements and the results discussed below a common experimental setup at the Cooler Synchrotron COSY has been used. A polarized deuteron beam with an intensity of approximately 10^9 particles was accumulated, accelerated to the final momentum of 970 MeV/c, and electron-cooled to reduce the equilibrium beam emittance. The beam polarization, perpendicular to the ring plane, was alternated from cycle to cycle using two vector-polarized states. An RF cavity was used to bunch the beam during the full cycle, while after the beam was prepared the electron cooler was turned off for the remaining measurement period. An RF solenoid induced spin resonance was employed to rotate the spin by 90° from the initially vertical direction into the horizontal plane. Subsequently, the beam was slowly extracted onto a carbon target using a white noise electric field applied to a stripline unit. Elastically scattered deuterons were detected in the scintillation detectors of the EDDA polarimeter consisting of rings and bars around the beam pipe and forming four quadrants up, down, right, and left. The corresponding rate asymmetries are used to analyze the polarization states of the beam throughout the cycle.

3.2.1 Record in-plane polarization lifetime

Since 2012, the new event time marking system has enabled COSY to measure the spin polarization of a deuteron beam as it precesses in the plane of the ring at about 120 kHz [Phys. Rev. STAB 17 (2014)]. This has made it possible to study the mechanisms that cause polarization loss and find ways to counteract them. The lifetime of this in-plane polarization may be lengthened by using a combination of beam bunching, electron cooling, sextupole field corrections, and beam currents not much larger then 10^9 deuterons/fill to stabilize the beam. The additional sextupole fields correct the path lengthening that occurs when particles in the beam undergo transverse oscillations. Studies were able to find the best balance of making these corrections in the horizontal plane by working at points with large beam sizes and other points with large momentum spreads simultaneously. One of the best values for an in-plane polarization lifetime at COSY is shown in Fig.18. In this case the beam was pre-cooled with electrons for 75 s. Then the polarization was sampled four times by bringing particles in the beam to a thick carbon target. Asymmetries in the scattered deuteron flux indicate the degree of polarization. The measurements have been normalized so that the initial polarization appears to be unity, which simplifies comparison with theories of the polarization decay. The curve shown in the figure agrees well with the data, as shown by the bottom panel containing the differences between the data and the curve. The calculated curve represents the polarization loss for Gaussian distributions of transverse particle oscillation amplitudes in both the vertical and horizontal directions. The curve then provides an estimate of the polarization lifetime. Using a Gaussian width definition, the lifetime is 782 ± 117 s. The exponential width is 2280 ± 336 s. This is a new record for in-plane polarization lifetime [submitted to Phys. Rev. Lett.], exceeding the Novosibirsk results for electrons by about three orders of magnitude. Such a lifetime is required if a storage ring experiment to search for an electric dipole moment on the deuteron is to be performed with a sensitivity near $10^{-29} e\cdot$cm, which is about three orders of magnitude above the current limits on the neutron. Searches with these sensitivities will either reveal a

dipole moment for the first time or put severe constraints on super-symmetry theories seeking to explain the excess of matter over anti-matter in the universe.

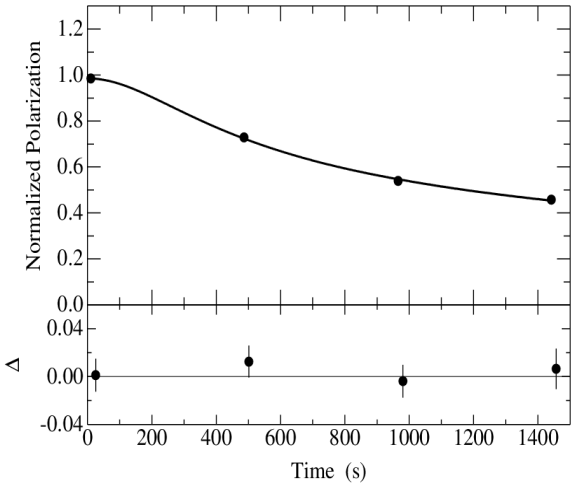

Fig. 18: Measurements of the normalized polarization. Least squares fits were made to the data acquired after rotation into the horizontal plane during four periods when the beam was extracted onto the polarimeter target. Data points taken with target extraction off are not shown. The residuals of the fit are given in the lower panel. The IPP lifetime is 782 ± 117 s.

3.2.2 Ultra-high precision spin tune measurement

When the deuteron spin polarization axis is placed in the plane of the COSY storage ring, the polarization rotates rapidly due to the action of the magnetic fields of the ring on the magnetic moment of the deuteron. That polarization may be observed as an up-down asymmetry in the scattering of deuterons from a carbon target placed in the ring, but only at those times when the polarization is pointing sideways, perpendicular to the direction of the beam. The scattering events associated with sideways polarization can be identified by measuring the clock time of the events from which one can calculate the number of times the deuterons have circled the ring since the experiment started. This leads directly to the amount by which the polarization has rotated. Keeping track of the polarization rotation rate allows all events in a chosen time interval to be combined to yield an accurate determination of the degree of polarization, the rate of rotation, and the direction, or phase, of the polarization when the time interval started. A sample of phase measurements made for every million turns around the ring, are shown in the top panel of Fig. 19. At the beginning, the statistical uncertainties in the phase are about 1% of a complete rotation. The rotation rate is usually given by a quantity known as the spin tune, which is the product of the anomalous part of the deuteron's magnetic moment times a relativistic correction factor, γ, which is close to unity. This precision in the rotation rate corresponds to an error bar of about 10^{-8} in the spin tune associated with each data point. The figure also shows that in COSY the phase varies smoothly with time as the measurement proceeds. By representing the change with a quadratic polynomial, information from the whole run may be combined to determine the polarization rotation rate at any point in the run. This is shown by the band around the spin tune seen in the lower panel of Fig. 19, which illustrates that the rotation rate varies linearly with time. When the time is about 38s, the highest precision of the spin tune determination (10^{-10}) is reached [Phys. Rev. Lett. 115 (2015,)094801]. This opens the possibility to use spin tune measurements to obtain unprecedented precision in the study of machine magnetic fields, closed-orbit corrections, and component stability. By introducing small field perturbations to represent hypothetical machine construction errors, the influence of these changes on the polarization history during an experiment may be observed. Such a level of precision exceeds what is needed in a feedback system (10^{-9}) in order to ensure that the signature of an electric dipole moment accumulates as it should during searches using storage rings operating at a sensitivity of $10^{-29} e\cdot$cm.

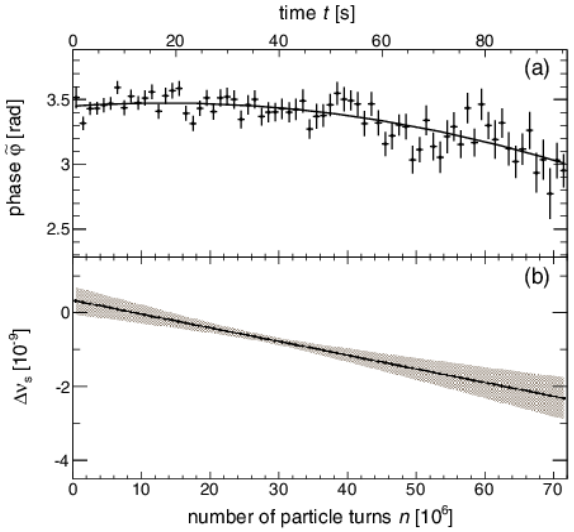

Fig. 19: (a) Polarization phase, or direction, in the plane of the ring as a function of time during an experiment along with a quadratic polynomial fit. (b) The deviation of the spin tune from a reference value of 0.160 975 407 along with an error band based on the statistical precision shown in the upper panel. At about 38 s, the most precise spin tune value is $(16097540628.3 \pm 9.7) \times 10^{-11}$.

3.2.3 Spin-tune based feedback system

For the precursor experiment, the build-up of the EDM induced vertical polarization strongly depends on the relative phase between the spin precession and RF Wien filter frequency. If one allows for a phase variation cor-

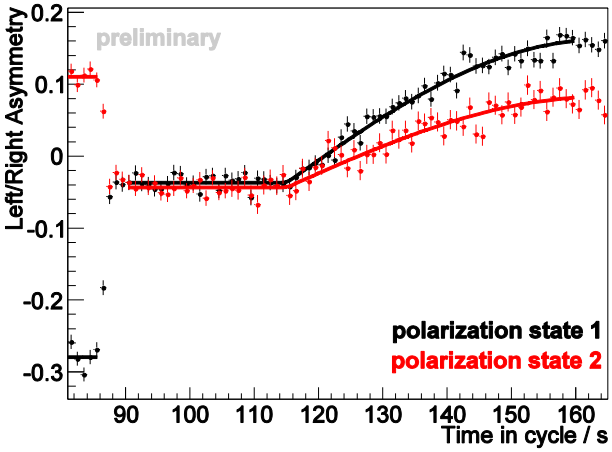

Fig. 20: Left/right asymmetry as a measure of the vertical polarization. At $t = 85\,\mathrm{s}$ the spins are rotated into the horizontal plane, at $t = 115\,\mathrm{s}$ the solenoid is turned back on. The absolute values for the build-up for the two states are different as the initial polarization differs.

responding to a reduction to 80% of the maximum signal the spin tune must not change by more than $\Delta\nu_s = 10^{-9}(10^{-10})$ during a 100 s (1000 s) cycle. In addition, also the cycle-by-cycle reproducibility has to be maintained at the same level. Recent measurements showed that this cannot be achieved without an active stabilization/feedback system based on the precise spin tune determination discussed in the previous section. A first prototype of such a feedback system aiming at the control of the spin direction by modifying the COSY RF has been developed and tested in 2015. In the absence of the actual RF Wien filter the RF solenoid has been used as reference and for phase-dependent spin manipulations. The experimental setup was similar as for the spin-tune and spin-coherence-time measurements discussed above. After the spin has been rotated into the horizontal plane (at $t = 85\,\mathrm{s}$), the COSY RF frequency is changed in steps of $\Delta f = 3.7\,\mathrm{mHz}$ — corresponding to the least significant bit of the frequency generator — such that the relative phase between the spin precession and the (external) solenoid RF is kept constant. This has been achieved by using a second, stand-alone data acquisition system providing a permanent data stream of the EDDA detector signals and the COSY RF and solenoid RF signals, and a dedicated spin-tune analysis passing the necessary frequency changes to the COSY RF generator. Then, at $t = 115\,\mathrm{s}$, the solenoid was switched on at a very low amplitude. The expectation is, that — independent from the original polarization state at injection — the spins will be slowly rotated back into the vertical direction and that the rotation speed has a sinusoidal dependence on the phase between spin and solenoid field: in case the field is at maximum when the spins point sideways the build-up should be largest, in case the spins are parallel the build-up should vanish. This measurement scheme has been repeated for different values of the relative phase. Figure 20 shows two example cycles for different initial polarization states and a (nominal[1]) relative phase of $\Delta\varphi = 3/5\pi$. Already in this plot one sees that the build-up is independent of the initial polarization and that the slope of the build-up is proportional to the initial degree of polarization. Figure 21 shows the initial slope of the build-up as function of the relative phase. The bin width corresponds roughly to the accuracy of the fixed relative phase provided by the feedback system. The statistical errors are in the order of the marker sizes, systematic uncertainties are not yet included. The plot confirms the expected sinusoidal dependence and shows that the spin direction at the solenoid is well under control. Besides the long spin coherence time this is another important milestone that has been achieved towards a first EDM measurement at COSY.

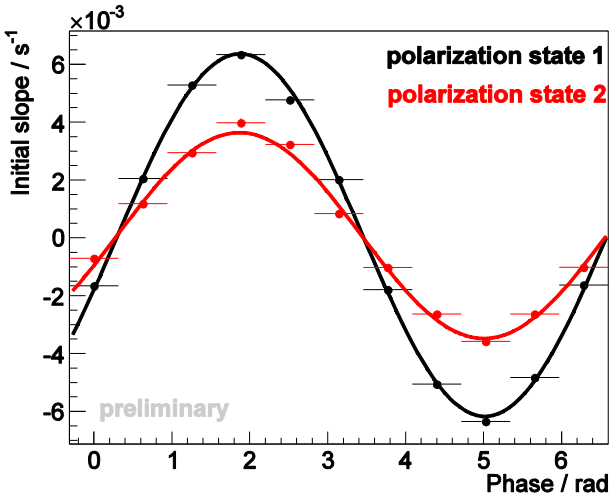

Fig. 21: Initial slope of the polarization build-up as function of the relative phase (online result). The difference in amplitude is due to the different degrees of polarization of the two initial states.

3.3 Technical developments

3.3.1 Design of a novel waveguide RF Wien filter

A prototype RF Wien filter, based on an already existing RF dipole with radial magnetic field, was recently developed and used at COSY-Jülich. The RF dipole was equipped with vertical electric field plates in order to provide an RF Wien filter configuration [S. Mey, Towards an RF Wien filter for EDM Experiments at COSY, Proceedings of the International Beam Instrumentation Conference, IBIC2015, Melbourne, Australia, 2015]. The RF electromagnetic field was generated using two coupled resonators; one that generates the electric field and an other one that generates the magnetic field. The approach of using separate systems to generate electric and magnetic fields, however, did not take into account the in-

[1] The actual phase at the solenoid differs from the set value due to cable and electronic delays.

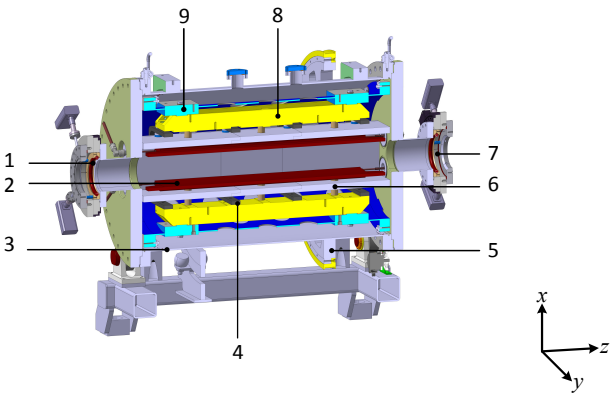

Fig. 22: Design model of the RF Wien filter showing the parallel-plates waveguide and the support structure. 1: BPM; 2: copper electrodes; 3: vacuum vessel; small angle rotor; 4: clamps to hold the ferrite cage; 5: belt drive for 90° rotation, with a precision of 0.01° (0.17 mrad); 6: ferrite cage; 7: CF100 feedthrough; 8: support structure of the electrodes; 9: inner support tube.

herent coupling between the electric and magnetic fields.

Therefore, the approach described here is based on a novel waveguide system, where by design the orthogonality between electric and magnetic fields is accomplished. The design calculations for the novel waveguide RF Wien filter were carried out using a full-wave simulation with CST Microwave Studio, and the electric and magnetic fields were modelled with an accuracy of 10^{-6}. The transverse electromagnetic (TEM) mode of a wave guide comes closest to the requirement of orthogonal electric and magnetic fields. For the use of the RF Wien filter at frequencies of about 100 kHz to 2 MHz, a parallel plate waveguide was chosen as the basic geometry (see Fig. 22). The axis of the waveguide points along the beam direction.

The aim was to create a structure that is strong enough to hold the electrodes and the ferrite blocks and has minimal effects on the field quality. The leakage of the electromagnetic field from the central section to the components of the support structure induced current that is time and space variation. Having the high values of the field homogeneity and low net Lorentz force computed with the electromagnetic simulator, the particle's simulation was a necessary step to evaluate the performance of the intended Wien filter based on realistic basis. The fields' maps were exported and the relativistic equation of motion has been solved.

In order to maintain an optimal Lorentz-force compensation, the beam width must be kept as small as possible so that the particles interact mainly with the central fields of the RF Wien filter, i.e., in the high-quality field region.

Within the COSY ring, the PAX low-β section provides the smallest beam size, therefore the RF Wien filter will be installed at this location. Using phase spaces of the particles at the section of the COSY ring over which the filter is expected to be installed as initial conditions, simulations with 5000 particles has been conducted. Two cases have been considered; small beam size with large angular dispersion (low-β section ON) and (relatively) large beam size with low angular dispersion (low-β section ON). The results show drift-like behavior (field-free) indication minimal influence of the RFWF on the particles. For each particle, the trajectory of a single pass is recorded and the full components of the corresponding field value $(E_x, E_y E_z, H_x, H_y, H_z)$ is registered.

3.3.2 Deflector development

For the final EDM ring, high-field electrostatic deflectors have to be developed. The highest electric field gradient of about 17 MV/m (foreseen for 30 m storage ring with electrostatic components only) was taken as reference value for building the prototype of the electrostatic deflector. Theoretically, a few meters long flat deflector, designed for several centimeters spacing between two capacitor plates, should not differ much from its small scaled version, made with the same accuracy and the electrode profile. Moreover, the minimization of the prototypes affects the following factors:

- the weight is not more a problem. A small-scaled deflector can be built from a bulk peace of material without special support,
- the laboratory-scale high voltage power supply is capable to produce the same field gradient at small distances between the electrodes,
- the safety restrictions for the laboratory room will be lower in case of smaller high voltage,
- cables, feedthroughs and flashover detection is much simpler.

Complementary requirements to perform these tests were ultra-high vacuum and the lack of dust inside the vacuum chamber. To achieve these conditions the test bench (shown in Fig. 23) for electrostatic deflector prototypes, built using UHV CF components, was assembled in ISO71 class clean room at RWTH Aachen University. The deflector prototypes (see Fig. 24) were made in two different sizes from stainless steel and aluminum. After machining they were mechanically polished. The small electrodes have ideal half-sphere shape with 10 mm radius. The large electrodes have additional flat region of 20 mm diameter (stainless steel) or 30 mm (aluminum) in the center with similar round edges. To increase the accuracy of measuring the distance between the deflectors, every new measurement procedure starts from positioning electrodes on top of each other; using a linear drive with precision of 0.01 mm.

First high voltage tests were made with the stainless steel half-sphere electrodes in the wide range of distances from 30 mm to 0.05 mm. Varying the spacing between them,

Fig. 23: The test bench for electrostatic deflectors at RWTH Aachen University.

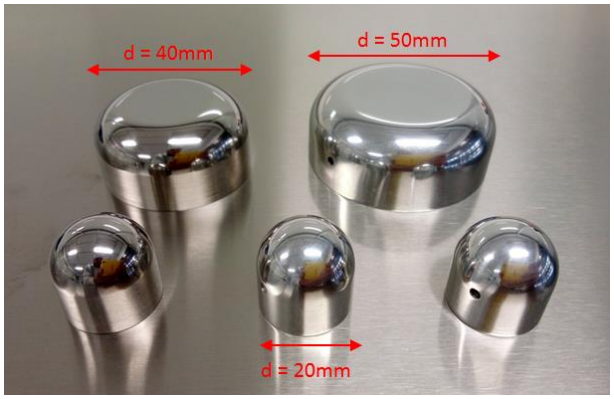

Fig. 24: Test electrodes made from the stainless steel (on the left) and from aluminum (on the right).

the discharge, if at all, happens in a smallest gap region, as it should be for the electrodes with spherical surface. The dark current at different distances between the electrodes behaved similarly (see Fig. 25) and, taking into account the field enhancement factor, could be scaled. This is another measure of the quality of surface polishing.

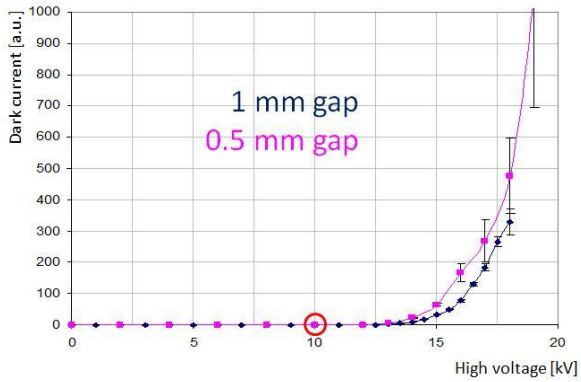

Fig. 25: Test electrodes made from the stainless steel (on the left) and from aluminum (on the right).

Similar tests were performed after exchange one of the electrodes to the largest stainless steel version. The measured field strength at 0.05 mm distance was about 200 MV/m which is the maximum possible in the vacuum. A second material for electrodes tests was aluminum. The polishing procedure was not very well established and the breakdown at smallest distances during measurements with two half-spheres happened not in the region of the minimum gap, but on the side. It could happen because of the strongest impact on field inhomogeneity at such short distances caused by the roughness of the surface.
The maximum field strength, achieved in that configuration, was about 30 MV/m. Measurements at the small distances showed a good agreement with theoretical predictions of the breakdown conditions and will require further tests with different materials. Special attention should be paid to the measurements at larger distances and higher voltages.

3.3.3 Status of polarimeter development

In the upcoming JEDI project the essential point would be to measure the tiny change of beam polarization over a long period. At present, the EDDA detector is being used to measure the beam polarizations of protons and deuterons circulating inside the storage ring COSY. For the future EDM experiments, based on the storage ring method, a dedicated high precision polarimeter is required. We have developed a concept based on the following principles: achieving the maximum identifaction efficiency for the elastic events of carbon target (polarimetry reaction), providing the dead-time less data taking, and avoiding strong magnetic and electric fields. The measurements will last over several years, so the long-term stability and strong radioactive hardness of the detector material is a crucial requirement as well.
The ongoing step of this development program is to study the choice for the detector material. The information collected after the first measurements in lab and then at COSY, will provide essential input for the development of the simulation code using the GEANT4 toolkit. In this version, the modular assembly with a standardized aluminum support structure is shown on Fig. 26. Such a construction allows us to build the polarimeter with an arbitrary number of crystals and with an optimal configuration.
At present, we already own five LYSO crystals needed to build four independent calorimeter modules, equipped with LYSO crystals from two different companies: Saint-Gobain (SG) and EPIC Crystals (EP). Among this crystals, two different module configuration can be assembled: three for low (large Θ angles) and one for high count rate (small Θ angles) use. The design of the LYSO modules is final (see Fig. 27). The prototype modules will be assembled and tested during the COSY test beamtime in March 2016. A new idea of target design is also under investigation, based on using small diamond pellets ($10 \div 100\ \mu m$) to sample the beam and provide a 2-dimensional polarization profile of the beam's cross section. Laboratory tests of the detector modules, the noise performance of the electronics, and the LED irradiation

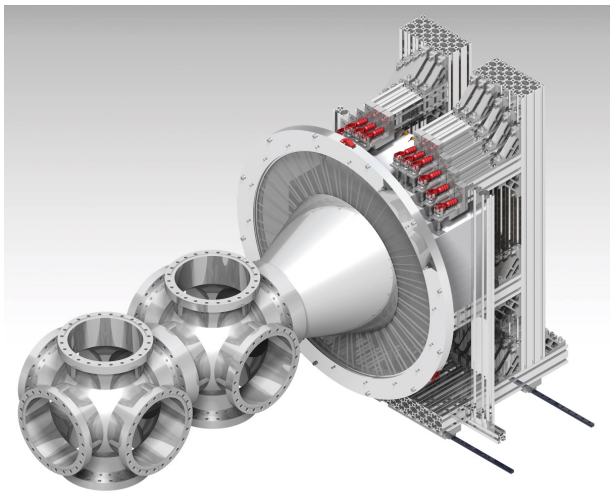

Fig. 26: The current engineering drawing (detector and the target chamber) together with the supporting system is shown. From left to right there are two cross type flanges, one for beam position monitors (BPM's) and the second one for the target. In the middle there is a vacuum chamber. Next, the two layer of ϕ-sensitive plastic scintillator and the LYSO HCAL are placed to absorb the total energy of the scattered particles.

of the different light sensors (like PMT's and SiPM's) are the ongoing activities.

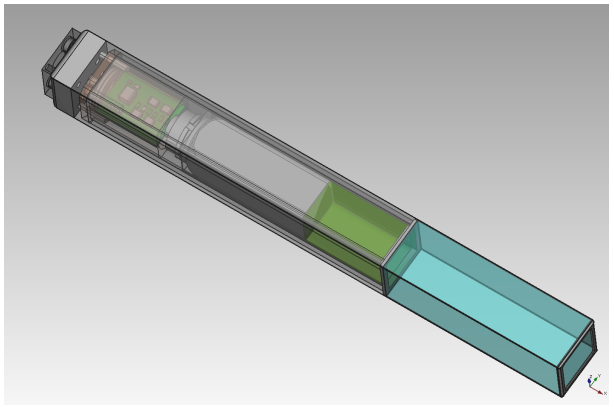

Fig. 27: The LYSO calorimeter module in the carbon fiber enclosure.

The read-out electronics of the Low Energy Polarimeter (LEP) was upgraded using a new system based on field-programmable gate arrays (FPGA). LEP is the polarimeter in the injection beam line of COSY. The polarizations measured there are used to monitor and calibrate the polarized particle source. The new read-out was tested successfully during the beam times in the summer and winter of 2015 and is now available for routine operation. In addition to the event selection by pulse height that was already possible using the old electronics, the new read-out system can also measure the time of flight for each particle (Fig. 28).
Other developments like beam position measurements,

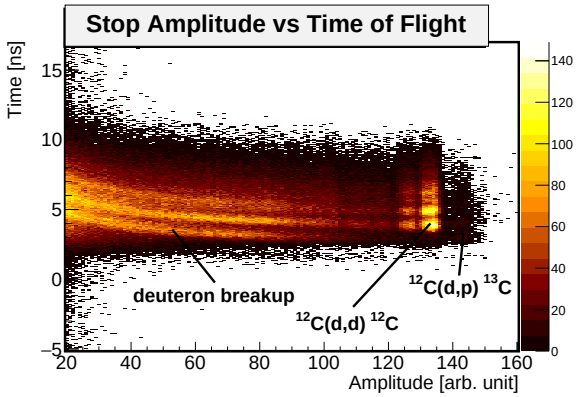

Fig. 28: Amplitude and time of flight of particles detected at a scattering angle of 40° using a carbon target at LEP.

and orbit response matrix measurements driven by the requirements of the EDM measurements are described in section 2.3.

3.4 Beam and spin dynamics

3.4.1 Systematic limitations for EDM measurements at COSY due to magnet misalignments

The proposed measurement method for Electric Dipole Moments at COSY makes use of a radiofrequency Wien filter. Initially, the particle spins are precessing perpendicular to the stable spin direction of the storage ring with is equal to the invariant axis of spin motion. To excite a spin resonance, the frequency of the radiofrequency fields is adjusted to this spin precession frequency. In an ideal storage ring, the corresponding resonance strength is directly proportional to the EDM magnitude, resulting in a slow oscillation of the vertical polarization component. To first order this oscillation is fully characterized by the slope of the vertical polarizion buildup. Additional electromagnetic fields introduced by magnet imperfections and misalignments bias the observed build-up. Those systematic contributions are investigated using a recently developed simulation framework. The functionality of this framework has been discussed in the IKP Annual Report (2014).
Different sets of randomly distributed vertical shifts of the quadrupole magnets are introduced and the impact on spin motion is studied. The RMS of the vertical orbit has been used as measure of the additional radial magnetic fields. The results are shown in Fig. 29. For small orbit deviations the vertical polarization buildup is clearly distinguishable for different EDM magnitudes, but towards larger orbit deviations the false signal contribution increases. According to the conducted study, the 90% upper confidence limit of the false signal at $\Delta y_{\mathrm{RMS}} \approx 1.6\,\mathrm{mm}$ is of equal magnitude as a pure EDM signal corresponding to $\eta_{\mathrm{EDM}} = 10^{-4}$. This value corresponds to an EDM magnitude of $d_d \approx 5 \cdot 10^{-19} e{\cdot}\mathrm{cm}$.

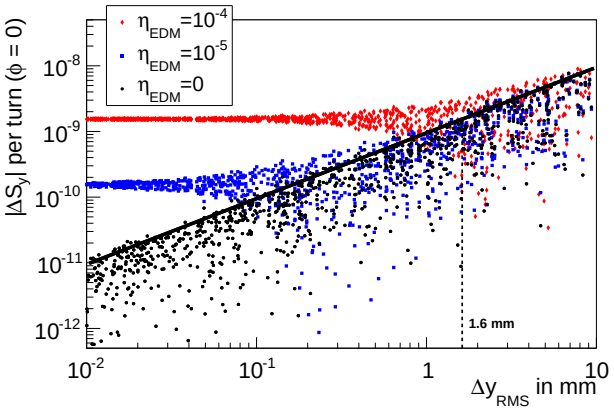

Fig. 29: Absolute average change of the vertical spin component $|\Delta S_y|$ per turn with respect to different Δy_{RMS} and an initial Wien filter phase $\phi = 0°$ in the simulation. A Wien filter magnetic field of 10^{-4} mT and corresponding electric field and its length of about 0.8 m are used. The different Δy_{RMS} have been generated by randomized vertical quadrupole shifts assuming Gaussian distributed misalignment errors. Furthermore different EDM magnitudes are considered. The solid line shows the 90% upper confidence limit for pure misalignments. The dashed line refers to the location for which the false signal by misalignments is equal to an EDM signal corresponding to $\eta_{\mathrm{EDM}} = 10^{-4}$.

3.4.2 Investigation of lattices for a deuteron EDM ring

The "frozen spin (FS)" and "quasi-frozen spin (QFS)" concept are investigated for a deuteron EDM storage ring [Yu. Senichev et al., Proceedings of IPAC 15, MOPWA044, p. 213]. In the FS concept the spins are always aligned to the momentum vector [Phys. Rev. Lett. 93, 052001 (2004)]. The QFS concept is based on the fact that the anomalous magnetic moment has a small negative value. Magnetic and electric fields can be spatial separated with magnetic arcs and either pour electric field or combined magnetic and electric field sections connecting the two arcs. The rotation of spin relative to the momentum in two parts of ring – the arc and the connecting sections – can compensate each other, leading a quasi-frozen spin rotation turn by turn.

Two possible options for a QFS lattice (Fig. 30) are considered and compare to a frozen spin lattice (see Fig. 31), where elements with combined electric and magnetic fields are used.

In the first QFS option completely separate electric and magnetic parts are used that form a structure. In the second option, we suggest using only two magnetic arcs with two straight sections having combined straight elements with magnetic and electric fields. The straight elements have a horizontal electric field of 120 kV/cm and a vertical magnetic field of 80 mT. They provide the compensation for the spin rotation in the arc and at the same time

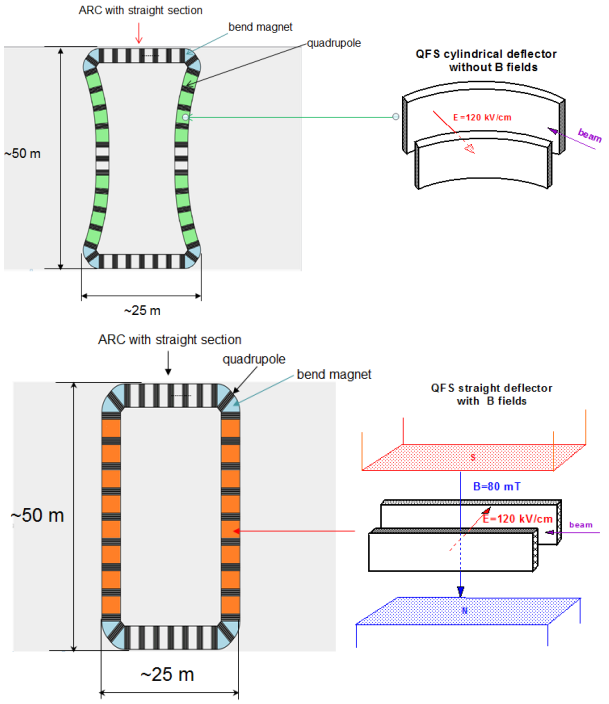

Fig. 30: Two options of QFS lattices with curved (left) and straight (right) electrostatic deflectors.

allow having straight electric plates without the higher orders field.

This scheme could be tested in the COSY ring at Forschungszentrum Jülich to prove the quasi-frozen spin concept. Obviously, this oscillation should lead to an EDM signal reduction. However, due to the small amplitudes oscillation the EDM signal is reduced by approximately a factor of 0.98 compared the FS case. In both options the free dispersion straight sections are placed between the magnetic arcs and are necessary to accommodate the polarimetry, the beam extraction and injection systems and RF cavity.

Also a FS lattice has been designed based on deflectors with incorporated E and B fields (see Fig. 31). Despite the difference in the concepts, the basic parameters, namely the size of the rings, the length of the straight sections, the number of focusing periods, and the number of deflecting and focusing elements and sextupoles all remain approximately the same.

A special role is given to sextupoles, all structures have at least six families of sextupoles for a flexible control of spin coherence time and chromaticity in all coordinates, and each family carries out its own functions. The proposed QFS method could simplify the lattice and would allow diagnosis of the presumably existing EDM signal, but it needs to be investigated in detail from the point of view of the systematic errors.

3.5 Summary and goals

For the feasibility of the precursor experiment at COSY and the design study of a dedicated EDM storage ring,

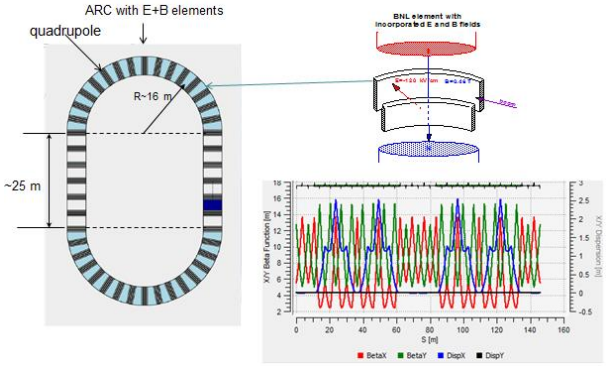

Fig. 31: QFS lattices with incorporated electrostatic and magnetic fields.

the JEDI collaboration is performing the necessary R&D work at COSY, prototyping critical hardware and performing dedicated beam and spin dynamics studies.
Record in-plane polarization lifetimes could be reached, ultra-high precision spin tune measurements are established and the feasibility of a spin-tune based feedback has been shown.
Prototyping of critical elements for accelerator and polarimeter has also successfully been carried out. Rogowski coil beam position monitor have been developed and successfully tested with COSY beam (see chapter 2.3), high-field electrostatic field tests have been performed and ultra-high field gradients could be reached, and a test setup has been equipped with LYSO crystals toward a dedicated JEDI polarimeter. In addition a Waveguide RF Wien filter has been developed for the precursor experiment.
In terms of beam- and spin dynamics studies an automatic orbit response matrix measurement has been established (see chapter 2.4), spin tracking simulations were performed to study the feasibility of a precursor experiment and different lattices for final deuteron EDM ring design are investigated utilizing the COSY Infinity [Nucl. Inst. and Meth. in Phys. Res. A 558 (2005)] and Mode [A. Ivanov et al., Proceedings of IPAC 14, MOPME011, p. 400] simulation programs.
In the upcoming year the R&D work has to continue to support the anticipated precursor experiment at COSY and to finalize the design of a dedicated Deuteron EDM storage ring.

4 COSY – operation statistics

4.1 Beam time at COSY

For 2015 in total 5544 hours of operation were scheduled.
2800 hours (32%) were scheduled for dedicated beam dynamic studies, equipment tests for HESR and FAIR related activities and 1960 hours (22%) for precursor experiments on EDM studies. 768 hours (9%) were used for COSY machine development and experimental set-up and 16 hours were devoted to students education (see Fig. 32). With a shutdown duration of 3216 hours (37%) the reliability of COSY amounts to more than 90%.
Within the FAIR related activities, 2 weeks of beam time were used in 2015 by the the external group CBM (Compressed Baryonic Matter) for detector-system tests and tests of FPGA-based read out boards. To this the radiation tolerance, i.e. single- and multiple-bit upset detection and correction methods were studied. The INT (Institut für nukleare Trendanalysen) of the Fraunhofer Institute Euskirchen spend one week of COSY beam time on the measurement of cross sections for single event effects on five different incident proton energies. The distribution of user weeks is listed in Table 3.

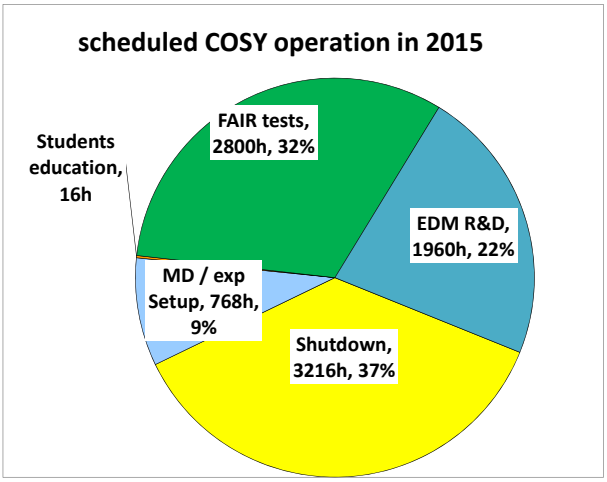

Fig. 32: COSY beam-time statistics in 2015.

Table 3: Overview COSY user beam time and EDM/FAIR weeks in 2015.

Date	Experiment	Duration	Reaction, experiment #
1.01.15.–08.02.15	Maintenance	6 week	shutdown of COSY
13.02.–22.02.	FAIR (CBM)	1 week	CBM measurements COSY Exp. D004
28.02.–15.03.	FAIR	2 weeks	FAIR electron cooling, Exp. A002
16.03.–22.03.	FAIR	1 week	FAIR stochastic cooling, Exp. A001
23.03.–26.04.	Maintenance	5 weeks	shutdown of COSY
01.05.–10.05.	FAIR (STT)	1 week	FAIR straw tube tracker, Exp. D002
11.05.–17.05.	FAIR (MVD)	1 week	FAIR micro Vertex detector, Exp. D001
22.05.–28.06.	EDM (JEDI)	5 week	EDM, COSY Exp. E001
07.08.–23.08.	FAIR	2 weeks	FAIR electron cooling, Exp. A002
24.08.–30.08.	FAIR	1 week	FAIR stochastic cooling, Exp. A001
31.08.–05.09.	MD	1 weeks	students training
06.09.–13.09.	FAIR (CBM)	1 week	CBM measurements COSY Exp. D004
18.09.–27.09.	INT	1 week	Irradiation measuerements (INT), D006
28.09.–18.10.	Maintenance	3 weeks	shutdown of COSY
23.10.–01.11.	FAIR/KOALA	1 week	KOALA COSY Exp. D005
06.11.–15.11.	COSY	1 week	beam optics studies, Exp. A005
16.11.–22.11.	COSY	1 week	beam instrumentation studies, A003
27.11.–20.12.	EDM (JEDI)	3 week	EDM, COSY Exp. E001
28.09.–18.10.	Maintenance	3 weeks	shutdown of COSY
user weeks 2015		23 weeks	
maintenance		17 weeks	
EDM		8 weeks	
FAIR		11 weeks	

5 Progress of the HESR at FAIR

5.1 Project status

IKP is leading the international consortium which is dedicated to build the HESR. It is strongly supported by colleagues from the Central Institutes for Engineering and Analytics (ZEA) of the Research Center Jülich. HESR component design and acquisition are on time and within budget. About 18 MEuro have been spent and about half of the project money is still available for contracting. Vacuum equipment is to be delivered just in time for installation once the HESR tunnel is ready for moving in. Thus the warranty for these components will still be valid for the commissioning and operation phase. The power converter for the dipole magnets will be ordered to arrive after all dipole magnets have been installed and connected.

Work in 2015 was dominated by delivery and acceptance tests of 16 dipole magnets (40 t each including girder) and 18 quadrupole magnets (6 t each). Upgrading storage capacity has also been a priority activity. Dipole preassembly is ongoing. The concept for ring assembly is constantly being optimized and adapted to new boundary conditions. Quadrupole power converters are delivered and stored at IKP until assembly in the ring is possible.

Fig. 33: Stored dipole magnets for HESR in Jülich.

A first power converter for sextupole and steering magnets has been tested with respect to electromagnetic compatibility. The results are being discussed in close contact with the manufacturer. Delivery of the series is expected for 2016.

Dedicated vacuum chambers to receive the vacuum pumps have been prototyped. A manufacturer for these chambers has been identified.

The first stochastic cooling pick-up tank has been assembled and is being commissioned in COSY.

5.2 Magnets, vacuum and power converters

After a slow start in the first quarter of 2015 the dipole and quadrupole magnets are being delivered regularly now: 2 dipole and 4 quadrupole magnets per month, or more. By the end of 2015 16 dipole magnets and 18 quadrupole magnets arrived in Jülich (see fig. 33). All vacuum chambers for the dipole magnets are produced. The first 12 chambers are already NEG coated and arrived in Jülich. The first dipole magnet has been operated with a normal thermal cycle for NEG activation, see fig. 34. Careful investigation revealed that special precautions have to be taken to minimize the friction between the heating jacket and paint on the magnet poles. Else the thermal cycling leads to a 4 mm hysteresis of the flange position at the fixed bearing relative to the magnet iron.

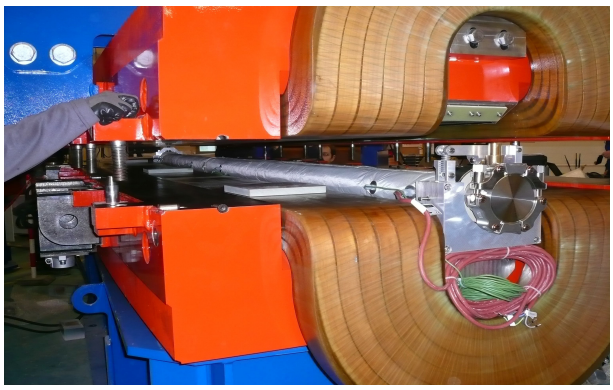

Fig. 34: Dipole magnet with vacuum chamber in heating jackets, view from the floating bearing side. Upper yoke lifted.

Measuring the multipole components of fabricated magnets is essential for providing detailed information for accelerator modeling. For straight magnets the method is well established. For curved magnets several measurement methods are under investigation at various laboratories. For the HESR curved dipole magnets (bending radius nearly 30 m) a solution with 16 Hall probes mounted on a disk is favoured. This disk can be moved along the central trajectory. As proof of principle pointwise measurements with a 3D device were performed. Acquisition of magnets for the PANDA chicane, the injection dipole and the magnetic septum had to be shifted to 2016. Detailing of the vacuum chambers with the pumping ports is finished. Two variants will be needed, one for pumps of DN 100, and one for pumps of DN160. The contract for production of 182 of these chambers has been awarded. Prototypes including RF grids are already on site and have been tested successfully.

The straight sections of HESR have already been designed in detail. Corresponding data bases have been updated. A solution for storing finished pre-assemblies in Darmstadt has been found.

27 power converters for the quadrupole magnet families were delivered, stored in Jülich (see fig. 35), and will be operated in regular intervals to avoid capacitor aging.

The manufacturer requested to shift the delivery of the PANDA chicane dipoles power converter to Q1/2016. Acquisition of power converters for injection dipole and magnetic septum had to be shifted to 2016.

Fig. 35: Stored quadrupole power converters.

5.3 Injection and stochastic cooling

The parts of the injection kicker system which will be contributed by Jülich are well advanced. They are regularly synchronized with the manufacturer of the current bearing parts. The test tank including peripherals has been finished. The resistor column with the connecting high voltage coaxial cables will rest on a ceramic flange. To minimize the weight on that flange, Jülich designed a lifting and holding mechanism which at the end of 2015 has been forwarded to production. Once the required rise time of 225 ns has been observed with a kicker magnet assembled into the kicker test tank, the production of the injection kicker magnets and their power converters can be released. The complete assembly of the test tank by the end of 2015 is shown in fig. 36.

Fig. 36: Photo of the test tank for injection kicker with heating jackets, pumps, and control rack.

The assembly of the first pick-up tank of the 2-4 GHz stochastic cooling system was completed, see fig. 37. The tank is being installed in COSY for commissioning. Assembly of the corresponding kicker tank is in progress.

Fig. 37: Assembly of pick-up tank. The full subassembly of the ring slot coupler structures for 2-4 GHz is only partially inserted. Cryogenic cooling heads are installed at the top. Assembly has been done under clean room conditions.

The contract for manufacturing and delivery of 32 power amplifiers for the 2-4 GHz range could be awarded.

5.4 Beam diagnostics

The present BPM design (diagonally cut cylinder, upper panel of fig. 38) and an alternative with higher sensitivity but poorer linear behaviour (4 capacitive strips, lower panel of fig. 38) have been presented to and examined by a Beam Instrumentation Panel at Jülich with members from CERN, DESY, and GSI. A comparison of both designs was recommended. The decision which design to choose will depend also on timely availability.

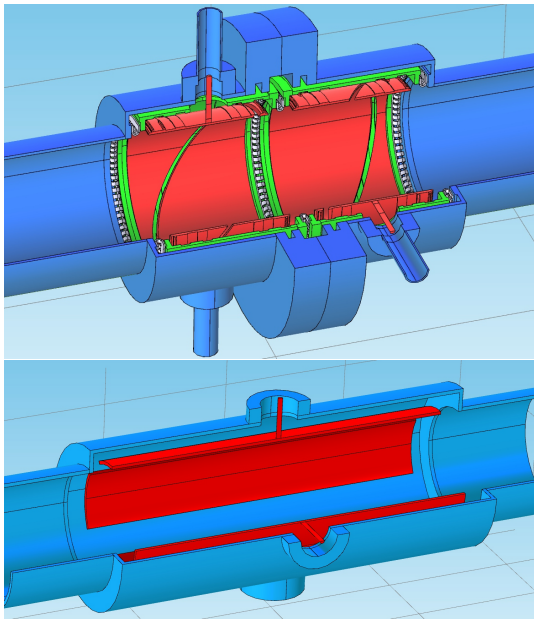

Fig. 38: Present (upper panel) and alternative (lower panel) of the HESR BPM design.

6 The $\overline{\text{P}}$ANDA experiment at FAIR

6.1 Introduction

The future Facility for Antiproton and Ion Research (FAIR) will be one of the largest accelerator facilities in the world giving access to new experiments to gain insights into the structure of matter and the evolution of the universe.

The antiProton ANnihilation at DArmstadt ($\overline{\text{P}}$ANDA) experiment is one of the main experiments of FAIR. It utilizes the intense anti-proton beam with excellent momentum resolution provided by the High Energy Storage Ring (HESR) to perform precision measurements in the charmonium energy regime to improve the understanding of Quantum Chromo Dynamics.

In this regime many new and unexpected hidden and open charm states were found in the last decade where the nature of many of theses states is not clear. First evidence was found that at least some of the new states could be exotic particles with more than three valence quarks. To distinguish the various theories about their origin a precise knowledge of mass and width is important. Here $\overline{\text{P}}$ANDA is the only experiment in the world which will be able to determine the width of these states down to 50 keV, compared to an upper limit of a few MeV now.

One challenging aspect not only in the analysis of the small charmonium-like states is the separation of the signal events from the huge background. To develop the needed algorithms and to determine the performance of $\overline{\text{P}}$ANDA once the experiment is running an intense simulation program is ongoing. One example for this are the simulations of the D_{sJ} mesons formed by a heavy c quark and a light s quark.

The signatures of the physics channels $\overline{\text{P}}$ANDA is interested in is very similar to the structure of the background reactions. One way to separate the signal of e.g. D mesons from the background is the precise measurement of the place of their decay (the decay vertex). Due to their lifetime this point is displaced by a couple of 100 μm from the place of their creation. Therefore, $\overline{\text{P}}$ANDA will use high precision tracking detectors to precisely measure the tracks of the generated particles. Two of theses tracking detectors, the Straw Tube Tracker (STT) and the Micro Vertex Detector (MVD) are developed by the IKP together with other partners.

One challenge in the development of these detectors is that $\overline{\text{P}}$ANDA is not able to select the physically interesting reactions based on a few, fast sub-detectors but has to read out the complete dataset of the whole detector. This requires from all detector components, that they are able to send out all hit data to an event selection network in a free running mode. Compared to existing particle physics experiments this is a novel approach which requires the development of new electronic devices which are capable to transmit large data rates.

For the pixel and the strip part of the Micro Vertex Detector two different front-end ASICs are under development: The ToPix ASIC for the pixel part, developed by INFN Torino and the PASTA ASIC for the strip part as a combined development from INFN Torino, the University of Gießen and the Forschungszentrum Jülich.

In the Straw Tube Tracker (STT) of $\overline{\text{P}}$ANDA two different approaches for the data taking are under study. The first one uses an ADC with a connected FPGA to do a complete pulse shape sampling, while in the second approach a dedicated ASIC PASTTREC was developed, which only measures the start time and the duration of a signal. Both approaches are under study in beam tests at COSY and in lab measurements.

6.2 A study of the decay $\bar{p}p \rightarrow D_{s0}(2317)^{*+}D_s^-$ at $\overline{\text{P}}$ANDA

In high energy physics, the spectrum of the mesons built by a c-quark and a s-quark is not well understood. In fact, until 2003 experimental observations and theoretical predictions had good agreement, as the non-perturbative calculations can predict well the potential of an heavy-light system, at that energy regime. Here we assume that the c-quark is a heavy quark; the s-quark is a light quark. The discovery of the resonant state $D_{s0}(2317)^{*+}$ opened questions that are still unanswered, about the nature of this state, whose mass was experimentally found to be $\sim$180 MeV/c^2 lower than predicted by potential models. Subsequent observations, as for example of the $D_{s1}(2460)^+$, gave a hint that the $D_{s0}(2317)^{*+}$ is probably the missing $J^P = 0^+$ state of the cs-spectrum. This statement needs to be confirmed by experimental data, which still has not happened. After the discovery of the $D_{s0}(2317)^{*+}$, several theoretical models have been elaborated, all of them strictly depending on the measurement of the width of the $D_{s0}(2317)^{*+}$:

- pure cs state, a model predicting $\Gamma(D_{s0}(2317)*+) \leq$10 keV
- molecular state, models predicting $\Gamma(D_{s0}(2317)^{*+}) \sim$ 140 keV
- tetraquark, a model predicting $\Gamma(D_{s0}(2317)^{*+}) \sim$ 100 keV

The B-factories have been limited in this kind of search, as they have measured mass resolutions of the order of a MeV, as well as LHCb which cannot determine the upper limit better than 1 MeV in this respect. The measurement of the $D_{s0}(2317)^{*+}$ total width will be possible only by a future machine, where the $D_{s0}(2317)^{*+}$ is seen in production, such as in the process $\bar{p}p \rightarrow D_{s0}(2317)^{*+}D_s^-$. As the $D_{s0}(2317)^{*+}$ is a charged state, we need another charged state of opposite sign to obtain it in $\bar{p}p$ interactions. We believe that in $\overline{\text{P}}$ANDA the study of the process $\bar{p}p \rightarrow D_{s0}(2317)^{*+}D_s^-$ and the measurement of the width of the $D_{s0}(2317)^{*+}$ are a unique physics case because of several reasons:

- $\overline{\text{P}}$ANDA is designed to obtain an excellent momentum resolution by utilizing the phase

space cooled beam of HESR with $\Delta p/p \sim 4 \cdot 10^{-5}$. The minimum antiproton momentum beam, needed to produce the $D_{s0}(2317)^{*+}$ in the $\bar{p}p \rightarrow D_{s0}(2317)^{*+}D_s^-$ process, is p = 8.80235 GeV/c. This leads to a width resolution of $\Delta m > 50$ keV. This would be sufficient to verify the molecular hypothesis of the $D_{s0}(2317)^{*+}$, scanning the $D_{s0}(2317)^{*+}D_s^-$ mass in 100-keV-steps. In case of success, this would have extremely important impact in the understanding of the cs-spectrum; in case of non-success, i.e. if a new upper limit is fixed because the width of the $D_{s0}(2317)^{*+}$ is much lower than about 50 keV, this would be an important measurement in any case, because we could exclude the molecular hypothesis at the 90% confidence level and fix a new upper limit. Both scenarios will open the doors to new theoretical interpretation, in any case. The current upper limit of the $D_{s0}(2317)^{*+}$ width at 90% confidence level is 3.8 MeV. No experiment at present can perform the scan of the $D_{s0}(2317)^{*+}D_s^-$ invariant mass in 100-keV-steps.

- $\overline{\text{P}}$ANDA proposes to analyse the $\bar{p}p \rightarrow D_{s0}(2317)^{*+}D_s^-$ process to avoid undesired effects of interference, as we do not choose the same final state particles (e.g., the $D_{s0}(2317)^{*+}$ and the D_s^- have different mass values). Actually, interference effects can occur in the final state $D_s^+D_s^-\pi^0$ of the process under investigation; but for the energy range analyzed it does not occur.

First simulations with PandaRoot have been performed, to study the feasibility of this analysis, once $\overline{\text{P}}$ANDA collects data, and evaluates the reconstruction efficiency and the ratio S/B with the correct status of the framework development. We perform an inclusive analysis, tagging the $D_s^- \rightarrow K^+K^-\pi^-$, only. On the $D_{s0}(2317)^{*+}$ we do not make any particular request. It is reconstructed simply as missing mass of the $D_{s0}(2317)^{*+}D_s^-$ event. With an easy kinematic fit, the D_s^- mass resolution is ~ 14 MeV/c^2; from the fit, the mass resolution of the $D_{s0}(2317)^{*+}D_s^-$ system is deduced to be less than 1 MeV/c^2.
We propose a mass scan of the $D_{s0}(2317)^{*+}D_s^-$ system in 15-scan-points, at 100 keV/c^2 intervals to measure the excitation function. Progress has been made this year in improving the track reconstruction efficiency for low momentum particles below p_t <350 MeV/c by almost a factor 2.
Unfortunately we do not know what is the cross section of the $\bar{p}p \rightarrow D_{s0}(2317)^{*+}D_s^-$ process. We assume a conservative range of [1-100] nb. Depending on this values, the ratio of signal events to background events (S/B) clearly changes, and also the analysis strategy could change. We propose different studies related to different assumptions of the ratio S/B. The challenge in this study is to improve the S/B ratio from$[10^{-8} - 10^{-6}]$ to a reasonable number, e.g. not smaller than 0.2. This cannot be reached by standard selection methods, thus a multivariate analysis must

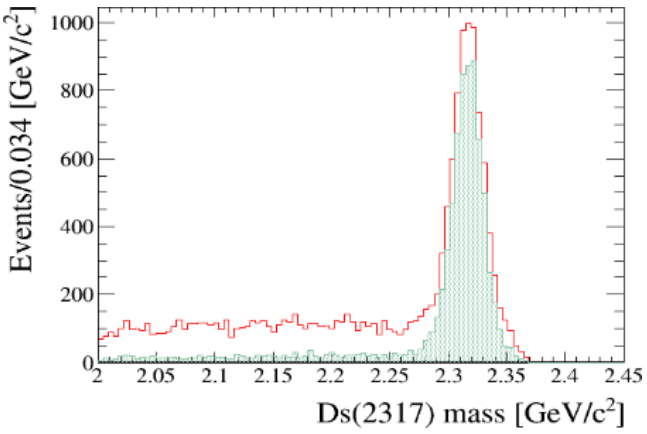

Fig. 39: Monte-Carlo study of the $\bar{p}p \rightarrow D_{s0}(2317)^{*+}D_s^-$ process based on a parametrization of the full simulation. The Fisher discriminant cut applied to the $D_{s0}(2317)^{*+}$ mass selection (red plot) is compared to the neural network cut (green plot). One can clearly see the much better background suppression capability of the neural network.

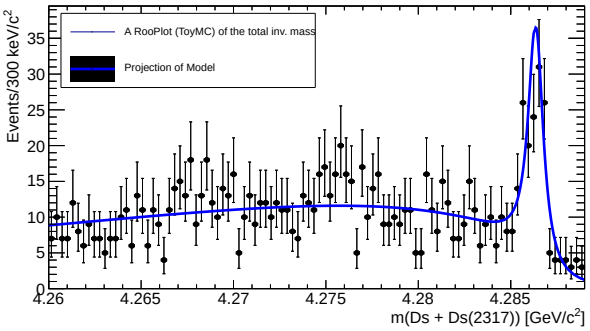

Fig. 40: Signal and background events of the combined $D_{s0}(2317)^{*+}D_s^-$ system at a beam momentum of 8.80235 GeV/c for one week of data taking and a signal to background ratio of 0.2.

be performed, and a neural network discriminant must be introduced in the analysis procedure. This work has been done, and the result is graphically shown in Fig. 39, where the big impact of the neural network discriminant (NN) cut has on the selection procedure can be seen in comparison to the previously used Fischer-discriminant cut. With additional selection criteria no background event survived which allows us to determine a lower limit of the rejection power of $> 4.5 \cdot 10^{-6}$. The optimization of this work in now ongoing. With the current selection we measure a reconstruction efficiency ∼3%, in a semi-inclusive simulation where the $D_{s0}(2317)^{*+}$ is supposed to decay to all possible decay modes. We expect then to produce [864-8640] events per day, assuming an average luminosity of L = 0.864 pb^{-1}/day; with the reconstruction efficiency that we determined with our simlu-

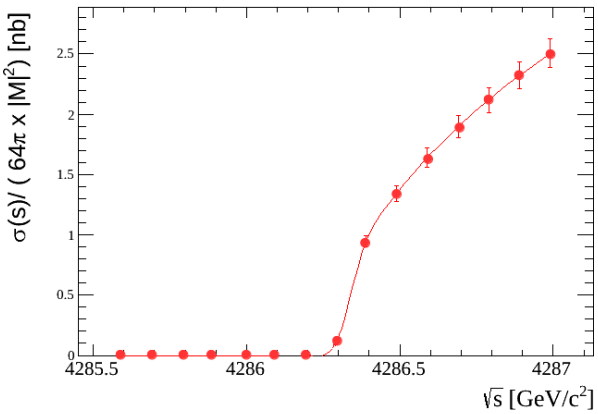

Fig. 41: Resulting excitation function for a signal to background ratio of 0.2 with 15 scan points and 1 week measurement time per scan point.

ation, we would obtain between [26-260] reconstructed $D_{s0}(2317)^{*+}$/day. The number of needed days to perform a 15-scan-point analysis in $\overline{\text{P}}$ANDA will depend on which precision we need to separate the different theoretical scenarios.

One example of one week of data taking per scan point is shown in Fig. 40. The diagram shows the events surviving all selection criteria for a signal to background ratio of 0.2 at a beam momentum slightly above the production threshold (p = 8.80235 GeV/c). One can clearly see the signal peak above the background. The number of events in the signal peak normalized with the luminosity gives one point of the excitation function. With 15 measurements at different beam momenta around the threshold one achieves an excitation function shon in Fig. 41. The shape of the excitation function depends on the width of the $D_{s0}(2317)^{*+}$ which can be extracted from the measurement.

6.3 Simulated measurement of the D_s semileptonic decay form factor

Measuring the semileptonic decay form factor of the D_s meson is one of the most challenging topics of open-charm physics at $\overline{\text{P}}$ANDA. The semileptonic D_s decays are governed by both weak and strong interactions. The strong interaction dynamics can be described by a form factor $f_+(q^2)$, where q^2 is the invariant mass of the lepton-neutrino system $M^2_{e^+\nu_e}$. To study this form factor in $\overline{\text{P}}$ANDA D_s pairs have to be created in $\bar{p}p$ collisions.

For the simulation it was assumed that the first D_s decays semileptonically via $D_s^+ \to e^+\nu_e\eta$ with further decays to $\eta \to \pi^+\pi^-\pi^0$; $\pi^0 \to \gamma\gamma$. The decay of the second D_s is needed to identify the generated D_s pairs as a so called *tag*. Two tag modes are studied: tag mode A: $D_s^- \to K^+K^-\pi^-$ and tag mode B: $D_s^- \to \pi^+\pi^-\pi^-$.

One million $\bar{p}p$ collisions have been simulated in this decay mode to evaluate the performance of the $\overline{\text{P}}$ANDA detector for this channel. Several improvements have been made compared to last year: new software tools for tracking and truth matching, as well as a better event reconstruction strategy. The correlation parameters for the neutral particle reconstruction have been studied to achieve an acceptable efficiency and significance for the reconstructed π^0 and η by optimizing the photon energy threshold. In addition, the beam momentum dependence of the reconstruction efficiency has been studied for three different $\bar{p}$ momenta above the production threshold, 7.3 GeV/c, 7.685 GeV/c and 8 GeV/c. A beam momentum of 8 GeV/c seems to have the best reconstruction efficiency. Table 4 summarizes the preliminary results on the reconstruction efficiency and resolution.

Table 4: Vertex resolution and reconstruction efficiency of the η candidates, the π^0 and the D_s^- for both tag modes (see text).

Tag		rec. eff. [%]	σ_{mass} [MeV/c^2]	σ_{vtx} [μm]		σ_{mom} [%]	
				x/y	z	p_t	p_z
	η	16.4	5.6	100	187	1.6	1.3
	π^0		4.8			1.9	1.8
A	D_s^-	15.1	13.1	62	130	2.2	0.7
B	D_s^-	23.4	17.2	51	89	2.2	0.7

After reconstructing the intermediate particles D_s^- and η, the kinematics of the undetected neutrino can be calculated based on four-momentum conservation. Fig. 42 shows the reconstructed $M^2_{e^+\nu_e}$ spectrum with a comparison to the event-wise MC truth matched data. It is shown that the reconstructed result is consistent with the MC data in the large momentum transfer region $M^2_{e^+\nu_e} > 0.2$ GeV$^2/c^4$.

Assuming the cross section of $\bar{p}p \to D_s^+D_s^-$ to be 20 nb at a $\bar{p}$ beam momentum of 8.0 GeV/c, we estimate the reconstruction rate to be approximately 60 events per month for a luminosity of 2×10^{32} cm^{-2}s^{-1}. The next steps will include a modification of the present software to improve the reconstruction efficiency and an investigation of the background channels.

6.4 The $\overline{\text{P}}$ANDA strip ASIC

The experimental setup of $\overline{\text{P}}$ANDA and the physics topics to be studied pose stringent requirements on the individual sub-detectors. This is especially true for the Micro Vertex Detector, which is the innermost detector component surrounding immediately around the interaction point. Here the track densities and the radiation levels are highest and special efforts have to be done to ensure a reliable operation of the detector over the full lifetime of the experiment. In addition, the material budget is very limited and high spatial and timing resolution are required. The PAnda STrip Asic (PASTA) is under development for the strip part of the MVD, which is based on

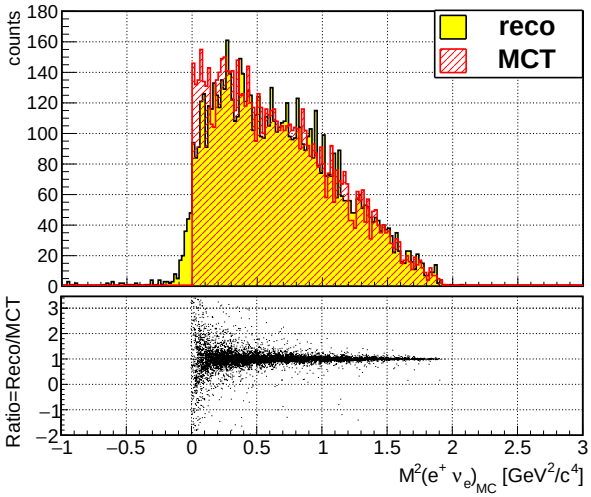

Fig. 42: Invariant mass squared distribution of the lepton-neutrino system with tagging mode A ($D_s^- \rightarrow K^+K^-\pi^-$). In the upper frame, the yellow field is the reconstructed result, and the red shadowed area is the result obtained by the MC truth matched data. Black dots in the lower frame show the ratio between "reco" and "MCT".

a predecessor for medical applications called TOFPET. Several design changes where necessary to modify the TOFPET ASIC to the needs of the PANDA experiment. The preamplifier stage had to be adopted for silicon strip sensors, the size of the chip had to be reduced, the power consumption had to go down and measures to protect the ASIC from single event upsets due to irradiation had to be implemented. A summary of the design parameters for PASTA can be found in Table 5.

Table 5: Parameters of the PASTA front-end ASIC

Input capacitance / charge	10 - 25 pF / 38 fC
Input channels / pitch	64 ch / 64 μm
Max. event rate	100,000 evt. / s / ch
Power consumption	$<$ 4 mW / ch
Time bin width	50 - 400 ps
Charge resolution	8 bit dyn. range
Radiation tolerance	10 kGy

All these changes were successfully conducted and a first prototype was submitted to the ASIC foundry in mid 2015. Figure 43 shows a photograph of the PASTA prototype received from the ASIC foundry at the end of 2015. Preparations to test the ASIC are ongoing in all collaborating institutes in order to be ready for a beam test in June 2016.

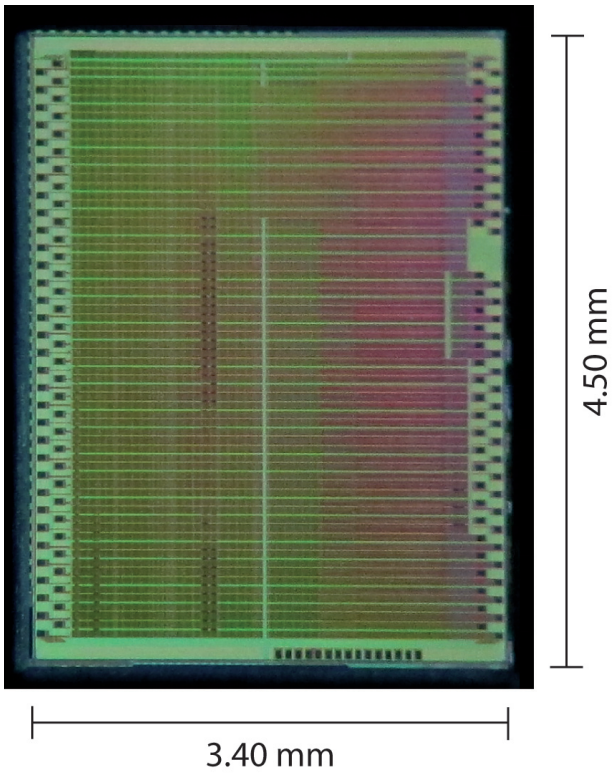

Fig. 43: Photograph of the first PASTA prototype.

6.5 The $\overline{\text{P}}$ANDA - Straw Tube Tracker

The construction and installation of the PANDA-Straw Tube Tracker (STT) is a joint project with partner groups in Germany, Italy, Poland, Romania, and USA. The FZ Jülich is involved in the system design and mechanical construction (IKP, ZEA-1), the readout system (ZEA-2) and in-beam tests of the system at the COSY accelerator. A major contribution is the assembly of the 4200 individual straw tubes for the STT which is carried out at IKP. The straw series production started in 2014 and continued in 2015. The first straw modules for the hexagonal STT layout were assembled and will be mounted in a prototype mechanical frame. In addition new modules consisting of the final straw type and close-packed geometry have been built for high-rate in-beam tests.

The STT prototype frame together with the Central Support Frame (CSF) and mounting rail system were designed and built by the group at LNF (Frascati, Italy). The components were shipped to Jülich and installed in the former COSY-TOF beam area. The CSF supports the whole inner part of the $\overline{\text{P}}$ANDA,Target Spectrometer with the beam and target cross pipe, the Micro-Vertex-Detector and the two STT semi-barrels. The rail system for the CSF mounting in the target spectrometer has a total length of about 5 m and is split into two sections. The mounting of the first section with the STT prototype frame and CSF is shown in Fig. 44.

The STT will feature a new custom-designed electronic readout system for the simultaneous measurement of the

Fig. 44: Installation of a prototype of the Central Support Frame (CSF) system for the PANDA target spectrometer in the former COSY-TOF beam area.

drift time for the spatial particle track information and deposited charge for the specific energy-loss (dE/dx) information, both with high resolution and in the $\overline{\text{P}}$ANDA specific environment of high particle intensities, variety of particle species, high multiplicities and broad momentum range.

Two concepts are investigated. One is based on a full pulse shape measurement and analysis by using an ADC with FPGA readout. The straws are directly connected to thin, about 12 m long coaxial cables with the amplifier located in the backend and integrated in the ADC readout system. This concept is developed by groups at Jülich (ZEA-2, IKP) and Krakow (IFJ PAN).

The other option measures the pulse start time and pulse width (time-over-threshold) for the charge information by a new, specific amplifier-shaper-discriminator ASIC which was designed by the group at AGH Krakow. The time and time-over-threshold are readout by TRB3 boards (designed by GSI, Darmstadt). The set up of the readout system, specific programming of the TRB3-FPGAs for the software control of the ASIC parameters and the readout algorithms are done by the group at the Jagiellonian University in Krakow.

After successful prototype tests proving the conceptual design and fulfilling the required drift time and charge measurement resolutions, the next step is to set up larger pre-series systems consisting of the final components. Fig.45 shows the front-end components of the ASIC/TRB readout system mounted at a straw test system. The STT-specific ASIC was named PASTTREC for PAnda STT REadout Chip. The ASIC tests, the front-end board design and bonding of the ASICs to the boards were done by the groups at AGH and the Jagiellonian University in Krakow. The ASIC features altogether more than 1000 combinations of parameter settings for amplifier gain, peak time, ion tail cancellation and further pulse shaping. The parameters are software controlled and are set via an FPGA in the TRB3 board. The main PASTTREC characteristics and straw signals for three different default settings are shown in Fig. 46 and Fig. 47.

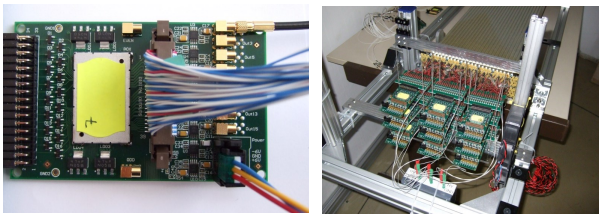

Fig. 45: Front-end board (left) with two PASTTREC chips under the cover shield (with yellow label) and mounted front-end boards at the straw test system (right).

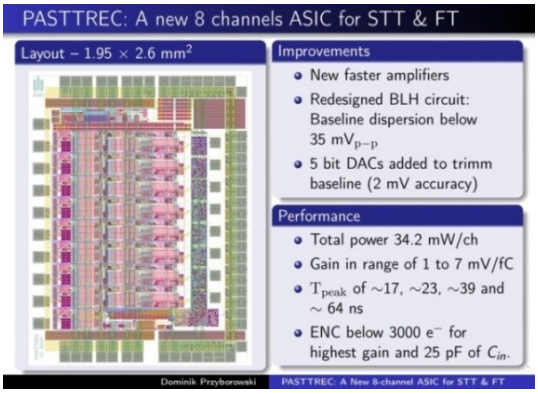

Fig. 46: Layout and main characteristics of the PASTTREC ASIC for the PANDA-STT.

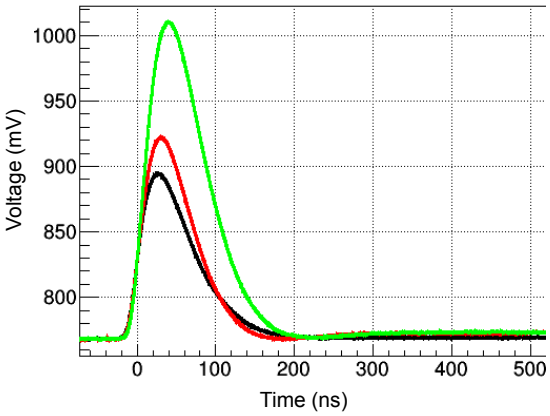

Fig. 47: Analog output signals for three different ASIC parameter settings for a straw illuminated by a ^{55}Fe source.

For the ADC based readout the final ADC chip (LTM9011-14, Linear Technology) was verified by a measurement of the achievable spatial resolution with a testboard, containing a commercial FPGA (Kintex-7) for the ADC readout. The set up of a larger test system for the upcoming beam tests in 2016 is ongoing.

The COSY proton and deuteron beams in the momentum range of 0.6 to 3.0 GeV/c are ideally suited to test the STT particle identification capability by the particle specific energy-loss. The measurements will allow a direct extrapolation to the proton, kaon and pion separation power in the lower momentum region below 1 GeV/c which is of interest for $\overline{\text{P}}$ANDA. Fig. 48 shows a summary of the dE/dx measurement results obtained so far with the prototype setups for both readouts and for a proton beam at different momenta. A nice agreement between the data

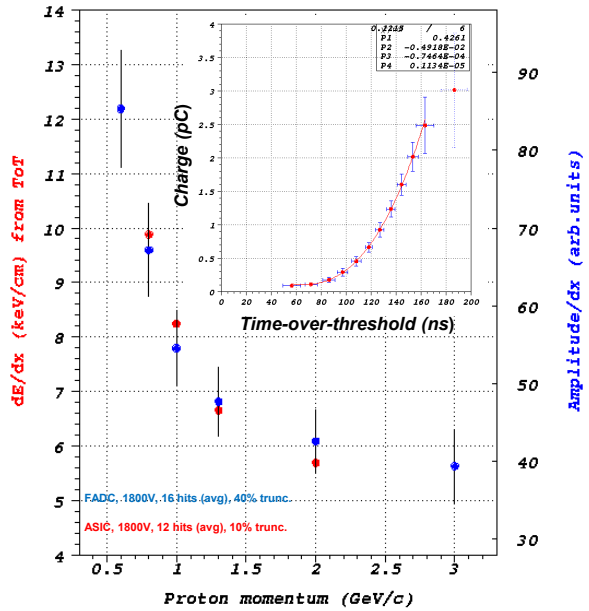

Fig. 48: Energy-loss (dE/dx) measurements for a proton beam at different momenta. The ADC data (blue dots and y-axis to the right) show the integrated signal amplitude divided by the track path length in the gas. The ASIC/TRB data (red dots and left y-axis) show the dE/dx extracted from the time-over-threshold measurement using the calibrated time-over-threshold to charge dependency (insert in right top corner).

for both methods is seen. Note that the energy-loss for minimum ionising particle is around 5.0 keV/cm for the Ar/CO_2 (90/10 %) gas mixture at 2 bar pressure. All data are for prototype systems with a reduced number of available channels. The next step is to set up pre-series systems with a larger number of channels and perform a measurement series to determine the proton deuteron separation power over the full momentum range at COSY.

6.6 KOALA experiment at HESR

One challenge of PANDA experiment is to achieve a precision of 3% of absolute luminosity determination by using antiproton-proton elastic scattering as reference channel. It is limited by the available data of antiproton-proton elastic scattering differential cross section in the relevant beam momentum range of PANDA. Therefore, the

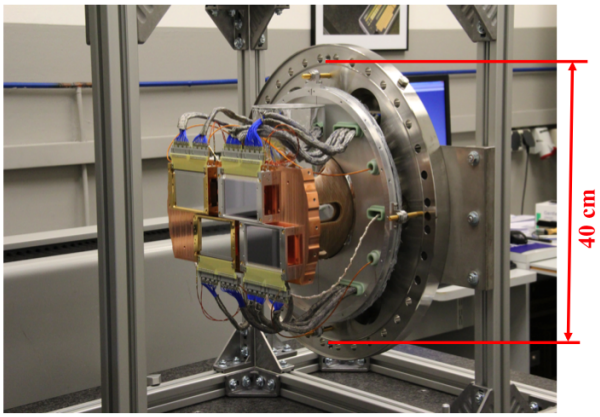

Fig. 49: Recoil detector assembled for a beam test at COSY.

KOALA experiment at HESR has been proposed to provide the required knowledge of antiproton-proton elastic scattering down to CNI (Coulomb-Nuclear-Interference) region.

The KOALA experiment will measure a large range of the squared 4-momentum transfer t-distribution of antiproton-proton elastic scattering in order to determine the parameters of total cross section σ_{tot}, the ratio, ρ, of the real part to the imaginary part of the forward elastic scattering amplitude and nuclear slope b, thus the differential cross section. The idea is to measure the scattered beam particles at forward angles by tracking detectors and the recoil target protons near 90° by energy detectors.

The PANDA luminosity monitor detector can be used for the forward measurement and the recoil protons will be measured by a new recoil detector. The forward measurement will track the scattered antiprotons. The recoil detector will measure both the kinetic energy and the polar angle of the recoil protons since t is directly proportional to the proton's kinetic energy T_p, i.e. $|t| = 2m_pT_p$. The recoil detector will measure the energy of the recoil protons within an angular range (recoil angle defined as $\alpha \equiv 90^\circ - \theta_{lab}$) $0^\circ < \alpha < 19^\circ$.

One of the recoil arms of the KOALA experiment has been designed and built. A picture of the recoil detector as used for the commissioning is shown in Fig. 49. Two silicon strip sensors produced by MICRON with customized dimensions of 76.8 mm (length) x 50 mm (width) x 1 mm (thickness) have been placed at about 1 m from the target to cover the recoil angles, α=0°–5.7°. This corresponds to the region in which the silicon detector can stop the recoil protons with energies up to 12 MeV. Each silicon detector has 64 strips with 1.2 mm pitch. In addition, two germanium strip detectors produced by SEMIKON with 5 and 11 mm thickness have been set up in 2 rows as well. They can measure the recoil protons with energies up to 60 MeV. Both germanium detectors have 67 readout strips and a strip pitch of 1.2 mm in a sensitive area of 80.4 mm (length) x 50 mm (width).

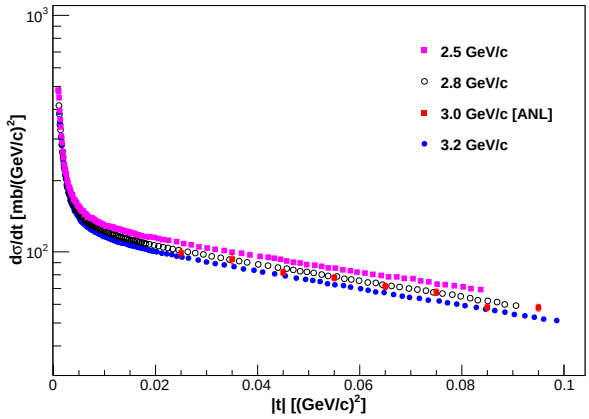

Fig. 50: The differential cross section of proton-proton elastic scattering at different beam momenta. The differential cross section data at 3.0 GeV/c is from reference [Phys. Rev. D (1974) 9: 1179].

The recoil detector was commissioned at COSY by measuring proton-proton elastic scattering since the recoil particles are exactly the same for both antiproton-proton elastic scattering at HESR and proton-proton elastic scattering at COSY. The commissioning experiment has been performed at ANKE hydrogen cluster target station at COSY.

Data of the proton-proton elastic scattering at the beam momenta of 2.5, 2.8 and 3.2 GeV/c have been taken in commissioning weeks. After energy calibration, acceptance correction and background subtraction the t-spectrum has been constructed based on the measured energy of the recoil protons. The parameters of σ_{tot}, ρ and b have been determined with expected small errors. The differential cross section of proton-proton elastic scattering at 3 beam momenta has been normalised as shown in Fig. 50. One existing experimental data of proton-proton elastic scattering at 3.0 GeV/c in a smaller range of t has also been plotted. It shows a well consistence between the KOALA data and the existing data.

Those preliminary results of the commissioning experiment have validated the proposal of KOALA experiment. The full setup of KOALA experiment will be performed at HESR as soon as the antiproton beam will be available.

7 Further experimental activities

7.1 Production and interaction of polarized molecules

The polarized atomic beam source (ABS), used before to feed the polarized internal target of the ANKE experiment at COSY, is still in use for other experiments in different fields of physics. For example, the influence of the nuclear spin in chemical reactions was observed, i.e., in the recombination of hydrogen or deuterium atoms to molecules or in the adsorption of polarized atoms on different surface materials. Even the interaction of polarized molecules with surface materials can be investigated.
For this purpose, a collaboration between the Petersburg Nuclear Physics Institute (PNPI), the Institut of Nuclear Physics of the University of Cologne, and the IKP built a dedicated reaction chamber where the polarized atoms in different hyperfine substates, produced with the ABS, can recombine into polarized molecules. The recombination takes place on the surface of T-shaped storage cells only and not in the gas phase, because the pressure inside does not exceed 10^{-4} mbar. The atoms and molecules are ionized by an electron beam and the produced protons/deuterons or H_2^+/D_2^+ and even HD^+ ions are accelerated into a Lambshift-Polarimeter, where the nuclear spin polarization is measured as a function of the magnetic field along the cell (up to 1 T).
With Monte-Carlo-Simulations the amount of wall collisions of the molecules inside the cell can be determined due to the well known and simple geometry of the storage cell tubes (400 mm long, 10 mm inner diameter). During these collisions the nuclear spin orientation can be destroyed by several mechanisms:

1. Coupling of the nuclear spins with the rotational magnetic moment of the molecule itself.
2. Interaction of the nuclear spins with magnetic fields on the surface.
3. Interaction of the nuclear spins with electric field gradients on the surface.

These polarization losses can be controlled by the magnetic field of the superconductive magnet.
For instance, if a cell with a gold surface is used, electric field gradients are suppressed and no magnetic fields on the surface influence the polarization. In this case, the coupling of the nuclear spins with the rotational magnetic moment is responsible for the polarization loss of the molecules. The external field can decouple both and at large fields no polarization losses are observed.
For deuterium, the coupling to the rotational magnetic moment depends on the temperature. If both nuclear spins are aligned, ortho-deuterium is produced in states of even rotational quantum numbers $J = 0, 2, 4, \ldots$. At 100 K about 75 % of the molecules are in the $J = 0$ state and only 25 % in the $J = 2$ state can contribute to the rotational magnetic moment. This changes for lower temperatures and at about 50 K, the lower cell temperature

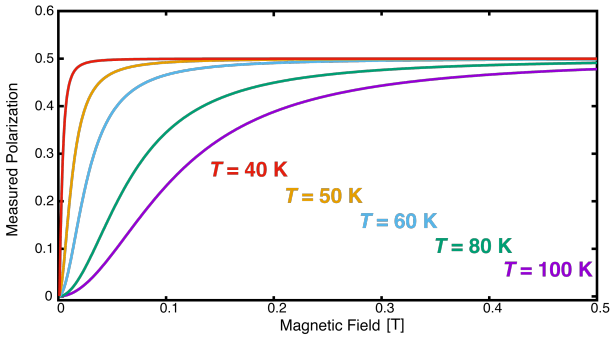

Fig. 51: Calculated molecular polarization as a function of the magnetic field B when fully polarized deuterium atoms recombine on a gold surface at temperatures between 40 and 100 K, and corresponding population of the rotational states.

limit of the apparatus, more than 95 % of the molecules will have $J = 0$. The polarization losses, corresponding to the rotational magnetic moment, are minimized.

The polarization losses for hydrogen do not depend on the temperature in the range of the apparatus, because for ortho-hydrogen J must be odd and changes in the occupation numbers for the different states are found at temperatures above 200 K only. With this experience it seems possible to store polarized deuterium molecules for a reasonable time, because the different sources for depolarization can be excluded at temperatures close to the condensation temperature of deuterium. In addition, former experiments with a Fomblin (Perfluropolyether) surface showed that the nuclear polarization of hydrogen atoms can be preserved completely during the recombination process. Therefore, with this method it seems possible to produce highly polarized deuterium molecules that can be collected and stored for further use. For example, the molecules itself or the polarized H_2^+/D_2^+ and even HD^+ ions can be used for next-generation laser spectroscopy or as target material for laser-acceleration experiments to produce polarized ion beams (JUSPARC). Another option is to increase the energy output or to reduce the costs of future energy production by nuclear fusion, because the use of polarized D_2 or DT molecules opens the door to increase the fusion cross sections and to control the trajectories of the fusion products, i.e., the neutrons.

In addition, this type of measurements allows for the first time a deep view on the effect by the nuclear spin in chemical reactions. Based on this experience it might be possible to add a nuclear polarized atom to substances that are used in medicine and to keep them polarized for a reasonable time. Then this polarized substances can be used in NMR investigations as tracer or to increase the resolution of this scans by orders of magnitude.

7.2 Laser-driven acceleration of (polarized) helium ions at PHELIX

A high-intensity laser pulse impinging on a suitable target can form relativistic plasmas out of which charged particles can be accelerated to energies of several MeV. An unsolved question in this context is the influence of the strong magnetic laser and plasma fields on the spins of the accelerated particles. Two scenarios are possible here: either these fields change the spin direction of the accelerated particles, or the spins are sufficiently robust that the short laser pulse has no effect on the spin alignment of a polarized target [Phys. Plasmas **21** 2, 023104 (2014)]. For the second scenario, there is no data on the behavior of nuclear spins ($\omega_{\mathrm{Larmor},^3\mathrm{He}} = 32.4\,\mathrm{MHz\,T^{-1}}\,B$) in magnetic laser–plasma fields ($B \sim O\left(10^3 - 10^5\,\mathrm{T}\right)$, temporal continuance of $10^2 - 10^3$ fs). It has to be experimentally investigated if the polarization can be conserved inside plasmas during laser–acceleration processes, which would also open up the possibility of nuclear fusion with polarized fuel, in which the cross-sections for nuclear fusion reactions theoretically can be enhanced, leading to higher energy yields compared to the case of unpolarized fuel. In order to investigate the polarization degree of laser-accelerated ^{3}He ions from a pre-polarized ^{3}He gas–jet target, several challenges have to be overcome beforehand. One of these includes the demonstration of the feasibility of laser-induced ion acceleration out of underdense gas–jet targets at PHELIX, GSI Darmstadt. As laser target, both ^{4}He and unpolarized ^{3}He gas were used. The laser–acceleration process was simulated on the Jülich supercomputer JURECA with the help of EPOCH 2D [PoS(PSTP2015)002 (2016)]. The simulated as well as experimental laser parameters were set to: $I_\mathrm{L} = 1.4 \times 10^{19}\,\mathrm{W\,cm^{-2}}$, $\lambda_\mathrm{L} = 1.053\,\mu\mathrm{m}$, $\tau_\mathrm{L} = 0.8\,\mathrm{ps}$, $n_\mathrm{c} = 10^{21}\,\mathrm{cm^{-3}}$, $a_0 \approx 3.3$. Different ^{4}He/^{3}He backing pressures were applied: in case of ^{4}He gas, the pressures were 30 bar ($n_\mathrm{gas}^\mathrm{max} \approx 0.06\,n_\mathrm{c}$) and 15 bar ($n_\mathrm{gas}^\mathrm{max} \approx 0.03\,n_\mathrm{c}$), and in case of unpolarized ^{3}He gas a maximal backing pressure of 8 bar ($n_\mathrm{gas}^\mathrm{max} \approx 0.02\,n_\mathrm{c}$) was available. As main ion diagnostics, a removable *GAFCHROMIC HD-V2* radiochromic film (RCF) wrap-around detector was mounted close to the interaction region cylindrically around the nozzle in order to measure the angular ion distribution qualitatively. The RCFs were wrapped in 5 µm thick Al foil (protection from side-scattered laser light). Hence, $\mathrm{He}^{1+,2+}$ ions with energies > 1.6 MeV were able to pass through the Al degrader and irradiate the RCF. In addition, three Thomson parabola spectrometers (TP) were placed at three angles relative to the laser direction (wedge-shaped capacitor with a HV of 3 kV, $B \approx 0.6$ T, covered solid angles $170 - 370$ nSr). The TPs were armed with *Agfa MD4.0* image plates (IP) and for one laser shot with *TASTRAK* CR-39 SSNTDs. Results: $^{3,4}\mathrm{He}^{1+,2+}$ ions could successfully be accelerated to MeV energies—the ion angular distribution as well as the energy spectra for all ion species for specific emission angles could be extracted. Figure 52 illustrates a lineout of the background-corrected angular $\mathrm{He}^{1+,2+}$–ion distribution on the height of the laser focus, obtained from the scanned RCF-raw data. In transversal direction (around $\pm 90°$), a peak in ion signal with a FWHM of $\varphi_\mathrm{fwhm} = 23°$ indicates the ion–emission angles at which the TPs were aligned for the following measurements: $-\{80°, 90°, 100°\}$. The IPs used in the experiment could not be calibrated with $^{3,4}\mathrm{He}^{1+,2+}$ ions beforehand. The ion–energy spectra, *i.e.* the normalized signal intensity (per MeV and Sr, $\log_{10}$ scale) against the ion energy in MeV, could be extracted from the detector raw data, exemplified in Fig. 53: both $^4\mathrm{He}^{1+,2+}$ Thomson parabolas are imaged on the IP. In order to get an impression of the real ion number, one TP was equipped with CR-39 SSNTDs for one laser shot. The high- and low-energy cut-offs in case of $^4\mathrm{He}^{2+}$ in Fig. 53 are given with 4.6 MeV (normalized energy uncertainty of $\Delta\mathcal{E}\,\mathcal{E}^{-1} = 0.032$) and 0.84 MeV ($\Delta\mathcal{E}\,\mathcal{E}^{-1} = 0.014$). The single CR-39 measurement ($-80°$, 356 nSr, low gas pressure) in total yielded $\sim 1.4 \times 10^{11}\,\mathrm{Sr^{-1}}$ He^{1+} and $\sim 5.7 \times 10^{10}\,\mathrm{Sr^{-1}}$ He^{2+} ions. A layout of a polarized ^{3}He gas–jet target for the exploration of spin effects in laser-induced plasmas is currently being developed (*i.e.* a magnetic holding field, a gas–compression system, and a fast piezo-driven valve). Two weeks of beamtime at PHELIX

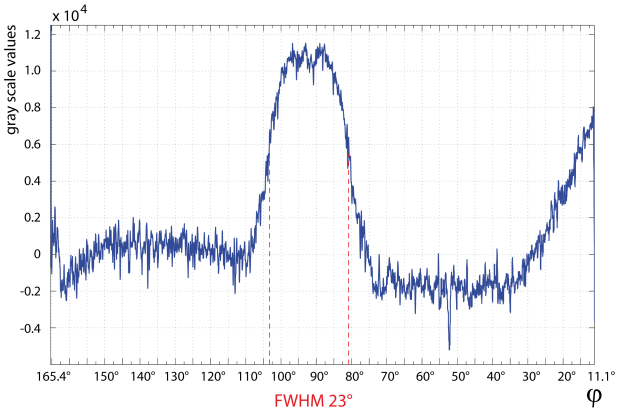

Fig. 52: BG-corrected angular $\mathrm{He}^{1+,2+}$–ion distribution.

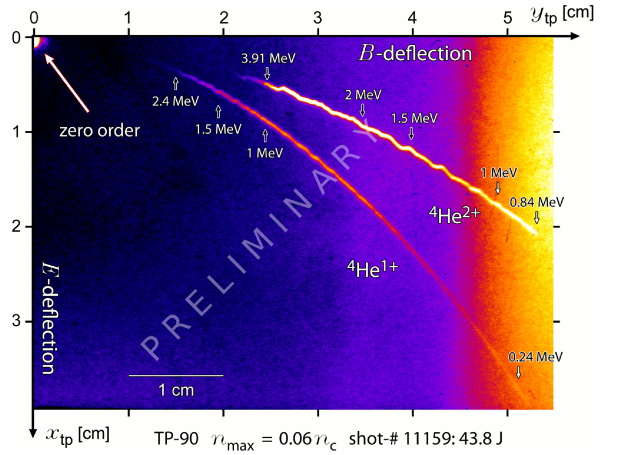

Fig. 53: IP raw data: $\mathrm{He}^{1+,2+}$ Thomson parabolas

(2016/17) were granted for polarization measurement of laser-accelerated ^{3}He ions from a polarized ^{3}He gas–jet target.

7.3 Neutrino activities

Along the strategy to extend the CP-violation search from the baryonic also to the leptonic sector, a new neutrino group is starting to grow at IKP. Livia Ludhova, an expert in neutrino physics, joined IKP in November 2015 via the recruiting initiative of the Helmholtz Association. She, as the head of this group, will work in a close collaboration with RWTH Aachen within the JARA–FAME section "Forces and Matter Experiments" of the "Jülich-Aachen Research Alliance". She has a 10-year long experience in neutrino physics by working in Borexino and SOX projects. Borexino is a 300 ton liquid scintillator detector placed in the underground Laboratori Nazionali del Gran Sasso in central Italy. The unprecedented radio-purity of the scintillator was at the base of a series of spectroscopic measurements of neutrino species from the pp-cycle (pp, pep, ^{7}Be, and ^{8}B neutrinos), a unique success of Borexino. Geoneutrinos, antineutrinos emitted along the decays of long-lived radioactive elements inside the Earth, are unique probes in order to determine the radiogenic heat produced in the deep Earth. Borexino, together with KamLAND in Japan, are the only two experiments being currently able to measure geoneutrinos. At the end of 2016, a strong ^{144}Ce/^{144}Pr antineutrino generator will be placed below the Borexino detector. This so called SOX project has the aim to search for a hypothetical sterile neutrino with mass squared of $\approx 1\ eV^2$. The data taking will last about 1.5 years. Borexino and SOX projects are important short and medium term targets of the IKP neutrino group. This includes a strong involvement in:

- a new complete solar neutrino analysis (after an extensive purification campaign of liquid scintillator), will lead to an improved measurement of ^{7}Be, pep and possibly also pp and ^{8}B neutrinos;
- an attempt to perform the first observation of neutrinos from the CNO cycle;
- final geoneutrino analysis based on the complete data-set, naturally closed after the insertion of the SOX antineutrino source;
- SOX-related sensitivity and Monte Carlo studies, data acquisition, detector calibration with radioactive sources and, naturally, final data analysis.

The principal long-term project of the group is the JUNO experiment in Jiangmen in China. The 20 kton liquid scintillator detector will start to take data in 2020. The project is based on a proven science case with the determination of the neutrino mass hierarchy (inverted versus normal) as the core measurement and a number of outstanding measurements of neutrinos from other sources (Sun, Earth, super novae, etc.). The determination of the mass hierarchy, at JUNO based on the measurement of the oscillation pattern of reactor antineutrinos at 60 km baseline, is a prerequisite for the detection of CPV with any neutrino experiment. JUNO, as the first multi-ton liquid scintillator detector ever built, is facing a wide range of scientific and technological challenges being addressed by a large international team. The Forschungzentrum is already involved in the JUNO project together with RWTH Aachen. The ZEA-2 is leading the effort to develop the smart sensor, the core element of the read-out electronics chain for each of about 20,000 photomultipliers mounted around the JUNO detector. The IKP neutrino group, already a new member of the JUNO collaboration, will enter in this effort. Special attention will be dedicated to the potential of JUNO to measure geoneutrinos.

7.4 Preparation for the TRIC experiment

The TRIC (Time-Reversal Invariance at COSY) is planned as a transmission experiment at the COSY storage ring by using a polarised proton beam and internal tensor polarised deuterium gas target located at the PAX target place of COSY. Information about a possible T-symmetry violation will be extracted from the slope difference for two different configurations of the beam and target polarisations. This demanding experiment requires: excellent understanding of the beam conditions at COSY, high density internal tensor polarized deuterium target, polarimeters for beam and target, and high precision beam current measurement system.
In the fall of 2015 the PAX Atomic Beam Source (ABS) and Breit-Rabi Polarimeter (BRP) were fully commissioned in the laboratory with a polarized deuterium gas. All deuterium states with high polarizations (about 80%) necessary for the realization of the TRIC experiment were prepared and tested using the BRP. Two Fast Current Transformer (FCT) - beam current sensors for bunched beam, produced by the Bergoz company, have been ordered and delivered to the IKP by the Bergoz company in 2015. A precision of better than 10^{-4} for 1 mA of averaged beam current has been shown in the laboratory using FCT readout by the new DAQ system, developed for the TRIC experiment. Hence, all the experimental equipment necessary for the realization of the TRIC project is now available and it is time to proceed with a next step towards the realization of this precision experiment.
Following the decision of the CBAC, two weeks of beam time have been granted for the TRIC experiment in summer of 2016. Aim of the beam time will be: accomplish the commissioning of the polarized proton beam for TRIC, commission target and polarimeter with beam, study the performance of the new beam current measurement system under real beam conditions, and to measure the $A_{Y,Y}$ observable in double polarized proton-deuteron scattering.

8 Theoretical investigations

8.1 Introduction

The IKP theory group studies the strong interactions in their various settings — spanning topics in hadron structure and dynamics, the nuclear many-body problem and symmetry tests in Quantum Chromodynamics (QCD), physics beyond the Standard Model and strongly correlated electron systems. The first focus of the theory group is the formulation and application of effective field theories for precision hadron and nuclear physics based on the symmetries of QCD. The second focus is related to high performance computing in nuclear and hadronic physics, spear-headed by the work on nuclear lattice simulations. Since July 2012, the group is heavily involved in the activities of the collaborative research center "Symmetries and the emergence of structure in QCD" (CRC 110) together with researchers from Bonn University, TU München, IHEP/CAS (Beijing, China), ITP/CAS (Beijing, China) and Peking University (China). Some of the high-lights of these activities are discussed in the following.

8.2 High-precision calculation of the pion-nucleon σ-term

The pion-nucleon (πN) σ-term measures the amount of the nucleon mass that is generated by the two lightest quarks. Since the dominant contribution originates from the energy content of the gluon field, due to the trace anomaly of the QCD energy-momentum tensor, the nucleon mass would only change moderately if the quark masses were turned off. Thus, $\sigma_{\pi N}$ encodes information on the explicit breaking of chiral symmetry and constitutes one of the fundamental low-energy parameters of QCD. In recent years, a precise determination of the σ-term has become increasingly urgent, given its relation to the scalar couplings of the nucleon that are prerequisite for a consistent interpretation of direct-detection dark matter searches.

We have combined two new sources of information on πN scattering that have become available over the last years. First, the measurement of level shifts and decay widths in pionic atoms at PSI has led to a precision determination of the πN scattering lengths. Second, a system of Roy–Steiner (RS) equations has been developed that combines general constraints on the πN scattering amplitude imposed by analyticity, unitarity, and crossing symmetry. The construction proceeds similarly to Roy equations for $\pi\pi$ scattering, where the solution for the low-energy phase shifts can be parameterized in terms of the S-wave scattering lengths. In the case of πN scattering, the construction and solution is complicated by the presence of the crossed channel $\pi\pi \to N\bar{N}$, as well as the increased number of relevant partial waves. At this level of accuracy the impact of isospin-violating corrections cannot be ignored, as demonstrated by the isoscalar πN scattering length. Therefore, we had to revise the Cheng–Dashen low-energy theorem that is used to extract the σ-term from the pion-nucleon scattering data. We have not only solved the corresponding Roy-Steiner integral equations to get the S- and P-wave phase shifts below the so-called matching point, but also have provided a detailed study of the theoretical uncertainties, cf. Fig. 54. This is a major achievement in the determination of the pion-nucleon interaction.

Apart from low-energy phase shifts, the RS solution provides a consistent set of subthreshold parameters. In particular, this allows us to pin down the σ-term from the various terms that appear in the improved Cheng-Dashen low-energy theorem. Putting pieces together, our result for the σ-term is

$$\sigma_{\pi N} = (59.1 \pm 3.5)\ \text{MeV}, \tag{7}$$

Although already 4.2 MeV are due to new corrections to the LET (thereof 3.0 MeV from isospin breaking), we do observe a significant increase compared to the earlier work by the Bern group ($\sigma_{\pi N} \simeq 45$ MeV). This effect can be immediately traced back to our modern knowledge of the πN scattering lengths as extracted from pionic atoms. By combining this information with the constraints from RS equations, the σ-term can be determined to a remarkable accuracy.

We have also determined the scalar couplings of the nucleon, which are of utmost importance for the direct-detection searches of weakly-interacting massive particles (WIMPs) as prominent dark matter candidates. Further, by matching the results of the RS equation to the pion-nucleon amplitudes described by chiral perturbation theory, we could pin down to high accuracy the important dimension two and three low-energy constants that play an important role in the effective field theory description of the forces between two and three nucleons.

8.3 How to reveal the exotic nature of the $P_c(4450)$

The LHCb Collaboration announced two pentaquark-like structures in the $J/\psi p$ invariant mass distribution, denoted as P_c, with masses (widths) of $(4380 \pm 8 \pm 29)$ MeV ($(205 \pm 18 \pm 86)$ MeV) and $(4449.8 \pm 1.7 \pm 2.5)$ MeV ($(39 \pm 5 \pm 19)$ MeV), respectively. Normally, such structures are observed as peaks in invariant mass distributions of certain final states, and fitted by using the Breit–Wigner parameterization to extract the masses and widths. However, such a procedure is problematic. On the one hand, many of these structures are very close to certain thresholds to which they couple strongly. In this case, a use of Breit–Wigner is questionable and one needs to account for the thresholds. This can be achieved using the Flatté parameterization. On the other hand, not every peak should be attributed to the existence of a resonance. In particular, kinematical effects may also show up as peaks. Such kinematical effects correspond to singularities of the S-matrix as well, but they are not

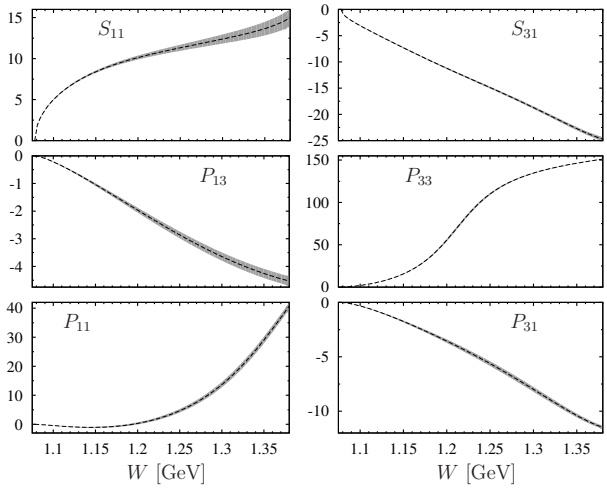

Fig. 54: Phase shifts δ of the s-channel S- and P-partial waves in degrees, obtained from the solution of the RS equations. The dashed line indicates our central solution, the bands the uncertainty estimate. The partial waves are labeled by the spectroscopic notation $L_{2I_s 2J}$, with L the orbital angular momentum, I_s the total s-channel isospin and J the total angular momentum.

poles. In general, they are the so-called Landau singularities including branch points at thresholds and more complicated ones such as the triangle singularity, also called anomalous threshold. We show that the current information on the narrow structure at 4.45 GeV is compatible with kinematical effects of the rescattering from $\chi_{c1}\,p$ to $J/\psi\,p$: First, it is located exactly at the $\chi_{c1}\,p$ threshold: $M_{P_c(4450)} - M_{\chi_{c1}} - M_p = (0.9 \pm 3.1)$ MeV. Second, according to the Coleman–Norton theorem, the singularity of the triangle diagram is in the physical region only when the process can happen classically, which means that all the intermediate states are on shell, and the proton emitted from the decay of the Λ^* moves along the same direction as the χ_{c1} and can catch up with it to rescatter. We find that just at the $\chi_{c1}\,p$ threshold, this condition is fulfilled for the mass of the well-established four-star $\Lambda(1890)$ resonance, see Fig. 55. Further, there is a narrow structure at the $\chi_{c1}\,p$ threshold but not at the $\chi_{c0}\,p$ and $\chi_{c2}\,p$ thresholds. This is consistent with the leading order perturbative QCD arguments. In order to check whether that structure corresponds to a real exotic resonance, one can measure the process $\Lambda_b^0 \to K^-\chi_{c1}\,p$. If the $P_c(4450)$ structure exists in the $\chi_{c1}\,p$ invariant mass distribution as well, then the structure cannot be just a kinematical effect but is a real resonance, otherwise, one cannot conclude the $P_c(4450)$ to be another exotic hadron. In addition, it is also worthwhile to measure the decay $\Upsilon(1S) \to J/\psi\,p\,\bar{p}$: a narrow structure at 4.45 GeV but not at the $\chi_{c0}\,p$ and $\chi_{c2}\,p$ thresholds would exclude the possibility of a pure kinematical effect.

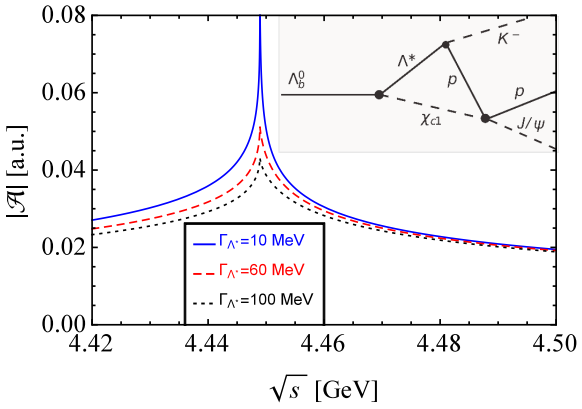

Fig. 55: Absolute values of amplitude corresponding to the triangle diagram (see inset) in arbitrary units. Here, a Λ^* with a mass of 1.89 GeV is exchanged and the solid, dashed and dotted lines correspond to a width of the $\Lambda(1890)$ of 10, 60 and 100 MeV, in order.

8.4 Could the near–threshold XYZ states be simply kinematic effects?

In recent years a large number of structures were discovered in production data with either $Q\bar{Q}$ states or $Q\bar{q}$-$\bar{Q}q$ pairs in the final state close to the thresholds of the latter, where Q ($\bar{Q}$) and q ($\bar{q}$) denote a heavy and a light (anti-)quark, respectively. Examples are the famous $X(3872)$ seen in $J/\psi\pi\pi$, $J/\psi\pi\pi\pi$, $J/\psi\gamma$, $\psi'\gamma$ as well as $D^0\bar{D}^{*0}$ final states, the $Z_b(10610)$ and $Z_b(10650)$ decaying into the $B^{(*)}\bar{B}^*$ open-bottom and $\pi\Upsilon(nS)/\pi h(mP)$ (n = 1,2,3, m = 1,2) hidden-bottom channels and their charmed cousins $Z_c(3900)$ and $Z_c(4020)$ seen $D^{(*)}\bar{D}^*$ as well as $\pi Q\bar{Q}$ channel. Besides other interpretations, the proximity of these states to the mentioned open flavor thresholds suggested that they are either hadronic molecules (bound systems of the mentioned open flavor states) or simply cusps — kinematic effects that necessarily occur at the oping of any S–wave threshold as soon as one loop diagrams contribute significantly that are not connected to any pole of the S–matrix.

In a recent publication we showed that in order to distinguish the signature of a cusp (that appears as the result of a perturbative rescattering process) from that of a pole (that appears as a result of non–perturbative processes either at the level of quark or of hadron dynamics) it is crucial to study the elastic channel — the signal in the channel close to which the pole is located — for only in this channel is it possible to disentangle the contribution from the source term and the contribution from the perturbative, one–loop rescattering as is demonstrated in Fig. 56 on the example of data collected in the $D\bar{D}^*$ channel for the $Z_c(3900)$: the source term, shown as green dotted line, dominates the region beyond the signal while the signal itself is driven by the rescattering which is shown as the solid red line. Once this observation is made all it takes to demonstrate that the $Z_c(3900)$ can not be simply a kinematic effect is to show that the double (=two–loop

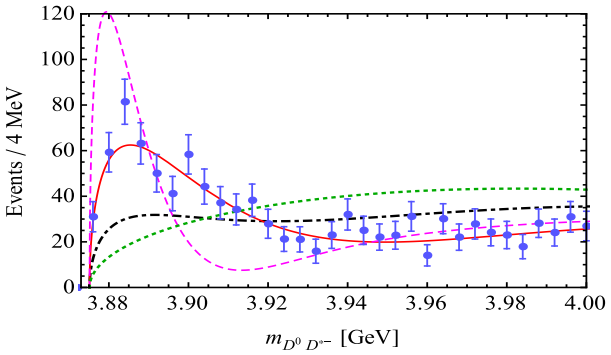

Fig. 56: Results for the $D\bar{D}^*$ invariant mass distribution in $Y(4260) \to \pi D\bar{D}^*$. The data were taken at BESIII and the results from the tree level, full one-loop and full two-loop calculations are shown by the dotted, solid and dashed curves, respectively. The dot–dashed line shows the one-loop result with the strength of the rescattering requested to be small to justify a perturbative treatment as described in the text.

contribution) rescattering is significantly more important than the one–loop rescattering, when calculated using the parameters fixed in the fit including only the source term and the one–loop rescattering as can be seen by the magenta dashed line in Fig. 56. Thus, a perturbative treatment appears to be unjustified.

The argument reversed: if we demand the double scattering to be only half of the single scattering (which would clearly be a boundary case for the application of a perturbative approach) the resulting signal turns out to be as little as shown by the black dot–dashed line. To summarize, on the example of $Z_c(3900)$ we demonstrated that the recently discovered near threshold states can not be the result of a pretrubative rescattering since it takes non–petrubative rescatterings to produce so pronounced narrow structures in the elastic channel. This qualifies these many near threshold states discovered recently as very interesting case studies for the inner workings of QCD.

8.5 Near-threshold enhancement of the $\bar{p}p$ mass spectrum in J/ψ decay

The origin of the enhancement in the antiproton-proton ($\bar{p}p$) mass spectrum at low invariant masses observed in heavy meson decays like $J/\psi \to \gamma\bar{p}p$, $B \to K\bar{p}p$ and $\bar{B} \to D\bar{p}p$, but also in the reaction $e^+e^- \leftrightarrow \bar{p}p$, is an interesting and still controversially discussed issue. In particular, the spectacular near-threshold enhancement in the $\bar{p}p$ invariant mass spectrum for the reaction $J/\psi \to \gamma\bar{p}p$, first observed in a high-statistics and high-mass-resolution experiment by the BES Collaboration has led to numerous publications with speculations about the discovery of a new resonance or of a $\bar{p}p$ bound state (baryonium), and was even associated with exotic glueball states.

However, in the above processes the hadronic final-state interaction (FSI) in the $\bar{p}p$ system should have an influ-

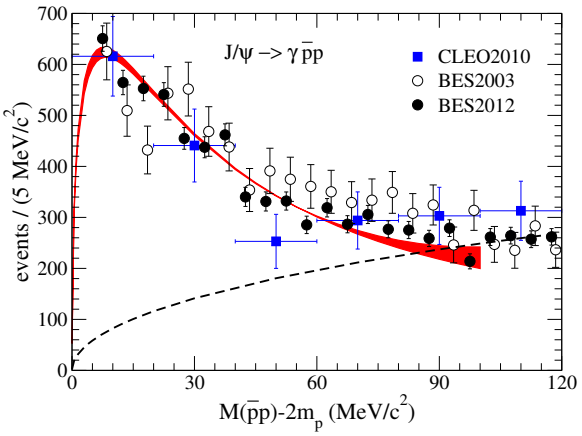

Fig. 57: $\bar{p}p$ invariant mass spectrum for the decay $J/\psi \to \gamma\bar{p}p$. The dashed curve denotes the pure phase space behavior. The band represents our result with inclusion of the $\bar{p}p$ interaction in the final state. The experiments are from the BES and CLEO collaborations.

ence too. Therefore, we performed a systematic analysis of the near threshold enhancement in the reactions $J/\psi \to x\bar{p}p$ and $\psi'(3686) \to x\bar{p}p$ ($x = \gamma, \omega, \rho, \pi, \eta$) with emphasis on the role played by the $\bar{p}p$ interaction. Its aim was to see whether one can achieve a simultaneous and consistent description of all $\bar{p}p$ invariant mass spectra measured in the various reactions based on the $\bar{p}p$ interaction alone.

Our calculation relies on a rigorous treatment of the FSI effects within the distorted wave Born approximation and is, thus, technically superior to past studies with a similar goal. Secondly, it is based on $\bar{p}p$ amplitudes that have been determined from a partial-wave analysis. An exemplary result is shown in Fig. 57. It concerns the reaction $J/\psi \to \gamma\bar{p}p$ where a rather large near-threshold enhancement was observed in the experiments. As can be seen from Fig. 57 this enhancement is nicely explained by the $\bar{p}p$ interaction employed in our study. The enhancements observed in other decays involving the $\bar{p}p$ in the final state are less pronounced, but they are also described quantitatively within our approach.

8.6 Ab initio calculation of α-α scattering

Nuclear lattice simulations have been established as a new quantum many-body method that allows for truely *ab initio* calculation of the properties of atomic nuclei. The method has recently been extended to the calculation of scattering and inelastic processes. In particular, processes involving alpha particles and alpha-like nuclei comprise a major part of stellar nucleosynthesis and hypothesized mechanisms for thermonuclear supernovae. As a first step towards a systematic analysis of these processes, we have performed the first *ab initio* calculation of alpha-alpha scattering, based on the same microscopic Hamiltonian from chiral EFT that was used for the *ab initio* calculation of the Hoyle state in ^{12}C and the structure of ^{16}O. It should be noted that conventional *ab initio* calculations of scattering and reactions suffer from the

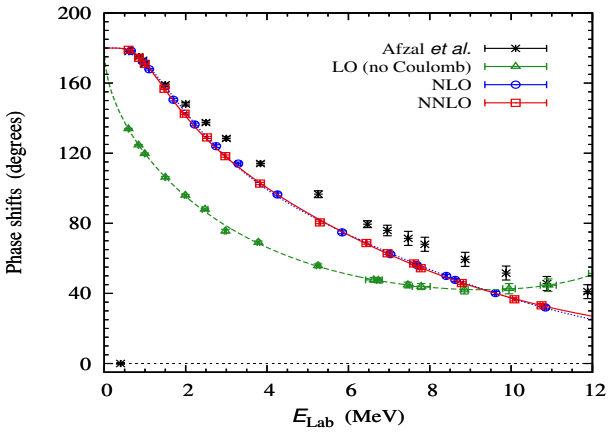

Fig. 58: S-wave phase shifts for low-energy α-α scattering at LO (green triangles), NLO (blue circles) and NNLO (red squares) in comparison with the experimental data (black stars). Note that the effect of the Coulomb interaction is only included at NLO and beyond.

computational scaling with the number of nucleons in the clusters, whereas our lattice EFT approach exhibits a mild, quadratic scaling, that is $t_{\rm CPU} \sim (A_1 + A_2)^2$, with A_i the number of nucleons in cluster i. To be more precise, the calculation of the scattering process proceeds into two steps: First, the so-called adiabatic projection method is used to reduce the eight-body system to an effective two-cluster system. The low-energy effective theory is constructed by generating all two-cluster states with a separation $\vec{R}$ and evolving the corresponding state $|\vec{R}\rangle$ in Euclidean time with the chiral EFT Hamiltonian. This generates the so-called dressed cluster states, where all effects from polarization, the Pauli principle, etc, are included. This gives a systematically improvable description of the low-lying scattering states and it can be shown to become exact in the limit of large Euclidean time. For very large separations, one thus deals with a free (non-interacting) two-cluster system with respect to the strong force but still interacting via the long-range Coulomb force. The scattering phase shifts for such configurations can easily be calculated using the so-called spherical wall method in the second step. While the strong part can be calculated in a lattice volume of about $(16\ {\rm fm})^3$, the long-range electromagnetic interaction is included by matching to asymptotic Coulomb wave functions in a large volume of about $(120\ {\rm fm})^3$. We have calculated the S- and D-wave α-α phase shifts at low energies, these compare well with the data, cf. the S-wave in Fig. 58. Due to the mild computational scaling, the *ab initio* calculation of carbon-carbon fusion or even the holy grail of nuclear astrophysics, $\alpha + {}^{12}{\rm C} \to {}^{16}{\rm O} + \gamma$, is within reach.

8.7 Calculating the Mott gap of carbon nanotubes with lattice Monte Carlo

Carbon nanotubes have proven to be a prime testing ground of our knowledge of quantum many-body physics. Viewed as rolled-up sheets of its parent material graphene, their electronic properties are closely related to those of graphene, and depend on how the graphene sheet has been compactified. In the absence of $e^- - e^-$ interactions, certain nanotube geometries exhibit a linear dispersion in the vicinity of the Dirac points which are characterized by a Fermi velocity of $v_F \sim c/300$, where c is the speed of light in vacuum. This feature contributes to the remarkable electronic properties of nanotubes, and coupled with their excellent mechanical and thermal properties, has spurred interest in using them as a replacement for silicon in future electronic applications.

The low dimensionality of carbon nanotubes provides an excellent enrironment for investigating strong-interaction phenomena. Here the interaction between electrons has non-perturbative effects on the energy dispersion relation of quasi-particles, and in particular, can induce an energy gap at the Dirac point. Using lattice Monte Carlo techniques originally developed within the high-energy particle physics community, we have calculated the energy spectrum of the (3,3) carbon nanotube in the presence of strong-electron interactions. In particular, we find an interaction-induced gap that cannot be attributed to any symmetry-breaking mechanism, e.g. curvature effects. Our results suggest a deviation from a näive scaling with empirical results from larger radii tubes (Fig. 59).

The possibility of comparing our results with empirical measurements at larger radii provides a procedure for determining the strength of electron-electron correlations within these systems, something that is poorly understood theoretically. We are actively pursuing this line of research. Our lattice methods will also allow us to investigate other non-perturbative behavior due to strong electron interactions, such as multi-particle dispersion relations and the effects of background external magnetic fields. This information is necessary for quantifying the behavior of such systems in electronic applications.

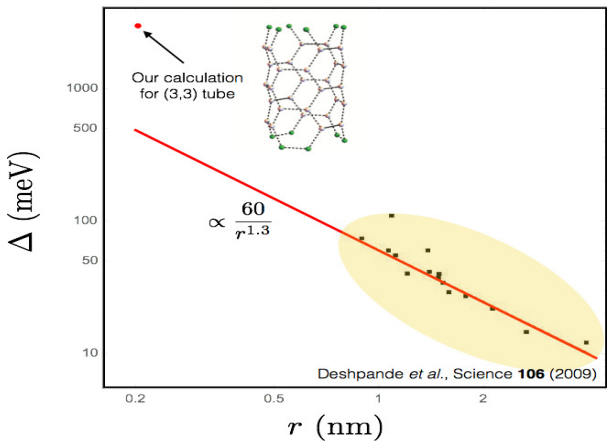

Fig. 59: Interaction-induced Mott gaps Δ as a function of tube radii. Black dots give experimental results, red dot gives lattice result for (3,3) nanotube (uncertainties too small to be seen here).

9

A Councils

A.1 CBAC – COSY Beam Time Advisory Committee

Prof. K. Aulenbacher	Universität Mainz, Germany
Prof. A. Chao	SLAC Stanford, USA
Prof. O. Kester	GSI Darmstadt, Germany
Prof. C.J. Schmidt	GSI Darmstadt, Germany
Prof. E. Steffens	Universität Erlangen-Nürnberg, Germany (Chairperson)
Prof. G. Trubnikov	JINR Dubna, Russia
Prof. M. Weber	KIT, Karlsruhe, Germany

Note: In the committee of Forschungszentrum Jülich, the "Wissenschaftlicher Beirat" (WB, Scientific Council), Prof. Thomas Roser (Brookhaven National Laboratory, USA) is assigned to IKP.

B Publications–journal articles

1. **Measurement of central exclusive $\pi^+\pi^-$ production in $p\bar{p}$ collisions at $\sqrt{s} = 0.9$ and 1.96 TeV at CDF**
   T. Aaltonen *et al.*
   Phys. Rev. D **91** 091101 (2015)

2. **Impact of the phonon coupling on the photon strength function**
   O. Achakovskiy *et al.*
   Phys. Rev. C **91** 034620 (2015)

3. **Θ -dependence of the lightest meson resonances in QCD**
   N.R. Acharya *et al.*
   Phys. Rev. D **92** 054023 (2015)

4. **ABC effect and resonance structure in the double-pionic fusion to ^{3}He**
   P. Adlarson *et al.*
   Phys. Rev. C **91** 015201 (2015)

5. **Measurement of the $np \to np\pi^0\pi^0$ reaction in search for the recently observed $d^*(2380)$ resonance**
   P. Adlarson *et al.*
   Phys. Lett. B **743** 325 - 332 (2015)

6. **A Gas Target Internal to the LHC for the Study of pp Single-Spin Asymmetries and Heavy Ion Collisions**
   C. Barschel *et al.*
   Adv. High Energy Phys. **2015** 1 - 6 (2015)

7. **Remarks on study of $X(3872)$ from effective field theory with pion-exchange interaction**
   V. Baru *et al.*
   Phys. Rev. D **91** 034002 (2015)

8. **Binding energy of the $X(3872)$ at unphysical pion masses**
   V. Baru *et al.*
   Phys. Rev. D **92** 114016 (2015)

9. **Analysis Tools for Next-Generation Hadron Spectroscopy Experiments**
   M. Battaglieri *et al.*
   Act. Phys. Pol. B **46** 257 - (2015)

10. **Ab initio Lattice Results for Fermi Polarons in Two Dimensions**
    S. Bour *et al.*
    Phys. Rev. Lett. **115** 185301 (2015)

11. **Nuclear reactions from lattice QCD**
    R.A. Briceño, Z. Davoudi and T. Luu
    J. Phys. G **42** 023101 - (2015)

12. **Features of cooling dynamics in a high-voltage electron cooling system of the COSY**
    M.I. Bryzgunov *et al.*
    Tech. Phys. **60** 1227 - 1233 (2015)

13. **Nuclear electric dipole moments in chiral effective field theory**
    J. Bsaisou *et al.*
    J. High Energ. Phys. **2015** 104 (2015)

14. **Erratum to: Nuclear electric dipole moments in chiral effective field theory**
    J. Bsaisou *et al.*
    J. High Energ. Phys. **2015** 83 (2015)

15. **P- and T-violating Lagrangians in chiral effective field theory and nuclear electric dipole moments**
    J. Bsaisou *et al.*
    Ann. Phys. **359** 317 - 370 (2015)

16. **Investigation of the Deuteron Breakup on Proton Target in the Forward Angular Region at 130 MeV**
    I. Ciepal *et al.*
    Few-body systems **56** 665 - 690 (2015)

17. **Coulomb Force Effects in Deuteron–Proton Breakup Reaction**
I. Ciepal *et al.*
Act. Phys. Pol. B **46** 459 - (2015)

18. **Employing spin symmetry to disentangle different models for the X Y Z states**
M. Cleven *et al.*
Phys. Rev. D **92** 014005 (2015)

19. **Thermal properties of hot and dense matter with finite range interactions**
C. Constantinou *et al.*
Phys. Rev. C **92** 025801 (2015)

20. **Degenerate limit thermodynamics beyond leading order for models of dense matter**
C. Constantinou *et al.*
Ann. Phys. **363** 533 - 555 (2015)

21. **Parity violation in neutron capture on the proton: Determining the weak pion-nucleon coupling**
J. de Vries *et al.*
Phys. Lett. B **747** 299 - 304 (2015)

22. **Baryon mass splittings and strong CP violation in SU(3) chiral perturbation theory**
J. de Vries, E. Mereghetti and A. Walker-Loud
Phys. Rev. C **92** 045201 (2015)

23. **Complex-mass renormalization in hadronic EFT: Applicability at two-loop order**
D. Djukanovic *et al.*
Eur. Phys. J. A **51** 101 (2015)

24. **A Monte-Carlo simulation of the equilibrium beam polarization in ultra-high energy electron (positron) storage rings**
Z. Duan *et al.*
Nucl. Instr. Meth. Phys. Res. A **793** 81 - 91 (2015)

25. **Analysing powers and spin correlations in deuteron-proton charge exchange at 726 MeV**
S. Dymov *et al.*
Phys. Lett. B **744** 391 - 394 (2015)

26. **Ab initio alpha-alpha scattering**
S. Elhatisari *et al.*
Nature **528** 111 - 114 (2015)

27. **Baryon chiral perturbation theory extended beyond the low-energy region**
E. Epelbaum *et al.*
Eur. Phys. J. C **75** 499 (2015)

28. **Improved chiral nucleon-nucleon potential up to next-to-next-to-next-to-leading order**
E. Epelbaum, H. Krebs and U. Meißner
Eur. Phys. J. A **51** 53 (2015)

29. **Precision Nucleon-Nucleon Potential at Fifth Order in the Chiral Expansion**
E. Epelbaum, H. Krebs and U. Meißner
Phys. Rev. Lett. **115** 122301 (2015)

30. **New Method for a Continuous Determination of the Spin Tune in Storage Rings and Implications for Precision Experiments**
D. Eversmann *et al.*
Phys. Rev. Lett. **115** 094801 (2015)

31. **Study of the $p\,\vec{d}\to n\{pp\}_s$ charge-exchange reaction using a polarised deuterium target**
B. Gou *et al.*
Phys. Lett. B **741** 305 - 309 (2015)

32. **Search for Polarization Effects in the Antiproton Production Process**
D. Grzonka *et al.*
Act. Phys. Pol. B **46** 191 - (2015)

33. **Electric Dipole Moment of the Neutron from 2 + 1 Flavor Lattice QCD**
F. Guo *et al.*
Phys. Rev. Lett. **115** 062001 (2015)

34. **What can radiative decays of the $X(3872)$ teach us about its nature?**
F. Guo *et al.*
Phys. Lett. B **742** 394 - 398 (2015)

35. **Could the near-threshold X Y Z states be simply kinematic effects?**
F. Guo *et al.*
Phys. Rev. D **91** 051504 (2015)

36. **Cumulants of the QCD topological charge distribution**
F. Guo and U. Meißner
Phys. Lett. B **749** 278 - 282 (2015)

37. **How to reveal the exotic nature of the $Pc(4450)$**
F. Guo *et al.*
Phys. Rev. D **92** 071502 (2015)

38. **Production of the spin partner of the $X(3872)$ in e^+e^- collisions**
F. Guo, U. Meißner and Z. Yang
Phys. Lett. B **740** 42 - 45 (2015)

39. **New insights into the D s 0 * (2317) and other charm scalar mesons**
Z. Guo, U. Meißner and D. Yao
Phys. Rev. D **92** 094008 (2015)

40. **ψ (3770) resonance and its production in $\overline{p}p \to D\overline{D}$**
J. Haidenbauer and G. Krein
Phys. Rev. D **91** 114022 (2015)

41. **A study of hyperons in nuclear matter based on chiral effective field theory**
J. Haidenbauer and U. Meißner
Nucl. Phys. A **936** 29 - 44 (2015)

42. **Do $\Xi\Xi$ bound states exist?**
J. Haidenbauer, U. Meißner and S. Petschauer
Eur. Phys. J. A **51** 17 (2015)

43. **Origin of the structures observed in e^+e^- annihilation into multipion states around the $\overline{p}p$ threshold**
J. Haidenbauer *et al.*
Phys. Rev. D **92** 054032 (2015)

44. **Practical Parametrization for Line Shapes of Near-Threshold States**
C. Hanhart *et al.*
Phys. Rev. Lett. **115** 202001 (2015)

45. **Erratum to: Dispersive analysis for $\eta \to \gamma\gamma^*$**
C. Hanhart *et al.*
Eur. Phys. J. C **75** 242 (2015)

46. **High-Precision Determination of the Pion-Nucleon σ Term from Roy-Steiner Equations**
M. Hoferichter *et al.*
Phys. Rev. Lett. **115** 092301 (2015)

47. **Matching Pion-Nucleon Roy-Steiner Equations to Chiral Perturbation Theory**
M. Hoferichter *et al.*
Phys. Rev. Lett. **115** 192301 (2015)

48. **$\overline{K}+N \to K+\Xi$ reaction and S = - 1 hyperon resonances**
B.C. Jackson *et al.*
Phys. Rev. C **91** 065208 (2015)

49. **Near-threshold $\overline{p}p$ invariant mass spectrum measured in J/ψ and ψ' decays**
X. Kang, J. Haidenbauer and U. Meißner
Phys. Rev. D **91** 074003 (2015)

50. **Kaon pair production in proton-nucleus collisions at 2.83 GeV kinetic energy**
Y.T. Kiselev *et al.*
Phys. Rev. C **92** 065201 (2015)

51. **Regularization methods for Nuclear Lattice Effective Field Theory**
N. Klein *et al.*
Phys. Lett. B **747** 511 - 516 (2015)

52. **Uncertainties of Euclidean time extrapolation in lattice effective field theory**
T. Lähde *et al.*
J. Phys. G **42** 034012 - (2015)

53. **Nuclear Lattice Simulations using Symmetry-Sign Extrapolation**
T. Lähde *et al.*
Eur. Phys. J. A **51** 92 (2015)

54. **Study of $B^{\pm,0} \to J/\psi K^+ K^- K^{\pm,0}$ and search for $B^0 \to J/\psi\varphi$ at BaBar**
J. Lees *et al.*
Phys. Rev. D **91** 012003 (2015)

55. **New structures in the proton-antiproton system**
I. Lorenz, H. Hammer and U. Meißner
Phys. Rev. D **92** 034018 (2015)

56. **Theoretical constraints and systematic effects in the determination of the proton form factors**
I. Lorenz *et al.*
Phys. Rev. D **91** 014023 (2015)

57. **Breaking and restoration of rotational symmetry for irreducible tensor operators on the lattice**
B. Lu *et al.*
Phys. Rev. D **92** 014506 (2015)

58. **Isoscalar and isovector giant resonances in a self-consistent phonon coupling approach**
N. Lyutorovich *et al.*
Phys. Lett. B **749** 292 - 297 (2015)

59. **Intermediate mass fragment emission in 32S + 51V, 109Ag, and 238U collisions at E = 31.6 MeV A**
H. Machner *et al.*
Eur. Phys. J. A **51** 146 (2015)

60. **Constraints on the chiral unitary $\bar{K}N$ amplitude from $\pi\Sigma K^+$ photoproduction data**
M. Mai and U. Meißner
Eur. Phys. J. A **51** 30 (2015)

61. **Charmante Pentaquarks?**
U. Meißner
Phys. J. **14** 21-22 (2015)

62. **Anthropic considerations in nuclear physics**
U. Meißner
Sci. Bull. **60** 43 - 54 (2015)

63. **Testing the $\chi_{c1}\,p$ composite nature of the $P_c(4450)$**
U. Meißner and J.A. Oller
Phys. Lett. B **751** 59 - 62 (2015)

64. **Spectrum of Three-Body Bound States in a Finite Volume**
U. Meißner, G. Ríos and A. Rusetsky
Phys. Rev. Lett. **114** 091602 (2015)

65. **Refined analysis on the $X(3872)$ resonance**
C. Meng *et al.*
Phys. Rev. D **92** 034020 (2015)

66. **Non-resonant kaon pair production and medium effects in proton-nucleus collisions**
E.Y. Paryev, M. Hartmann and Y.T. Kiselev
J. Phys. G **42** 075107 - (2015)

67. **Predictions for the$\vec{\Lambda}_b \to J/\psi\,\Lambda(1405)$decay**
L. Roca *et al.*
Eur. Phys. J. C **75** 218 (2015)

68. **Eta photoproduction in a combined analysis of pion- and photon-induced reactions**
D. Rönchen *et al.*
Eur. Phys. J. A **51** 70 (2015)

69. **Erratum to: Photocouplings at the pole from pion photoproduction**
D. Rönchen *et al.*
Eur. Phys. J. A **51** 63 (2015)

70. **Determination of the COSY Proton Beam Polarization Using the WASA Detector**
I. Schätti-Ozerianska, P. Moskal and M. Zieli´nski
Act. Phys. Pol. B **46** 153 - (2015)

71. **Energy spectra of two interacting fermions with spin-orbit coupling in a harmonic trap**
C.D. Schillaci and T. Luu
Phys. Rev. A **91** 043606 (2015)

72. **Exact calculations of a quasibound state in the $\overline{KK}N$ system**
N.V. Shevchenko and J. Haidenbauer
Phys. Rev. C **92** 044001 (2015)

73. **Nucleon electric dipole moment with the gradient flow: The Θ -term contribution**
A. Shindler, T. Luu and J. de Vries
Phys. Rev. D **92** 094518 (2015)

74. **Experimental access to Transition Distribution Amplitudes with the $\overline{\mathrm{P}}$ANDA experiment at FAIR**
B.P. Singh *et al.*
Eur. Phys. J. A **51** 107 (2015)

75. **Heavy ion storage and acceleration in the HESR with stochastic cooling and internal target**
H. Stockhorst *et al.*
Phys. Scr. **T166** 014041 - (2015)

76. **Simulating Trajectories of Hydrogen and Deuterium Atoms in Polarized Sources**
A.A. Vasilyev *et al.*
Izv. Vyssh. Uchebn. Zaved., Priborostr. **12** 1008 - 1015 (2015)

77. **Photoproduction of hidden charm pentaquark states P c + (4380) and P c + (4450)**
Q. Wang, X. Liu and Q. Zhao
Phys. Rev. D **92** 034022 (2015)

78. **Toward polarized antiprotons: Machine development for spin-filtering experiments**
C. Weidemann *et al.*
Phys. Rev. ST Accel. Beams **18** 020101 (2015)

79. **States generated in the K -multi- ρ interactions**
C. Xiao
Phys. Rev. D **92** 054011 (2015)

80. **$J/\psi(\eta_c)N$ and $\Upsilon(\eta_b)N$ cross sections**
C. Xiao and U. Meißner
Phys. Rev. D **92** 114002 (2015)

81. **One-loop analysis of the interactions between charmed mesons and Goldstone bosons**
D. Yao *et al.*
J. High Energ. Phys. **2015** 58 (2015)

82. **Multidimensionally constrained relativistic Hartree-Bogoliubov study of spontaneous nuclear fission**
J. Zhao *et al.*
Phys. Rev. C **92** 064315 (2015)

83. **Multidimensionally constrained relativistic mean-field study of triple-humped barriers in actinides**
J. Zhao *et al.*
Phys. Rev. C **91** 014321 (2015)

C Talks and colloquia

C.1 Conference and workshop contributions

1. O. Achakovskiy *et al.*
   Microscopic nature of the photon strength function: stable and unstable Ni and Sn isotopes
   CGS15-Capture Gamma-Ray Spectroscopy and Related Topics, Dresden, Germany: 2014-08-25 - 2014-08-29

2. M. Bai
   Accelerator Physics Challenges in Electric Dipole Moment Measurements
   European Physical Society High Energy Physics conference, Vienna, Austria: 2015-07-22 - 2015-07-29

3. M. Bai
   High Energy Polarized Beams Status and Challenges
   The 2015 International Workshop on Polarized Sources, Targets & Polarimetry, Bochum, Deutschland: 2015-09-14 - 2015-09-18

4. L. Bianchi *et al.*
   Online tracking with GPUs at the PANDA Experiment
   DPG-Frühjahrstagung, Heidelberg, Germany: 2015-03-23 - 2015-03-27

5. L. Bianchi *et al.*
   Online Tracking with GPUs at PANDA
   21st International Conference on Computing in High Energy and Nuclear Physics (CHEP2015), OIST, Okinawa, Japan: 2015-04-13 - 2015-04-17

6. L. Bianchi *et al.*
   Online Tracking Algorithms on GPUs for the $\overline{\text{P}}$ANDA Experiment at FAIR
   J. Phys.: Conf. Ser. **664** 082006 - (2015)

7. C. Böhme *et al.*
   Studies for a BPM Upgrade at COSY
   International Beam Instrumentation Conference, Melbourne, Australia: 2015-09-13 - 2015-09-17

8. L. Cao, J. Ritman and PANDA-Collaboration
   Simulation of D_s semileptonic decay with the PANDA detector
   DPG-Frühjahrstagung, Heidelberg, Germany: 2015-03-23 - 2015-03-27

9. M. Cleven *et al.*
   The nature of near-threshold XYZ states
   The 10th International Workshop on the Physics of Excited Nucleons, Osaka, Japan: 2015-05-25 - 2015-05-28

10. C. Constantinou
    Thermal and Adiabatic Indices in Binary Mergers
    Workshop on Binary Star Mergers, Thessaloniki, Greece: 2015-05-27 - 2015-05-29

11. C. Constantinou
    Thermal Properties of Dense MatterThe Homogeneous Phase
    Workshop on Microphysics In Computational Relativistic Astrophysics, Stockholm, Sweden: 2015-08-17 - 2015-08-21

12. M.G. Endres *et al.*
Photon mass term as an IR regularization for QCD+QED on the lattice
33rd International Symposium on Lattice Field Theory, Kobe, Japan: 2015-07-14 - 2015-07-18
arXiv:1512.08983

13. S. Esch and PANDA-Collaboration
Gruppenbericht: The Micro Vertex Detector for the PANDA Experiment
DPG-Frühjahrstagung, Heidelberg, Germany: 2015-03-23 - 2015-03-27

14. A. Gillitzer
Antiproton Nucleus Collisions
PANDA LV. Collaboration Meeting, Vienna, Austria: 2015-11-30 - 2015-12-04

15. A. Gillitzer
Baryon Spectroscopy
PANDA LV. Collaboration Meeting, Vienna, Austria: 2015-11-30 - 2015-12-04

16. A. Gillitzer
Hadrons in Nuclei - What Can Be Done with PANDA?
Workshop "PANDA Physics Perspective at Stefan-Meyer-Institut", Vienna, Austria: 2015-02-19 - 2015-02-20

17. A. Gillitzer
Excited Hyperons at PANDA
EMMI Workshop "Resonances in QCD", Darmstadt, Germany: 2015-10-12 - 2015-10-14

18. A. Gillitzer
Antiproton Nucleus Collisions at PANDA
EMMI Workshop "Cold Dense Nuclear Matter", Darmstadt, Germany: 2015-10-13 - 2015-10-17

19. D. Gotta *et al.*
Pionic hydrogen and friends
International conference on exotic atoms, Vienna, Austria: 2014-09-15 - 2014-09-19
Hyperfine Interact. 234 105 - 111

20. D. Gotta
Remarks on a Johann spectrometer for exotic-atom research and more
colloquium spectroscopicum internationale XXIX, Figueira da Foz, Portugal: 2015-08-30 - 2015-09-03

21. G. Guidoboni on behalf of the JEDI Col
Spin coherence time studies of a horizontally polarized deuteron beam at COSY
Phys. Scr. **T166** 014036 (2015)

22. J. Haidenbauer
Hyperons in nuclear matter studied in chiral EFT
The 8th International Workshop on Chiral Dynamics 2015, Pisa, Italy: 2015-06-29 - 2015-07-03

23. J. Haidenbauer
Baryon-baryon interaction from chiral effective field theory
The 12th International Conference on Hypernuclear and Strange Particle Physics, Sendai, Japan: 2015-09-07 - 2015-09-12

24. J. Haidenbauer
DN and $\bar{K}N$ interactions with the Jülich meson-exchange model
ELPH Workshop C013 "Meson Production and Meson-Baryon Interaction", Sendai, Japan: 2015-09-12 - 2015-09-14

25. C. Hanhart
Hadron spectroscopy with light and heavy quarks
Arbeitstreffen Kernphysik, Schleching, Germany: 2015-02-19 - 2015-02-26

26. C. Hanhart
Remarks about Resonances
Hadron spectroscopy with light and heavy quarks, Jinan, China: 2015-06-07 - 2015-06-12

27. C. Hanhart
Theoretical description of resonance production
Photon 2015, Novosibirsk, Russia: 2015-06-15 - 2015-06-19

28. C. Hanhart
Amplitude Analysis for Mesons and Baryons: Tools and Technology
XVI International Conference on Hadron Spectroscopy, Neport News, VA, USA: 2015-09-13 - 2015-09-18

29. C. Hanhart
Z states as molecules (and related topics)
Workshop on Z states, Gießen, Germany: 2015-07-07 - 2015-07-07

30. C. Hanhart
Remarks about Resonances
International Conference on the Structure and the Interactions of the Photon, Novosibirsk, Russia: 2015-06-15 - 2015-06-19

31. Y. Hao *et al.*
Experimental Demonstration of an Interaction Region Beam Waist Position Knob for Luminosity Leveling
International Particle Accelerator Conference, Richmond, USA: 2015-05-03 - 2015-05-08

32. F. Hauenstein
Hadron Physics at COSY
CLAS12 - 4th European Workshop, INFN Catania, Italy: 2015-02-17 - 2015-02-20

33. F. Hauenstein
Strangeness Production at COSY
HYP2015: 12th International Conference on Hypernuclear and Strange Particle Physics, Tohoku University, Sendai, Japan: 2015-09-07 - 2015-09-12

34. F. Hauenstein
Two-pion Production Reactions and the Observation of the d*(2380) Dibaryon
ELPH workshop C013 "Meson Production and Meson-Baryon Interaction", Tohoku University, Sendai, Japan: 2015-09-12 - 2015-09-14

35. F. Hauenstein and COSY-TOF-Collaboration
Determination of the Spin Triplet $p\Lambda$ Scattering Length from the Reaction $pp \to pK\Lambda$
DPG-Frühjahrstagung, Heidelberg, Germany: 2015-03-23 - 2015-03-27

36. V. Hejny
Measurement of Electric Dipole Moments of Charged Particles at Storage Rings
DPG-Frühjahrstagung Heidelberg 2015, Heidelberg, Germany: 2015-03-23 - 2015-03-27

37. V. Hejny
Polarimetry for monitoring long coherent spin precession and polarisation based feedback
Beam Dynamics meets Diagnostics, Florence, Italy: 2015-11-04 - 2015-11-06

38. N. Hempelmann
FPGA-Based Upgrade of the Read-Out Electronics for the Low Energy Polarimeter at the Cooler Synchrotron
DPG Frühjahrstagung Hadronen und Kerne, Heidelberg, Germany: 2015-03-23 - 2015-03-27

39. N. Hempelmann
FPGA-Based Upgrade of the Read-Out Electronics for the Low Energy Polarimeter at COSY/Jülich
The 2015 International Workshop on Polarized Sources, Targets & Polarimetry, Bochum, Germany: 2015-09-14 - 2015-09-18

40. N. Hempelmann
FPGA-Based Upgrade of the Read-Out Electronics for the Low Energy Polarimeter at COSY/Jülich
The 2015 International Workshop on Polarized Sources, Targets & Polarimetry, Bochum, Germany: 2015-09-14 - 2015-09-18

41. A. Herten
Introduction to Analysis with PandaRoot
LIV. PANDA Meeting, GSI Darmstadt, Germany: 2015-09-07 - 2015-09-11

42. A. Herten
GPU-based Online Track Reconstruction for PANDA and Application to the Analysis of $D \to K\pi\pi$
LIV. PANDA Meeting, GSI Darmstadt, Germany: 2015-09-07 - 2015-09-11

43. A. Herten
GPU-based Online Tracking for the PANDA Experiment.
GPU Computing in High-Energy Physics Conference 2014 GPUHEP2014, Pisa, Italy: 2014-09-10 - 2014-09-12

44. A. Herten
Opportunities in open charm physics with PANDA
2015 European Nuclear Physics Conference, EuNPC2015, Martiniplaza, Groningen, The Netherlands: 2015-08-31 - 2015-09-04

45. J. Hetzel, U. Bechstedt and J. Böker
Influence of the Manufacturing Process on the Harmonic Content of the HESR Quadrupoles
Intrnational Conference on Magnet Technology 24, Seoul, Korea: 2015-10-18 - 2015-10-23

46. J. Hetzel *et al.*
Inclusion of the Multipole Components in Beam Dynamics Simulations for the HESR
DPG Frühjahrstagung, Wuppertal, Germany: 2015-03-09 - 2015-03-13

47. Q. Hu, H. Xu and J. Ritman
Commissioning of the KOALA Experiment by Proton Beam at COSY
DPG-Frühjahrstagung, Heidelberg, Germany: 2015-03-23 - 2015-03-27

48. V. Kamerdzhiev *et al.*
Performance of the 2 MeV Electron Cooler at COSY
International Workshop on Beam Cooling and Related Topics, Newport News, USA: 2015-09-28 - 2015-10-02

49. T. Katayama *et al.*
Antiproton chain of the FAIR storage rings
Phys. Scr. **T166** 014073 - (2015)

50. A. Khoukaz *et al.*
Recent results from ANKE, WASA-at-COSY, and PAX
Phys. Scr. **T166** 014014 (2015)

51. S. Krewald
Nuclear Physics in Juelich
Workshop Struttura nucleare e reazioni, Lecce, Italy: 2015-11-06 - 2015-11-06

52. B. Kubis, J.R. de Elvira, M. Hoferichter and U.-G. Meißner
"Pion-nucleon scattering: from chiral perturbation theory to Roy-Steiner equations," The 8th International Workshop on Chiral Dynamics (CD 2015), Pisa, Italy: July 2015, PoS(CD15)021.

53. M.C. Kunkel
Light Meson Decays from Photon-Induced Reactions with CLAS
GHP Conference, Baltimore, MD, USA: 2015-04-08 - 2015-04-10

54. M.C. Kunkel
Light Meson Decays in CLAS
CLAS Collaboration Workshop, Catania, Italy: 2015-02-17 - 2015-02-20

55. M.C. Kunkel
Regge Theory Application to CLAS g12 data
2015 International Summer Workshop on Reaction Theory, Bloomington, Indiana, USA: 2015-06-08 - 2015-06-19

56. M.C. Kunkel and CLAS-Collaboration
Light Meson Decays from Photon-Induced Reactions with CLAS
DPG Frühjahrstagung, Heidelberg, Germany: 2015-03-23 - 2015-03-27

57. A. Lehrach
Challenges in optics requirement and control of storage ring for precision measurement of EDM
EuCARD2-ICFA workshop "Advanced Optics Control, Cern, Geneve, Schweiz: 2015-02-05 - 2015-02-06

58. A. Lehrach
Beam and Spin Dynamics for Charged Particle EDM Searches in Storage Rings
EUCARD workshop "Search for the electron EDM in an electrostatic storage ring", Mainz, Germany: 2015-09-11 - 2015-09-11

59. A. Lehrach
Beam and Spin Dynamics for Storage Ring Based EDM Search
Sixth International Particle Accelerator Conference, R, Germany: 2015-05-03 - 2015-05-08

60. A. Lehrach
Searching electric dipole moments in storage rings – challenges, status and computational needs
International Computational Accelerator Physics Conference, Shanghai, China: 2015-10-12 - 2015-10-16

61. D. Lersch
The η-meson decay program at WASA-at-COSY
2015 European Nuclear Physics Conference, EuNPC2015, Martiniplaza, Groningen, The Netherlands: 2015-08-31 - 2015-09-04

62. D. Lersch and WASA-at-COSY-Collaboration
Analysis of η-Meson Decays from the WASA Campaign at COSY
DPG-Frühjahrstagung, Heidelberg, Germany: 2015-03-23 - 2015-03-27

63. B. Lorentz *et al.*
Antiproton Acceleration and Deceleration in the HESR
6th International Particle Accelerator Conference, Richmond, VA, USA: 2015-05-03 - 2015-05-08

64. S. Lu *et al.*
Study of 2.13GeV Cusp in $p+p \to p+K^{+}+\Lambda$ with Partial wave Analysis using Flatté distribution.
DPG Frühjahrstagung, Heidelberg, Germany: 2015-03-23 - 2015-03-27

65. U.-G. Meißner
"Dispersion relations and the proton radius," Fundamental Constants Meeting 2015, Eltville, Germany: February 2015

66. U.-G. Meißner
"Chiral nuclear dynamics," invited talk, CRC 634 – Concluding Conference, Darmstadt, Germany: June 2015

67. U.-G. Meißner
"Clustering in nuclei from ab initio nuclear lattice simulations," invited lead parallel session talk, The 8th International Workshop on Chiral Dynamics (CD 2015), Pisa, Italy: July 2015, PoS(CD15)038.

68. U.-G. Meißner
"Alpha-cluster physics from ab initio nuclear lattice simulations," Workshop on "Clusters in Nuclear Systems," Rostock, Germany: August 2015

69. U.-G. Meißner
"Musings about pentaquarks," Workshop on "Frontiers in hadron and nuclear physics with strangeness and charm," ECT*, Trento, Italy
October 2015

70. S. Mey
An RF Wien Filter as Spin Manipulator
Matter and Technologies Student Retreat, DESY, Hamburg, Germany: 2015-02-23 - 2015-02-24

71. S. Mey
High Precision Spin Manipulation at COSY
Matter and Technologies Kickoff Meeting, DESY, Hamburg, Germany: 2015-02-23 - 2015-02-26

72. S. Mey and R. Gebel
Towards an RF Wien-Filter for EDM Searches in Storage Rings
DPG-Frühjahrstagung der Sektionen Didaktik der Physik, Extraterrestrische Physik, Strahlen- und Medizinphysik, Teilchenphysik und des Arbeitskreises Beschleunigerphysik, Wuppertal, Germany: 2015-03-09 - 2015-03-13

73. S. Mey and R. Gebel
Towards an RF Wien-Filter for EDM Experiments at COSY
6th International Particle Accelerator Conference, Richmond, VA, USA: 2015-05-03 - 2015-05-08

74. S. Mey and R. Gebel
Towards an RF Wien-Filter for EDM Experiments at COSY
6th International Particle Accelerator Conference, Richmond, VA, USA: 2015-05-03 - 2015-05-08

75. S. Mey and R. Gebel
Spin Manipulation with an RF Wien-Filter at COSY
XVIth International Workshop in Polarized Sources, Targets, and Polarimetry, Bochum, Germany: 2015-09-14 - 2015-09-18

76. R. Münzer *et al.*
Analysis of the reaction $p+p \rightarrow p+K^{+}+\Lambda$ with Partial Waves*
DPG Frühjahrstagung, Heidelberg, Germany: 2015-03-23 - 2015-03-27

77. A. Nogga
Light nuclei including hypernuclei - Role of few-body forces
7th Bethe Center Workshop on "Challenges in Strong Interaction Physics", Bad Honnef, Germany: 2015-09-29 - 2015-10-02

78. H. Ohannessian, P. Wintz and J. Ritman
Spatial and Energy-loss Measurements of a PANDA STT Prototype
DPG-Frühjahrstagung, Heidelberg, Germany: 2015-03-23 - 2015-03-27

79. E. Prencipe
Search for exotics at BABAR
3rd International Conference on New Frontiers in Physics (ICNFP 2014), Kolymbari, Crete, Greece: 2015-07-28 - 2015-08-06
Eur. Phys. J. Web of Conferences 95 01012 -

80. E. Prencipe
Hadrons with c-s content: present, past, and future
53rd International Winter Meeting on Nuclear Physics (Bormio 2015), Bormio, Italy: 2015-01-26 - 2015-01-30

81. E. Prencipe
Challenges in open-charm physics with PANDA
XLVI. Arbeitstreffen Kernphysik, Schleching, Germany: 2015-02-19 - 2015-02-26

82. E. Prencipe
New spectroscopy with PANDA at FAIR
HADRON2015 XVI International Conference on Hadron Spectroscopy, Newport News, Virginia, USA: 2015-09-13 - 2015-09-18

83. E. Prencipe
Planned measurement of the width of the Ds(2317)
EMMI Rapid Reaction Task Forces - Resonances in QCD, GSI Darmstadt, Germany: 2015-10-12 - 2015-10-14

84. E. Prencipe
X Y Z states at PANDA

EMMI Rapid Reaction Task Force: Resonances in QCD, GSI Darmstadt, Germany: 2015-10-12 - 2015-10-14

85. E. Prencipe
XYZ rates at PANDA
LIV. PANDA Meeting, GSI Darmstadt, Germany: 2015-09-07 - 2015-09-11

86. E. Prencipe, C. BaBar and C. Belle
Search for exotic charmonium states
12th International Conference on Heavy Quarks and Leptons (HQL 2014), Mainz, Germany: 2014-08-25 - 2014-08-29

87. E. Prencipe *et al.*
Open-charm Physics Opportunities at PANDA
DPG-Frühjahrstagung, Heidelberg, Germany: 2015-03-23 - 2015-03-27

88. E. Prencipe and C. PANDA
Hadrons with c-s content: past, present and future
53rd International Winter Meeting on Nuclear Physics (Bormio 2015), Bormio, Italy: 2015-01-26 - 2015-01-30

89. E. Prencipe *et al.*
Kalman Filter based algorithms for PANDA@ FAIR
DPG-Frühjahrstagung, Heidelberg, Germany: 2015-03-23 - 2015-03-27

90. E. Prencipe and BaBar-Collaboration
Search for exotics in the rare decay $B \to J/\psi KKK$ at BABARBa
Eur. Phys. J. Web of Conferences **95** 05012 - (2015)

91. E. Prencipe and PANDA-Collaboration
Perspectives of open charm physics at $\overline{\text{P}}$ANDA
Eur. Phys. J. Web of Conferences **95** 04052 - (2015)

92. J. Pretz on behalf of the JEDI collaboration
Measurement of electric dipole moments at storage rings
Phys. Scr. **T166** 014035 (2015)

93. F. Rathmann
Challenges of Electric Dipole Moment searches using Storage Rings
Beam Dynamics meets Diagnostics, Florence, Italy: 2015-11-04 - 2015-11-06

94. K. Reimers *et al.*
Upgrade of the Beam Profile Monitoring System in the Injection Beam Line of COSY
IBIC 2015, Melbourne, Australia: 2015-09-13 - 2015-09-17

95. J. Ritman
Hadron Physics with Antiprotons at PANDA/FAIR
International Review of FAIR, GSI Darmstadt, Germany: 2015-02-16 - 2015-02-17

96. J. Ritman
What Can We Learn About Hadron Spectroscopy With Antiproton Annihilation?
International Conference on Hadron and Nuclear Physics 2015, Krabi, Thailand: 2015-07-07 - 2015-07-11

97. J. Ritman
Role of IKP in Matter
MU Jahrestagung, Forschungszentrum Jülich, Germany: 2015-09-29 - 2015-09-30

98. J. Ritman
Baryon Spectroscopy with PANDA
Resonances in QCD, EMMI Rapid task force, GSI Darmstadt, Germany: 2015-10-12 - 2015-10-14

99. J. Ritman
Hadron Physics with Antiprotons at PANDA/FAIR
PANDA Russia-Treffen, FAIR, Russia Research Centre, ITEP, Moscow, Russia: 2015-05-25 - 2015-05-27

100. M. Rosenthal and A. Lehrach
Spin Tracking Simulations towards Electric Dipole Moment Measurements at COSY
International Particle Accelerator Conference "'15, Richmond, USA: 2015-05-03 - 2015-05-08

101. R. Schnell *et al.*
The readout chain for the $\overline{\text{P}}$ANDA MVD strip detector
J. Instrum. **10** C02003 - C02003 (2015)

102. Y. Senichev *et al.*
Quasi-frozen Spin Method for EDM Deuteron Search
6th International Particle Accelerator Conference, Richmond, VA, USA: 2015-05-03 - 2015-05-08

103. A. Shindler
Beyond the Standard model matrix elements with the gradient flow: the case of the nucleon electric dipole moment
Bound states in QCD and beyond, St. Goar, Germany: 2015-03-24 - 2015-03-27

104. A. Shindler
Beyond the Standard model matrix elements with the gradient flow: the case of the nucleon electric dipole moment
Lattice BSM Workshop, Odense, Denmark: 2015-05-11 - 2015-05-15

105. A. Shindler
Beyond the Standard model matrix elements with the gradient flow: the case of the nucleon electric dipole moment
5th International Workshop on Lattice Hadron Physics, Cairns, Australia: 2015-07-20 - 2015-07-24

106. A. Shindler
Beyond the Standard model matrix elements with the gradient flow: the case of the nucleon electric dipole moment
Challenges in Strong Interaction Physics, Bad Honnef, Germany: 2015-09-29 - 2015-10-02

107. A. Shindler
Beyond the Standard model matrix elements with the gradient flow: the case of the nucleon electric dipole moment
Intersections of BSM Phenomenology and QCD for New Physics Searches, Seattle, USA: 2015-09-14 - 2015-10-23

108. A. Shindler, T. Luu and J. de Vries
Beyond the Standard model matrix elements with the gradient flow: the case of the nucleon electric dipole moment
33rd International Symposium on Lattice Field Theory, Kobe, Japan: 2015-07-14 - 2015-07-18

109. T. Stockmanns
Continuous Readout Simulation with FairRoot on the Example of the PANDA Experiment
21st International Conference on Computing in High Energy and Nuclear Physics (CHEP2015), Okinava, Japan: 2015-04-13 - 2015-04-17

110. T. Stockmanns
Continuous-Readout Simulation with FairRoot on the Example of the $\overline{\text{P}}$ANDA Experiment
J. Phys.: Conf. Ser. **664** 072046 - (2015)

111. H. Stroeher
Electric Dipole Moments - A Window for New Physics
European Physical Society Conference on High Energy Physics 2015, Vienna, Austria: 2015-07-22 - 2015-07-29

112. H. Stroeher
Schicksal der Antimaterie - Wieso existieren wir?
Wissenschaftliches Symposium im Rahmen des 20-jährigen Helmholtz-Jubiläums, Berlin, Germany: 2015-06-25 - 2015-06-25

113. H. Stroeher
Cross Topic "Antimatter"
Matter and the Universe - Annual Meeting, Jülich, Germany: 2015-09-29 - 2015-09-30

114. R. Tölle *et al.*
Injection Kicker for HESR at FAIR using Semi-Conductor Switches
6th International Particle Accelerator Conference, Richmond, VA, USA: 2015-05-03 - 2015-05-08

115. Y. Uzikov, J. Haidenbauer and C. Wilkin
$dp \to pp_sN\pi$ in the Δ isobar region
22nd International Baldin Seminar on High Energy Physics Problems, Dubna, Russia: 2014-09-15 - 2014-09-20

116. C. Weidemann
Toward polarized antiprotons: machine development for spin-filtering experiments at COSY
Phys. Scr. **T166** 014038 - (2015)

117. P. Wintz
Detector Topic: STT
PANDA LV Collaboration Meeting, Vienna, Austria: 2015-11-30 - 2015-12-04

118. A. Wirzba
Electric Dipole Moments of Light Ions
Bethe Workshop on Challenges in Strong Interaction Physics, Bad Honnef, Germany: 2015-09-29 - 2015-10-02

119. C. Xiao
From $e^+e^- \to \pi^+\pi^-\eta$ to $\eta \to \gamma^*\gamma^*$ using dispersion theory
the 7th Bethe Center Workshop "Challenges in Strong Interaction Physics", Physikzentrum Bad Honnef, Germanny: 2015-09-29 - 2015-10-02

120. A. Zambanini *et al.*
The PASTA Chip - A Free-Running Readout ASIC for Silicon Strip Sensors in PANDA
DPG-Frühjahrstagung, Heidelberg, Germany: 2015-03-23 - 2015-03-27

121. M. Zurek
Central exclusive $\pi^+\pi^-$ production in $p\bar{p}$ collisions at $\sqrt{s}$=0.9 and 1.96 TeV at CDF
International Workshop on Diffraction in High-Energy Physics, Primosen, Croatia: 2014-09-10 - 2014-09-16

122. M. Zurek
Measurement of central exclusive $\pi^+\pi^-$ production in $\overline{p}p$ collisions at $\sqrt{s} = 0.9$ and 1.96 TeV at CDF
International Wilhelm and Else Heraeus Physics School, Bad Honnef, Germany: 2015-08-17 - 2015-08-21

123. M. Zurek
Exclusive Central pi+pi- Production in Proton Antiproton Collisions at $\sqrt{s}$ = 1960 GeV and 900 GeV at the CDF
XLV International Symposium on Multiparticle Dynamics, Wildbad Kreuth, Germany: 2015-10-04 - 2015-10-09

124. M. Zurek
Charge symmetry breaking in the $dd \to {}^4\mathrm{He}\pi^0$ reaction with WASA-at-COSY
INTERNATIONAL SCHOOL OF NUCLEAR PHYSICS 37th Course, Probing Hadron Structure with Lepton and Hadron Beams, Erice, Italy: 2015-09-16 - 2015-09-24

125. M. Zurek and WASA-at-COSY-Collaboration
Charge Symmetry Breaking in the $dd \to {}^4\mathrm{He}\pi^0$ Reaction with WASA-at-COSY
DPG-Frühjahrstagung, Heidelberg, Germany: 2015-03-23 - 2015-03-27

C.2 Colloquia

1. R.W. Engels
"'Nuclear Polarized Hydrogen/Deuterium Molecules: Evidence, Production and for what they can be used"
PNPI Gatchina, Russia

2. R.W. Engels
"'Polarized Molecules: A new Option for Internal Storage-Cell Targets¿'
PSTP 2015, Bochum University, Germany: 2015-09-18 - 2015-09-18

3. R.W. Engels
"'Hyper-polarized deuterium molecules: A new option to produce and store polarized fuel for nuclear fusion".
INFN, Ferrara University, Italy: 2015-07-23 - 2015-07-23

4. D. Gotta
Remarks on a Johann Spectrometer for Exotic-Atom Research and more
colloquium spectroscopicum internationale XXXIX (CSI2015), 2015-08-30 - 2015-09-03

5. J. Haidenbauer
Charm production in antiproton-proton collisions
Gießen, Germany: 2015-11-12

6. A. Halama and V. Kamerdzhiev
Automated adjustment of the electron beam line of the 2 MeV Electron Cooler at COSY
DPG-Frühjahrstagung 2015, Wuppertal, Germany: 2015-03-09 - 2015-03-13

7. C. Hanhart
How can we unravel the mysteries of the XYZ states?
GSI, Darmstadt, Germany: 2015-05-12

8. V. Kamerdzhiev
High Energy Electron Cooling
CANU/FFE/CBAC Meeting, Bad Honnef, Germany, 17-18 Dec. 2015, Bad Honnef, Germany: 2015-12-17

9. A. Lehrach
Hadron Accelerators - Progress and Plans
Matter and Technologies Kickoff Meeting, Hamburg, Germany: 2015-02-22 - 2015-02-26

10. A. Lehrach and H. Gast
Auf der Suche nach der Antimaterie
JARA-Ringvorlesung im Rahmen der "‘RWTH extern“ Veranstaltungsreihe, Aachen, Germany: 2015-11-24 - 2015-11-24

11. U.-G. Meißner
”Nuclear Physics as Precision Science“, Grosses Kolloquium, UniversitÃ¤t zu KÃ¶ln: 17. Nov. 2015

12. U.-G. Meißner
”Theory of nulceon and nuclear EDMs“, Kolloquium, Institute for Theoretical Physics, CAS, Beijing, China: 21. April 2015

13. U.-G. Meißner
”Charming Pentaquarks,“ Kolloquium, Institute for Theoretical Physics, CAS, Beijing, China: 28. August 2015

14. U.-G. Meißner
”Alpha-Cluster Physics,“ Kolloquium, Peking Univeersity, Beijing, China: 8. September 2015

15. U.-G. Meißner
”Life on Earth - an Accident?,“ LNS Colloquium, MIT, Cambridge, USA: May 11, 2015

16. S. Mey and R. Gebel
An RF Wien-Filter as Spin Manipulator in Storage Rings
Freitags Seminar, III. Physikalisches Institut B, RWTH Aachen, Aachen, Germany: 2015-11-13

17. D. Prasuhn
Status of HESR
PANDA Collaboration Meeting, Gießen, Germany: 2015-03-18

18. D. Prasuhn
HESR
FAIR-MAC, Darmstadt, Germany: 2015-04-28 -

19. D. Prasuhn
Overview HESR
HIC4FAIR Workshop, Hamburg, Germany: 2015-07-29 -

20. E. Prencipe
X, Y, Z rates at PANDA
Workshop on Z States, Heyligenstaedt, Germany: 2015-07-07 - 2015-07-07

21. F. Rathmann
Spin Physics with COSY:Search for Electric Dipole Moments in Storage Rings
Kolloquium, Bonn, Germany: 2015-01-29 - 2015-01-29

22. F. Rathmann
Search for permanent electric dipole moments of protons and deuterons using storage rings
Physikalisches Kolloquium, Erlangen, Germany: 2015-10-19 - 2015-10-19

23. F. Rathmann
Search for permanent electric dipole moments of protons and deuterons using storage rings
Barschall Haeberli Symposium, Madison, Wisconsin, USA: 2015-04-10 - 2015-04-10

24. V. Reva *et al.*
Experimental Observation of Longitudinal Electron Cooling of DC and Bunched Proton Beam at 2425 MeV/c at COSY
International Workshop on Beam Cooling and Related Topics, Newport News, VA, USA: 2015-09-28 - 2015-10-02

25. M. Rosenthal
Impact of orbit distortions on EDM measurements
Beam Dynamics meets Diagnostics Workshop, Florence, Italy: 2015-11-04 - 2015-11-06

26. A. Shindler
Introduction to the gradient flow in quantum field theory and applications
Jüliich, Germany

27. A. Shindler
Beyond the Standard model matrix elements with the gradient flow: the case of the nucleon electric dipole moment
Jülich, Germany

28. A. Shindler
Beyond the Standard model matrix elements with the gradient flow: the case of the nucleon electric dipole moment
Washington DC, USA

29. A. Shindler
Beyond the Standard model matrix elements with the gradient flow: the case of the nucleon electric dipole moment
College Park, USA

30. A. Shindler
Beyond the Standard model matrix elements with the gradient flow: the case of the nucleon electric dipole moment
Livermore, USA

31. A. Shindler
Beyond the Standard model matrix elements with the gradient flow: a new method for the calculation of the electric dipole moment
Jülich, Germany

32. A. Shindler
Nuclear physics from QCD on supercomputers
East Lansing, USA

33. A. Shindler
Nucleon electric dipole moment with the gradient flow
Boston, USA

34. R. Stassen *et al.*
STOCHASTIC COOLING OF HEAVY IONS IN THE HESR
COOL Workshop 2015, Newport News, USA: 2015-09-28 - 2015-10-02

35. H. Stockhorst
Introduction to Stochastic Cooling
BND Summer School 2015, Heimbach, Germany: 2015-08-31 - 2015-09-11

36. H. Stockhorst *et al.*
Stochastic cooling system for HESR –theoretical and simulation studies–
COOL"'15 Conference, Newport News, VA, September 28 to October 2, 2015

37. H. Ströher
    Schicksal der Antimaterie - Wieso existieren wir?
    20 J. - 20 Vorträge (Veranstaltungsreihe zum 20-jährigen Jubiläum der HGF, Potsdam, GFZ, Germany

38. H. Ströher
    New Area of Activity - Leptogenesis
    Jara-Fame Annual Meeting, Aachen, Germany: 2015-02-19 -

D Diploma and Ph.D. theses

1. Bachelor, Master, Diploma

1. M. Dung
   Bachelor Thesis: Consequences of a diquark-antidiquark structure of tetraquarks
   Rheinische Friedrich-Wilhelms-Universität Bonn, Germany

2. I. Hammer
   Bachelor Thesis: Constraints of the θ-term from BBN
   Rheinische Friedrich-Wilhelms-Universität Bonn, Germany

3. P. Matuschek
   Diploma Thesis: Systematic studies of line shapes of near-threshold states
   Rheinische Friedrich-Wilhelms-Universität Bonn, Germany

4. M. Schever
   Master Thesis: Towards Measuring the Electromagnetic Structure of eta'-Mesons with CLAS
   RWTH Aachen University, Germany

5. J. Schumann
   Master Thesis: Beschleunigung eines Spurfindealgorithmus für den Straw Tube Tracker des $\bar{\text{P}}$ANDA-Detektors durch Parallelisierung mit CUDA C
   Fachhochschule Aachen, Campus Jülich, Germany

6. N. Vaidya
   Master Thesis: Combined Analysis of Lorentz- and Stieltjes-transformed Electromagnetic Response Functions of Light Nuclei
   German Research School for Simulation Sciences, Germany

2. Ph.D.

1. Dariusch Deermann
   Development of the PANDA MVD Trapezoidal Sensors and a Feasibility Study of the $\bar{p}p \to \bar{\Lambda}_c\Lambda_c$ Reconstruction
   Ruhr-Universität Bochum, Germany

2. I. Engin
   Towards Polarization Measurements of Laser-accelerated Helium-3 Ions
   Heinrich-Heine-Universität Düsseldorf, Germany

3. B. Gou
   Initial Investigations of (np)-Scattering with a Polarized Deuterium Target at ANKE-COSY
   Institute of Modern Physics, Chinese Academy of Science, Lanzhou, China

4. A. Herten
   GPU-based Online Track Reconstruction for PANDA and Application to the Analysis of $D \to K\pi\pi$.
   Ruhr-Universität Bochum, Germany

5. Q. Hu
   Development of the Recoil Detector for the HESR Day-One Experiment and Commissioning at COSY by Measuring pp Elastic Scattering
   University of Chinese Academy of Sciences, China

6. S. Sharma
   Validation of Spallation Models
   Jagiellonian University Krakow, Poland

7. A. Zambanini
   Developement of a Free-Running Readout ASIC for the PANDA Micro Vertex Detector and Investigation of the Performance to Reconstruct Antiproton-Proton $\to \Xi^+\Xi^-(1690)$
   Ruhr-Universität Bochum, Germany

3. Habilitation

1. Prof.Dr. K. Pysz
   Experimental and Theoretical Studies of Proton Induced Nuclear Spallation
   Jagiellonian University Krakow, Poland

E Awards & offers for professorships

M. Bai: Ernest Orlando Lawrence Award given by the U.S. Department of Energy

J. Haidenbauer: Outstanding Referee by the APS in January 2015

A. Herten: Awarded the "PANDA PhD Prize"

C. Köber: Awarded Bonn-Cologne Graduate School (BCGS) Stipend and accepted into Honors PhD program

L. Ludhova: Awarded "Recruitment initiative of the Helmholtz Association of 2015"

L. Ludhova: Accepted Professorship at Rheinisch-Westfälische Technische Hochschule Aachen

R. Maier: JARA-Seniorprofessor, RWTH-Aachen und Forschungszentrum Jülich GmbH, 30.01.2015

U.-G. Meißner: Awarded Professorship (honorary) under the Chinese Academy of Sciences President's International Fellowship Initiative for Visiting Scientists in 2015

U.-G. Meißner: Editorial Board of EPJA, Managing Editor—Reviews

H. Ströher: Editorial Board of EPJA, Co-Editor

J. de Vries: Awarded VENI grant from NWO (Nederlandse Organisatie voor Wetenschappelijk Onderzoek)

Q. Wang: Awarded "The Excellent PhD Thesis of the Chinese Academy of Sciences, 2015"

F Funded projects

Project	Responsible	Funded by
HGF - Fellow Award C.Roberts Preisgeld	U. Meißner	HGF
SFB/TRR 110 Quantenchromodynamik TP A05	U. Meißner	SFB
SFB/TRR 110 Quantenchromodynamik TP B03	U. Meißner	SFB
SFB/TRR 110 Quantenchromodynamik TP B07	U. Meißner	SFB
SFB/TRR 110 Quantenchromodynamik TP Z01	U. Meißner	SFB
SFB/TRR 110 Quantenchromodynamik TP Z02	U. Meißner	SFB
POLPBAR 25200 Management	H. Ströher	EU Projekt
POLPBAR 25200 Research	H. Ströher	EU Projekt
HESR	R. Tölle	Industrieprojekt mit der FAIR GmbH
HESR -sonstige Magnete	U. Bechstedt	Industrieprojekt mit der FAIR GmbH
Straw Tube Tracker	J. Ritman	Industrieprojekt mit der GSI GmbH
HESR -Netzgeräte	M. Retzlaff	Industrieprojekt mit der FAIR GmbH
Micro Vertex Detector	J. Ritman	Industrieprojekt mit der GSI GmbH
HESR -Hochfrequenz	R. Stassen	Industrieprojekt mit der FAIR GmbH
HESR-Injektion P1	R. Toelle	Industrieprojekt mit der FAIR GmbH
HESR-Strahldiagnose	V. Kamerdzhiev	Industrieprojekt mit der FAIR GmbH
HESR- Vakuum P1	F. Esser	Industrieprojekt mit der FAIR GmbH
HESR- Stochastische Kühlung	R. Stassen	Industrieprojekt mit der FAIR GmbH
HESR- Panda-Integration P1	D. Prasuhn	Industrieprojekt mit der FAIR GmbH
PPP-Polen (Polarisation Antiproton Prod.)	D. Grzonka	DAAD

G JCHP-FFE projects

Project	Institute	Responsible
PD Dr. A. Khoukaz	Westfälische Wilhelms-Universität Münster	Mesonenproduktion in Nukleon-Nukleon- und Nukleon-Kern-Stößen an COSY
Prof. Dr. A. Vasilyev	PNPI Gatchina	Development, commissioning and operation of components for the COSY Experiments WASA and ANKE and spin-filtering studies at COSY as preparation for PAX at FAIR
Prof. Dr. Vorobyev	PNPI Gatchina	ANKE
Prof. Dr. M. Nioradze	Tbilisi State University	NN-elastic scattering studies at COSY
PD M. Jezabek	Polish Academy of Sciences	Development of the signal processing method for high performance PANDA STT
Prof. Dr. P. Moskal	Jagellonian University Krakow	η meson production with polarized proton beam
Prof. T. Johansson	Uppsala University	Study oft he omega →pi+pi-pi0 Dalitz plot distribution with WASA
PD Dr. D. Eversheim	HISKP Universität Bonn	Time Reversal Invariance Test at COSY (TRIC)
Prof. N. Nikolaev	L.D. Landau Institute Moscow, Russia	Numerical simulations of spin dynamics for JEDI experiments, searching for permanent Electric Dipole Moments of deuterons and protons at COSY
Dr. J. G. Messchendorp	University of Groningen, Kernfysisch Versneller Instituut, Netherlands	Momentum Dependent electron Reconstruction for WASA and the PANDA Pre-Assembly
Prof. A. Roy	Indian Institute of Technology Indore, India	The η meson decay into γγ* in pp reactions with WASA-at-COSY
Prof. Dr. P. Moskal	Jagellonian University Krakow	Analysis of hyperon production with polarized proton beam
Prof. A. Gerasimov	ITEP Moscow	Development of a Frozen-Pellet Target
Prof. Dr. W. Kühn	Universität Giessen	Realtime Tracking for the PANDA Target Spectrometer
Prof. Dr. P. Lenisa	Università degli Studi di Ferrara, Italy	Spin-filtering studies in storage rings
Dr. A. Kulikov	JINR Dubna, Moscow Region, Russia	Spin Experiments at ANKE
Prof. J. Wang	Chinese Academy of Sciences, Lanzhou, China	Commissioning of the HESR day one experiment at COSY
Prof. Dr. A. Schäfer	Universität Regensburg	Mesonen Distributions-Amplituden
Prof. Dr. U. Wiedner	Ruhr-Universität Bochum	Development for the forward endcap of the PANDA EMC and buildup of the final endcap within PANDA in Jülich
Prof. Dr. U. Wiedner	Ruhr-Universität Bochum	Development of the Cryogenic Supply System for tests of the PANDA Target Spectrometer Solenoid
Prof. H. Chen	Southwest University, School of Physical Science and Technology, China	Simulation and optimization of the PANDA detector to measure the form factor of the Ds→e+ν+π,η,η`decay

Project	Institute	Responsible
Prof. U. Wiedner	Ruhr-Universität Bochum	Entwicklung für das Slow-control-System von PANDA
Prof. A. Schmeink	RWTH Aachen, Dept. of Electrical Engineering	A secure real-time remote control and operation of COSY subcomponents
Prof. Dr. K. Brinkmann	Justus-Liebig-Universität Gießen	Development and Validation of Detector Components and Preassembly for the PANDA MVD

H Conferences (co-)organized by the IKP

H.1 MUJ 2015 / Annual meeting 'Matter and the Universe'

On September 29./30. 2015, the first annual meeting of the programme 'Matter and the Universe' (MU) in the research field 'Matter' of the programme-oriented funding (PoF) took place at the research center Jülich. The meeting aimed to bring together the different programme communities and to strengthen the co-operation across the different programme topics. About 130 participants from HGF research centers and co-operating universities attended the meeting. The activities from the MU topics elementary particle physics, hadron physics, nuclear physics and astroparticle physics as well as contributions from the strongly linked programme 'Matter and Technology' (MT) and the Helmholtz Alliances Terascale, EMMI and HAP were presented in plenary sessions. More detailed discussions took place in parallel sessions covering the topics of dark matter, neutrino properties, antimatter, and strongly interacting matter. In final highlight lectures news from the Planck telescope and LHC-b experiment at CERN were presented.

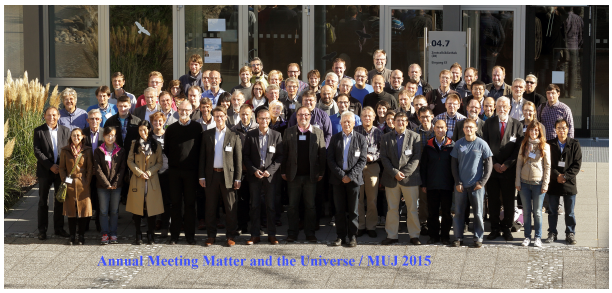

Fig. 60: Participants at the MU meeting in the research center Jülich.

H.2 2^{nd} Autumn lectures in Tbilisi

Within the framework of the "Georgian-German Science Bridge" (GGSB), institutes of Forschungszentrum Jülich (FZJ) - IKP, INM, and ZEA - together with its Georgian partner institutions - the Georgian Technical University (GTU) and the Ivane Javakishvili Tbilisi State University (TSU), have organized the second bi-annual meeting called "Autumn Lectures in Tbilisi" which took place during October 6 to 14, 2015, in Tbilisi (GTU) (see the corresponding website http://fz-juelich.gtu.ge/autumn-lectures/2015/). The lectures were devoted to "Nuclear Physics for Medicine" with the focus on: (i) Structure of Matter (Atoms, Nuclei, Particles, and Forces) (H. Stroeher, IKP); (2i) Radiation and Radiation Detection/and Protection (D. Gotta, IKP); (3i) Detectors: Electronics and Readout (D. Eversheim (Bonn Uni), I. Keshelashvili, A. Kacharava (IKP)); (4i) Applications in Medicine: Diagnosis (MRI, PET) (J. Shah, F. Grinberg (INM)); (5i) Technology for Science: Equipment Design and Construction (G. Natour, J. Wolters (ZEA)). About 50 selected students (Bachelor, Master, and PhD level) from the Georgian university consortium attended the course of lectures and practices. A special focus was laid on the practical exercises in laboratories.

At the same time a special meeting was organized with the Ministry of Education and Science of Georgia (MoE). The cooperation of Jülich and Georgian partners has been put on solid ground by a Memorandum-of-Understanding signed between MoE and JÜLICH to support and further develop their long-term scientific and educational cooperation. In this regard the foundation of so called SMART/Labs (SMART is the abbreviation for Science, Medicine, Applied Research and Technology) between a consortium of Georgian Universities and particular JÜLICH institutes (Institute of Energy and Climate Research (IEK), Nuclear Physics Institute (IKP), Institute of Neuroscience and Medicine (INM), Jülich Center for Neutron Science (JCNS) and Central Institute of Engineering, Electronics and Analytics (ZEA)) is envisaged. On October 7, 2015, contracts between Georgia and JÜLICH have been concluded and signed to establish a SMART/EDM_Lab, within the project devoted to search of electric dipole moments (EDM) of charged particles using storage rings. In addition discussions and brain storming about ongoing and future scientific projects were conducted and educational programs (in particular student exchanges) were fostered.

For 2016, JÜLICH and TSU are planing to organize the 7^{th} Georgian-German School and Workshop in Basic Science, this time devoted to the topic: "Spin Physics, Symmetries and Applications". The meeting will be held in Tbilisi, during August 29 - September 2, 2016. http://collaborations.fz.juelich.de/ikp/cgswhp/cgswhp16/

Fig. 61: Participants of the 2nd Autumn Lectures in Tbilisi (GTU).

Fig. 62: Participants of the 2nd Schülerakademie Teilchenphysik

H.3 Outreach: High–School–Student and teacher training program in hadron and particle physics

Funded by the Collaborative Research Center 110 and organized by members of the IKP/IAS of the Forschungszentrum as well as the Physikalisches Institut of Bonn University both a two–day teacher training program ('Lehrerfortbildung Teilchenphysik' with 20 participants) as well as a one–week program for high–school students ('Schülerakademie Teilchenphysik' with 27 participants) took place in the TU Munich and the Science College of Haus Overbach in Jülich Barmen, respectively. Fundamentals as well as current issues in nuclear, hadron and particle physics were discussed like the Higgs mechanism, the formation of elements, computer simulations as well as exotic hadrons. The high–school students had in addition the opportunity to visits of COSY as well as the supercomputer in the Forschungszentrum Jülich and to work on an own project in a small group.

H.4 Bethe workshop 2015: Challenges in strong interaction physics

The Bethe Center Workshop 2015, organized by scientists of both IKP/IAS of the Forschungszentrum Jülich as well as the HISKP of the Bonn University, was held in the Physikzentrum Bad Honnef, Germany, from September 29th to October 2nd. The nearly 70 international participants intensely discussed current challenges in Strong Interaction Physics focussing on nuclear and hadron physics. The four workshop days had the following themes:

- Non-perturbative Hadron-Hadron Interactions: few-particle systems,
- Strongly interacting many-body systems,
- Hadronic transitions form factors and (g-2),
- Hunting for physics beyond the SM.

H.5 International workshop on QCD exotics

Fig. 63: Participants of the "International Workshop on QCD Exotics"

The "International Workshop on QCD Exotics" was held in Jinan, China, on 8-12 June, 2015. The meeting was hosted by Shandong University and jointly organized by the Institute of High Energy Physics, Chinese Academy of Sciences and Shangdong University as well as the IAS/IKP of Forschungszentrum Jülich.
There has been a lot of progress in the experimental and theoretical study of the quarkonium and quarkonium-like XYZ states. In particular, various physical pictures were confronted with the recent observations. However, so far there has not been a single state for which the mission to identify the nature is fully accomplished. The 80 participants — theoreticians as well as experimentalists — discussed what is necessary from the theoretical side to disentangle the different scenarios proposed as well as what is feasible experimentally in this respect in the foreseeable future.

H.6 Topical meeting of spin tracking for precision measurements

The storage ring based search for a charged particle electric dipole moment (EDM) has received very positive responses in the latest US High Energy physics P5 report, and the Symmetries Town Meeting for the current US Nuclear Physics Long Range Plan as well as the latest

funding review by the German Helmholtz Association (HGF). To achieve the unprecedented precision of the EDM measurement requires not only a number of critical technology developments, such as polarimetry, high precision radial magnetic field measurements, high voltage electrostatic deflectors, high precision beam control, etc., but also

- Robust and advanced numerical tracking codes for exploring various systematic effects.
- Sophisticated lattice design tools for storage rings in the energy range of 0.7-1.5GeV/c with all electrostatic elements as well as combined magnetic and electric elements.
- Currently, a number of numerical tracking codes are available for spin tracking, including SPINK, Teapot, COSY-Infinity, zgoubi, BMAD, etc. Each code has its own unique characteristics based on its algorithm and architecture. To fulfill the requirements of the storage ring based EDM search, the following capabilities are essential:
- Accurate description of all ring elements including fringe fields.
- Allowing various error inputs for systematics investigation.
- Accurate implementation of RF spin manipulation elements.
- Calculation of both orbital and spin motion with a high accuracy for over 109 orbital revolutions.
- Allowing multipole particle tracking for exploring IBS as well as beam-beam effects.
- User friendly graphic interfaces for extracting physical information such as orbit, betatron tune, and spin tune from tracking data.

We organized a satellite meeting during the IPAC15 in Richmond, VA to identify the best approach using numerical simulation codes as well as lattice design tools. Discussions included how to benchmark the simulation codes against first-principle based models as well as well experimental results. (see https://juser.fz-juelich.de/record/282930.)

I Teaching positions

Institute	Name	University
IKP-1	PD Dr. A. Gillitzer	Bonn
	PD Dr. F. Goldenbaum	Wuppertal
	Prof. Dr. J. Ritman	Bochum
	PD Dr. S. Schadmand	Köln
	Dr. T. Stockmanns	Bochum
IKP-2	Prof. Dr. D. Gotta	Köln
	Prof. Dr. L. Ludhova	Aachen
	Prof. Dr. Dr. h.c. H. Ströher	Köln
	Prof. Dr. J. Pretz	Aachen
IKP-3/IAS-4	Univ. Doz. Dr. J. Haidenbauer	Graz
	Prof. Dr. C. Hanhart	Bonn
	Prof. Dr. S. Krewald	Bonn
	Prof. Dr. T. Luu	Bonn
	Prof. Dr. U.-G. Meißner	Bonn
	Dr. A. Nogga	Bonn
	PD Dr. A. Wirzba	Bonn
IKP-4	Prof. Dr. M. Bai	Bonn
	Prof. Dr. A. Lehrach	Aachen

J Personnel

DP A. Apostolou (IKP-1) (since 1st March 2015)
MSc. Z. Bagdasarian (IKP-2)
Prof. M. Bai (IKP-4)
Dr. U. Bechstedt (IKP-4)
C. Berchem (IKP-TA)
DP L. Bianchi (IKP-1)
Dr. C. Böhme (IKP-4)
M. Böhnke (IKP-4)
Dr. J. Böker (IKP-4) (since 1st February 2015)
DI N. Bongers (IKP-4)
Dr. B. Breitkreutz (IKP-4) (since 1st February 2015)
DI R. Brings (IKP-4) (until 31st March 2015)
P. Brittner (IKP-4)
Dr. J. Bsaisou (IKP-3/IAS-4) (until 31st March 2015)
J. But (IKP-TA)
Dr. L. Cao (IKP-1)
MBA A. Cebulla (IKP-1)
W. Classen (IKP-4)
M. Comuth-Werner (IKP-TA)
Dr. C. Constantinou (IKP-3/IAS-4)
B. Dahmen (IKP-4)
DI F.U. Dahmen (IKP-4)
DP D. Deermann (IKP-1) (until 15th August 2015)
Dr. J. de Vries (IKP-3/IAS-4)
C. Deliege (IKP-4)
G. D'Orsaneo (IKP-2)
R. Dosdall (IKP-1)
Dr. Y. Dutheil (IKP-4) (since 1st September 2015)
C. Ehrlich (IKP-4)
Dr. R. Engels (IKP-2)
Dr. I. Engin (IKP-4)
B. Erkes (IKP-4)
Dr. S. Esch (IKP-1) (until 28th February 2015)
DI F.-J. Etzkorn (IKP-4)
Dr. O. Felden (IKP-TA)
H.-W. Firmenich (IKP-TA)
Dr. R. Gebel (IKP-4)
I. Geerkens (IKP-2) (1st April – 30th Sept. 2015)
Dr. J. Gegelia (IKP-3/IAS-4) (since 1st June 2015)
R. Geppert (IKP-TA) (since 3rd August 2015)
DI N. Giese (IKP-TA)
PD Dr. A. Gillitzer (IKP-1)
J. Göbbels (IKP-TA)
PD Dr. F. Goldenbaum (IKP-1)
Prof. Dr. D. Gotta (IKP-2)
Dr. D. Grzonka (IKP-1)
Univ. Doz. Dr. J. Haidenbauer (IKP-3/IAS-4)
BSc. I. Hammer (IKP-3/IAS-4) (since 24th Aug. 2015)
Prof. Dr. C. Hanhart (IKP-3/IAS-4)
T. Hahnraths-von der Gracht (IKP-TA)
BEng. A. Halama (IKP-4)
Dr. M. Hartmann (IKP-2)
Dr. F. Hauenstein (IKP-1)
DI R. Hecker (IKP-TA)
Dr. V. Hejny (IKP-2)
DP N. Hempelmann (IKP-2)
Dr. A. Herten (IKP-1) (until 31st October 2015)
DP J.-H. Hetzel (IKP-4)
DP F. Hinder (IKP-4)
M. Holona (IKP-TA)
Dr. J. Hu (IKP-3/IAS-4)
Dr. Q. Hu (IKP-1)
MSc. M. Jabua (IKP-2)
Dr. A. Kacharava (IKP-2)
MSc. C. Kalitz (IKP-2) (1st April – 30th Sept. 2015)
Dr. V. Kamerdzhiev (IKP-4)
Dr. X. Kang (IKP-3/IAS-4) (since 31st August 2015)
P. Kaniewski (IKP-2) (since 1st September 2015)
Dipl.-Kffr. A. Kelleners (IKP-TA)
Dr. I. Keshelashvilli (IKP-2)
A. Kieven (IKP-4)
S. Kistemann (IKP-TA)
B. Klimczok (IKP-TA)
MSc. C. Körber (IKP-3/IAS-4)
M. Kremer (IKP-TA)
Prof. Dr. S. Krewald (IKP-3/IAS-4) (until 31st Aug. 2015)

DI T. Krings (IKP-TA) (since 1st April 2015)
G. Krol (IKP-4) (until 31st May 2015)
M. Küven (IKP-4)
Dr. T. Lähde (IKP-3/IAS-4)
DP A. Lai (IKP-1) (since 1st July 2015)
K.-G. Langenberg (IKP-4)
Prof. Dr. A. Lehrach (IKP-4)
Dr. D. Lersch (IKP-1)
Dr. N. Li (IKP-3/IAS-4)
Dr. S. Liebig (IKP-3) (until 31st August 2015)
Dr. B. Lorentz (IKP-4)
Dr. B. Lu (IKP-3/IAS-4)
Prof. Dr. L. Ludhova (IKP-2) (since 1st November 2015)
Prof. Dr. Th. Luu (IKP-3/IAS-4)
Prof. Dr. R. Maier (IKP-4)
DP P. Matuschek (IKP-3/IAS-4)
DI H.-P. May (IKP-4)
Prof. Dr. U.-G. Meißner (IKP-3/IAS-4)
Dr. S. Merzliakov (IKP-2)
DP S. Mey (IKP-4)
Dr. S. Mikirtytchiants (IKP-2)
C. Müller (IKP-TA)
DP F. Müller (IKP-2) (since 1st December 2015)
S. Müller (IKP-TA)
DP P. Musiol (IKP-1) (since 1st November 2015)
Dr. A. Naß (IKP-2)
Dr. A. Nogga (IKP-3/IAS-4)
H. Ohannessian (IKP-1) (until 30th April 2015)
Dr. H. Ohm (IKP-2) (until 31st October 2015)
BSc J. T. Peters (IKP-4)
Dr. D. Prasuhn (IKP-4)
Dr. E. Prencipe (IKP-1)
D. Prothmann (IKP-TA)
H. Pütz (IKP-4)
DP J. Pütz (IKP-1) (since 1st April 2015)
MSc. S. Quilitzsch (IKP-4) (since 2nd February 2015)
PD Dr. F. Rathmann (IKP-2)
DI K. Reimers (IKP-4)
DI M. Retzlaff (IKP-4)
DI A. Richert (IKP-4) (until 31st August 2015)
Prof. J. Ritman (IKP-1)
Dr. E. Roderburg (IKP-1)
G. Roes (IKP-TA)
A. Rolofs (IKP-2) (since 1st September 2015)
DP M. Rosenthal (IKP-4)
N. Rotert (IKP-4)
D. Ruhrig (IKP-4)
DP A. Saleev (IKP-2)
PD Dr. S. Schadmand (IKP-1)
MSc. M. Schever (IKP-1) (until 31st October 2015)
Dr. R. Schleichert (IKP-2)
BSc. V. Schmidt (IKP-4) (since 1st October 2015)
W. Schoofs (IKP-4) (since 1st October 2015)
F. Scheiba (IKP-4)
H. Schiffer (IKP-TA)
M. Schmühl (IKP-4)
DI G. Schug (IKP-4) (until 30th November 2015)
J. Schumann (IKP-1) (until 30th September 2015)
Dr. Th. Sefzick (IKP-TA)
Prof. Dr. Y. Senichev (IKP-4)
Dr. V. Serdyuk (IKP-1)
Dr. A. Shindler (IKP-3/IAS-4)
MSc. N. Shurkhno (IKP-4) (since 1st October 2015)
DI M. Simon (IKP-4)
H. Simonsen (IKP-TA)
A. Skawran (IKP-4) (since 1st October 2015)
D. Spölgen (IKP-2)
S. Srinivasan (IKP-4) (since 1st November 2015)
Dr. R. Stassen (IKP-4)
G. Sterzenbach (IKP-1)
Dr. H. Stockhorst (IKP-4)
Dr. T. Stockmanns (IKP-1)
J. Strehl (IKP-TA) (until 30th April 2015)
Prof. Dr. Dr. h. c. H. Ströher (IKP-2)
D. Temme (IKP-4) (16th March – 15th Sept. 2015)
MSc. M. Thelen (IKP-4)
Dr. R. Tölle (IKP-4)
MSc. F. Trinkel (IKP-2)
Dr. S. Trusov (IKP-2)
J. Uehlemann (IKP-1)
MSc. N. Vaidya (IKP-3/IAS-4) (until 21st Sept. 2015)
DI T. Vashegyi (IKP-4)

DP S. Vejdani (IKP-1) (since 1st October 2015)
BEng. A. Vishwanantha (IKP-3/IAS-4) (since 1st Apr. 15)
Dr. Q. Wang (IKP-3/IAS-4)
Dr. C. Weidemann (IKP-4) (since 1st September 2015)
DP P. Weiß (IKP-2)
Dr. P. Wintz (IKP-1)
PD Dr. A. Wirzba (IKP-3/IAS-4)
DI J.-D. Witt (IKP-4)
BSc. J.-L. Wynen (IKP-3/IAS-4) (since 1st October 2015)
Dr. C. Xiao (IKP-3/IAS-4)
Dr. H. Xu (IKP-1)
Dr. D.-L. Yao (IKP-3/IAS-4)
Dr. A. Zambanini (IKP-1) (until 30th November 2015)
Dr. E. Zaplatin (IKP-4)
H. Zens (IKP-4)
Dr. L. Zhao (IKP-3/IAS-4) (since 1st April 2015)
DP M. Zurek (IKP-2)

IKP-1 = Experimental Hadron Structure
IKP-2 = Experimental Hadron Dynamics
IKP-3/IAS-4 = Theory of the Strong Interactions
IKP-4 = Large-Scale Nuclear Physics Equipment
IKP-TA = Technical Services and Administration

K Further contributions

articles available on-line: http://www.fz-juelich.de/ikp/DE/Service/Download/download_node.html

- Evidence for excitation of two resonance states in the isovector two-baryon system with a mass of 2.2 GeV/c^2 at ANKE
- Measurement of the spin correlation paramaters in the reaction pd$\rightarrow{}^3$He+π^0 with ANKE
- Deuteron breakup pd$\rightarrow$ppn and the contact d-term in the pN$\rightarrow$ppπ subprocesses at ANKE
- One-loop contribution of the Δ-isobar mechanism to the reaction pp$\rightarrow$pp+π^0 near the Δ-threshold region at ANKE
- Identification of the reaction p+d$\rightarrow$d+η+p$_{sp}$ with ANKE
- High precision study on the η-meson production channel d+p$\rightarrow{}^3$He+η with ANKE
- Identification of deuterons in p+d$\rightarrow$ d+X reactions with ANKE
- Study of the p(pol)n quasi-free elastic scattering with ANKE
- Comparison of COSY-TOF and SATURNE-SPES4 data for the scattering length determination
- Investigation of meson production in proton-deuteron fusion to ^{3}HeX with WASA-at-COSY
- Studies on C-violation at WASA-at-COSY: $\eta \rightarrow \pi^0 e^+ e^-$
- Charge symmetry breaking in the dd $\rightarrow{}^4$Heπ^0 reaction with WASA-at-COSY
- Experimental study of few nucleon interaction dynamics in dp collisions with WASA-at-COSY
- Status of the search for η-mesic Helium in *dd* and *pd* reactions with WASA-at-COSY
- Determination of the analysing power for the $\vec{p}p \rightarrow pp\eta$ reaction using WASA-at-COSY
- Final State Interactions and the Box Anomaly in $\eta \rightarrow \pi^+\pi^-\gamma$ with WASA-at-COSY
- Electromagnetic transition form factor of the η meson with WASA-at-COSY
- Double dilepton decay of the η meson with WASA-at-COSY
- Radiative Decays of the η' meson with CLAS
- Transition form factor of the ω meson with CLAS
- Photoproduction of the π^0 meson up to 5.5 GeV with CLAS
- Measurement of the pp Elastic Scattering Differential Cross Section with the KOALA Recoil Detector at COSY
- Study of Excited Ξ Baryons in $\bar{p}$p-Collisions with the $\bar{P}$ANDA Detector
- Simulated Measurement of the D$_s$ Semileptonic Decay Form Factor with the PANDA Detector
- Search for the $\Delta\Delta$ Component in the Deuteron in $\bar{p}d$ Collisions with PANDA
- Parallel algorithms for online trackfinding at PANDA
- A test system for the electronic components of the PANDA Microvertex Detector
- Measurement of the spatial and energy-loss resolution with a prototype Straw Tube Tracker (STT) for the PANDA experiment
- XYZ rates at PANDA
- genfit2: a general fitting tool
- Search for polarization effects in the antiproton production process

- Commission of a Magnetostatic Beam Position Monitor
- Spin Tune Determination using Fourier Transform
- Development of the electrostatic deflector for JEDI
- Introduction to the quasi-frozen spin (QFS) method
- Preparation of First Beam Tests of LYSO Modules for JEDI polarimetry
- Systematic studies of spin dynamics in preparation for the precursor EDM experiment with the RF Wien filter at COSY
- Closed orbit influencing effects at COSY
- Beam and Spin Dynamics in an RF Wien-Filter
- Extension of COSY Toolbox for the Analysis of the Final Electric Dipole Moment Storage Ring
- A candidate layout for the JEDI polarimeter
- Automation of the Orbit Response Matrix Measurement at COSY
- Systematic Limitations of EDM Measurements at COSY due to Magnet Misalignments
- Automation of Rogowski Coil Test Bench and data Acquisition System
- Differential cross section of the dC$\rightarrow$p+X reaction at Td=270 MeV
- First Results of the Upgraded Low Energy Polarimeter Read-Out
- Improvements in Barrier-Bucket Signal Shaping
- Development of MAD-X based LOCO algorithm for COSY optics measurement as well as model improvement
- Measurement of the Harmonic Contents of the HESR Dipoles with a Single 3D Hall Probe
- Development of an automatic model based adjustment of the beam transport in the 2 MeV electron cooler at COSY
- Comparative numerical study of two BPM designs for the HESR
- Design of a test bench to characterize BPMs for the HESR
- GaN-Based High Power Amplifier for the HESR Main Stochastic Cooling System
- Status of the HESR BPM
- Upgrade of the BPM Readout Electronics at COSY
- Prototype of DAQ for commercial stand-alone devices with Ethernet interface
- Feasibility study on muon production with laser-accelerated protons or ions
- SEU Tests with the STS-XYTER Version 1 ASIC for CBM
- Radiation hardness tests of electronic components for CBM-STS low voltage power supply